Spatial Tessellations: Concepts and Applications of Voronoi Diagrams
Edition by ATSUYUKI OKABE & BARRY BOOTS and SUNG NOK CHIU

CHAPTER 2

Definitions and Basic Properties of Voronoi Diagrams

In Chapter 1 we discussed the concept of a Voronoi diagram from a historical viewpoint. In this chapter we wish to fully develop this concept from a geometric viewpoint.

The chapter consists of six sections. In Section 2.1 we define a Voronoi diagram and introduce notations to be commonly used in this text. In Section 2.2 we define a Delaunay tessellation, in particular a Delaunay triangulation in terms of the 'dual tessellation' of a Voronoi diagram. Voronoi diagrams and Delaunay tessellations are, as we overviewed in Section 1.2, quite useful in various fields because of their nice geometric properties. In Sections 2.3 and 2.4 we show the basic geometric properties of Voronoi diagrams and Delaunay triangulations, respectively (specific properties only used in each chapter will be shown in that chapter). In Section 2.5 we refer to geometric graphs closely related to a Delaunay triangulation, such as a Gabriel graph, a relative neighbourhood graph and a minimum spanning tree. In Section 2.6 we show how to judge whether or not a given diagram is a Voronoi diagram.

2.1 DEFINITIONS OF THE ORDINARY VORONOI DIAGRAM

For ease of exposition, we first give a fairly intuitive definition of a Voronoi diagram in a plane. We next restate this definition more precisely in mathematical terms. Lastly, extending the definition in $\mathbb{R}^2$ to $\mathbb{R}^m$, we define an m-dimensional Voronoi diagram.

Suppose that a set of points is given in the Euclidean plane (for example, the filled circles in Figure 2.1.1). The number of points is assumed to be two or more but finite and they are all distinct in the sense that no points coincide in the plane. Given this point set, we assign every location in the plane to the closest member in the point set (in Figure 2.1.1, for example, the point p is assigned to the filled circle incident to the heavy broken line). If a location happens to be equally close to two or more members of the point set,

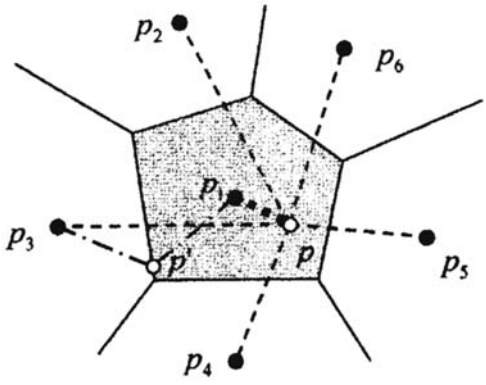

Figure 2.1.1 A planar ordinary Voronoi diagram.

we assign the location to those members (point p' in Figure 2.1.1 is assigned to the two filled circles incident to the dash-dot lines in Figure 2.1.1). As a result, the set of locations assigned to each member in the point set forms its own region (the shaded region in Figure 2.1.1). The resulting regions are collectively exhaustive in the plane because every location is assigned to at least one member in the point set. The set of locations assigned to two or more members in the point set forms the boundaries of the regions (the continuous lines in Figure 2.1.1). Hence adjacent regions overlap only on their boundaries. Thus the set of the regions is collectively exhaustive and mutually exclusive except for boundaries; namely, the set of the regions forms a tessellation. We call this tessellation a *planar ordinary Voronoi diagram*, and the regions constituting the Voronoi diagram *ordinary Voronoi polygons*.

To sum up, we have the following definition of a Voronoi diagram.

Definition V1 (a planar ordinary Voronoi diagram) Given a set of two or more but a finite number of distinct points in the Euclidean plane, we associate all locations in that space with the closest member(s) of the point set with respect to the Euclidean distance. The result is a tessellation of the plane into a set of the regions associated with members of the point set. We call this tessellation the *planar ordinary Voronoi diagram* generated by the point set, and the regions constituting the Voronoi diagram *ordinary Voronoi polygons*.

Note that when the Euclidean plane (space) is understood, or when there is no confusion with generalized Voronoi diagrams (to be shown in Chapter 3), we shall often refer to a planar ordinary Voronoi diagram simply as a *Voronoi diagram* and an ordinary Voronoi polygon as a *Voronoi polygon*. Also note that we exclude from our discussion the point set consisting of only one member, because such a Voronoi diagram is too trivial (it consists of only one Voronoi polygon which is the whole plane).

In the above definitions we define the Voronoi diagram for a set of finitely many points, but we can also define a diagram for a set of infinitely many points in the same manner. We also call the resulting diagram a Voronoi diagram (which is referred to as an *infinite Voronoi diagram* in Chapter 5). One diagram of this kind, the Poisson Voronoi diagram, is the subject of Chapter 5. In other chapters, however, we deal with only the former Voronoi diagram (which may be called a *finite Voronoi diagram*) because it is consistent with the applications to be presented throughout the book and, moreover, we want to avoid lengthy treatments resulting from the distinction between finite and infinite.

Let us now restate Definition V1 in mathematical terms. We consider a finite number, n, of points in the Euclidean plane, and assume that $2 \leq n < \infty$. The n points are labelled by $p_1, \ldots, p_n$ with the Cartesian coordinates $(x_{11}, x_{12}), \ldots, (x_{n1}, x_{n2})$ or location vectors $\boldsymbol{x}_1, \ldots, \boldsymbol{x}_n$. The n points are distinct in the sense that $\boldsymbol{x}_i \neq \boldsymbol{x}_j$ for $i \neq j$, $i, j \in I_n = \{1, \ldots, n\}$. Let p be an arbitrary point in the Euclidean plane with coordinates (x_1, x_2) or a location vector $\boldsymbol{x}$. Then the Euclidean distance between p and p_i is given by $d(p, p_i) = \|\boldsymbol{x} - \boldsymbol{x}_i\| = \sqrt{(x_1 - x_{i1})^2 + (x_2 - x_{i2})^2}$. If p_i is the nearest point from p or p_i is one of the nearest points from p, we have the relation $\|\boldsymbol{x} - \boldsymbol{x}_i\| \leq \|\boldsymbol{x} - \boldsymbol{x}_j\|$ for $j \neq i, j \in I_n$ (recall the heavy broken and dash-dot lines in Figure 2.1.1). In this case, p is assigned to p_i. Therefore, Definition V1 is written mathematically as follows.

Definition V2 (a planar ordinary Voronoi diagram) Let $P = \{p_1, \ldots, p_n\} \subset \mathbb{R}^2$, where $2 < n < \infty$ and $\boldsymbol{x}_i \neq \boldsymbol{x}_j$ for $i \neq j$, $i, j \in I_n$. We call the region given by

$$V(p_i) = \{\boldsymbol{x} \mid \|\boldsymbol{x} - \boldsymbol{x}_i\| \leq \|\boldsymbol{x} - \boldsymbol{x}_j\| \quad \text{for } j \neq i,\ j \in I_n\} \tag{2.1.1}$$

the *planar ordinary Voronoi polygon* associated with p_i (or the Voronoi polygon of p_i), and the set given by

$$\mathcal{V} = \{V(p_1), \ldots, V(p_n)\} \tag{2.1.2}$$

the *planar ordinary Voronoi diagram* generated by P (or the Voronoi diagram of P). We call p_i of $V(p_i)$ the *generator point* or *generator* of the ith Voronoi polygon, and the set $P = \{p_1, \ldots, p_n\}$ the *generator set* of the Voronoi diagram $\mathcal{V}$ (in the literature, a generator point is sometimes referred to as a *site*).

For brevity we may write V_i for $V(p_i)$. Also, we may use $V(x_{i1}, x_{i2})$ or $V(\boldsymbol{x}_i)$ when we want to emphasize the coordinates or location vector of the generator point p_i. In addition, we may use $\mathcal{V}(P)$ when we want to explicitly indicate the generator set P of $\mathcal{V}$.

In Definition V2 the reader should notice that the relation in equation (2.1.1) is defined in terms of $\leq$, but not $<$. A Voronoi polygon is hence a closed set. Alternatively, we may define a Voronoi polygon as

$$V^{\circ}(p_i) = \{\boldsymbol{x} \mid \|\boldsymbol{x} - \boldsymbol{x}_i\| < \|\boldsymbol{x} - \boldsymbol{x}_j\| \quad \text{for } j \neq i,\ j \in I_n\}, \tag{2.1.3}$$

which is an open set. Both definitions are acceptable, but in this text we

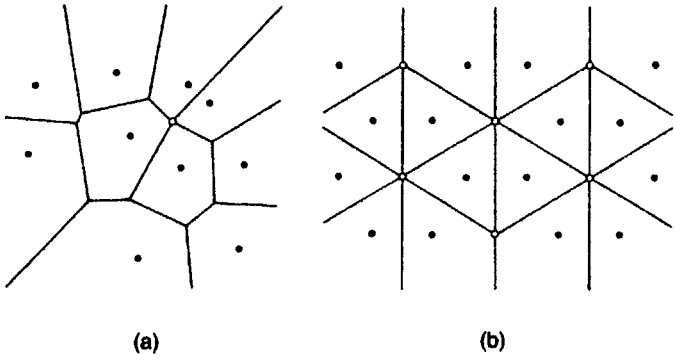

Figure 2.1.2 Degenerate Voronoi diagrams.

define a Voronoi polygon as a closed set. When we want to emphasize this property, we call $V(p_i)$ a *closed Voronoi polygon*, and $V^o(p_i)$ an *open Voronoi polygon.*

Since a Voronoi polygon is a closed set, it contains its boundary, which is denoted by $\partial V(p_i)$. The boundary of a Voronoi polygon may consist of line segments, half lines or infinite lines, which we call *Voronoi edges*. We denote a Voronoi edge by e_i. Note that a Voronoi diagram is sometimes defined by the union of Voronoi edges, i.e. $\cup_{i=1}^{n} \partial V(p_i)$ in place of the set $\{V(p_1), \ldots, V(p_n)\}$. Since the union of Voronoi edges may be regarded as a network, it is sometimes called a *Voronoi network* (Medvedev *et al.*, 1988; Bartkowiak and Mahan, 1995).

Noticing that = is included in the relation of equation (2.1.1), we may alternatively define a Voronoi edge as a line segment, a half line or an infinite line shared by two Voronoi polygons with its end points. Mathematically, if $V(p_i) \cap V(p_j) \neq \emptyset$, the set $V(p_i) \cap V(p_j)$ gives a Voronoi edge (which may degenerate into a point). We use $e(p_i, p_j)$ for $V(p_j) \cap V(p_j)$, which is read as the Voronoi edge generated by p_i and p_j. Note that $e(p_j, p_j)$ may be empty. If $e(p_i, p_j)$ is neither empty nor a point, we say that the Voronoi polygons $V(p_i)$ and $V(p_j)$ are *adjacent.*

An end point of a Voronoi edge is called a *Voronoi vertex*. Alternatively, a Voronoi vertex may be defined as a point shared by three or more Voronoi polygons. We denote a Voronoi vertex by q_i. When there exists at least one Voronoi vertex at which four or more Voronoi edges meet in the Voronoi diagram $\mathcal{V}$ (the unfilled circle in Figure 2.1.2(a)), we say that $\mathcal{V}$ is *degenerate*; otherwise, we say that $\mathcal{V}$ is *non-degenerate*. The Voronoi diagram in Figure 2.1.2(a) is degenerate and that in Figure 2.1.1 is non-degenerate. A degenerate Voronoi diagram often appears when generator points are regularly spaced, such as in Figure 2.1.2(b). In some derivations, a degenerate Voronoi diagram requires special lengthy treatments which are not always essential. To avoid this difficulty, we shall often make the following assumption.

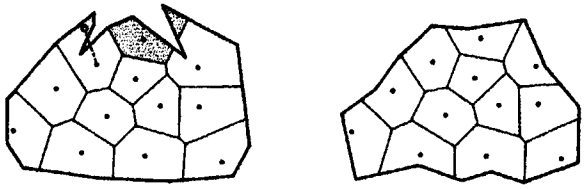

(a) (b)

Figure 2.1.3 Bounded Voronoi diagrams: (a) a disconnected boundary Voronoi region (the shaded region) and a non-star-shaped boundary Voronoi polygon with respect to its generator (the broken line segment); (b) star-shaped boundary Voronoi polygons with respect to their generator points.

Assumption V1 (the non-degeneracy assumption) Every Voronoi vertex in a Voronoi diagram has exactly three Voronoi edges.

In Definition V1 or V2, we defined a Voronoi diagram in an unbounded plane. In practical applications, however, we often deal with a bounded region S where generator points are placed (the heavy lines in Figure 2.1.3). In this case we consider the set, $\mathcal{V}_{\cap S}$, given by

$$\mathcal{V}_{\cap S} = \{V(p_1) \cap S, \ldots, V(p_n) \cap S\}. \tag{2.1.4}$$

We call this set a *bounded Voronoi diagram* or the *Voronoi diagram bounded by S* (which should be distinguished from the bounded Voronoi diagram defined by Wang and Schubert, 1987; see Section 3.4). If a Voronoi polygon $V(p_i)$ shares the boundary of S, we call the region $V(p_i) \cap S$ a *boundary Voronoi polygon* or *region* (the term 'region' is used when ∂S is curved or when $V(p_i) \cap S$ is not connected).

We should note that a boundary Voronoi region may be disconnected (the shaded region in Figure 2.1.3(a)), and that the line segment joining a point in $V(p_i)$ and p_i may not be contained in $V(p_i) \cap S$ (the broken line segment in Figure 2.1.3(a)). In practical applications, such boundary Voronoi polygons are often problematic, and so we have to define a more appropriate Voronoi diagram. We shall show such an alternative Voronoi diagram in Section 3.4. A bounded Voronoi diagram may be meaningful in practice if every boundary Voronoi region is star-shaped with respect to its generator point (Figure 2.1.3(b); recall Figure 1.3.15). In practice, we usually treat such a well-formed bounded Voronoi diagram.

As we observed in Figure 2.1.1, the ordinary Voronoi diagram consists of polygons. Recalling that a polygon is defined in terms of half planes (Section 1.3), we may alternatively define a Voronoi diagram in terms of half planes. To show this alternative definition, we consider the line perpendicularly bisecting the line segment $\overline{p_i p_j}$ joining two generator points p_i and p_j (Figure 2.1.4). We call this line the *bisector* between p_i and p_j and denote it by

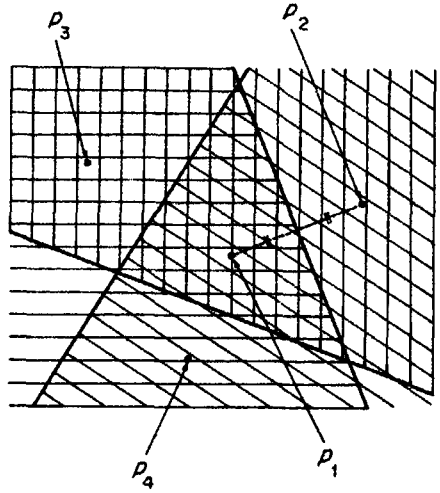

Figure 2.1.4 A Voronoi polygon obtained from half planes.

$b(p_i, p_j)$. Since a point on the bisector $b(p_i, p_j)$ is equi-distant from the generator points p_i and p_j, $b(p_i, p_j)$ is written as

$$b(p_i, p_j) = \{x \mid \|x - x_i\| = \|x - x_j\| \quad j \neq i. \tag{2.1.5}$$

The bisector divides the plane into two half planes and gives

$$H(p_i, p_j) = \{x \mid \|x - x_i\| \leq \|x - x_j\| \quad j \neq i. \tag{2.1.6}$$

We call the region $H(p_i, p_j)$ the *dominance region* of p_i over p_j. In Figure 2.1.4 we indicate the dominance regions of p_1 over p_2, p_3 and p_4 by the horizontally, diagonally and vertically hatched regions, respectively. Obviously, in the dominance region $H(p_i, p_j)$ the distance to the generator p_i is shorter than or equal to the generator p_j. In Figure 2.1.4, therefore, the distance from a point p in the intersection of the vertically, horizontally and diagonally hatched regions to the generator p_1 is shorter than or equal to the distance from p to the generator p_j, $j = 2, 3, 4$. This relation is equivalent to equation (2.1.1), and hence the intersection $H(p_1, p_2) \cap H(p_1 \cap p_3) \cap H(p_1, p_4)$ gives the Voronoi polygon associated with p_1. From this example, we understand that the following definition is an alternative to Definition V2.

Definition V3 (a planar ordinary Voronoi diagram defined with half planes) Let $P = \{p_1, \ldots, p_n\} \subset \mathbb{R}^2$, where $2 \leq n < \infty$ and $x_i \neq x_j$ for $i \neq j, i, j \in I_n$. We call the region

$$V(p_i) = \bigcap_{j \in I_n \setminus \{i\}} H(p_i, p_j) \tag{2.1.7}$$

the *ordinary Voronoi polygon* associated with p_i and the set $\mathcal{V}(P) = \{V(p_1), \ldots, V(p_n)\}$ the *planar ordinary Voronoi diagram* generated by P.

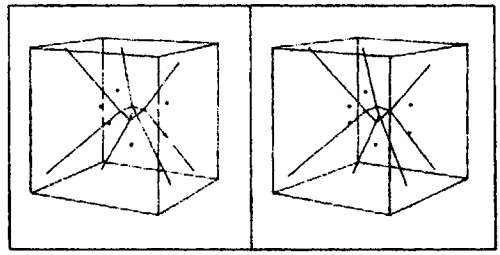

Figure 2.1.5 A stereographic view of a three-dimensional Voronoi diagram (view the left panel with the left eye and the right panel with the right eye at the same time, or use a stereographic viewer). (*Source*: Gen, 1983, p. 178.)

The equivalence of Definition V3 to Definition V2 is apparent, because $\|\boldsymbol{x} - \boldsymbol{x}_i\| \leq \|\boldsymbol{x} - \boldsymbol{x}_j\|$ if and only if $\boldsymbol{x} \in H(p_i, p_j)$ for $j \neq i$.

We can readily extend the above definition to the m-dimensional Euclidean space.

Definition V4 (an ordinary Voronoi diagram in $\mathbb{R}^m$) Let $P = \{p_1, \ldots, p_n\} \subset \mathbb{R}^m$, where $2 \leq n < \infty$ and $\boldsymbol{x}_i \neq \boldsymbol{x}_j$ for $i \neq j, i, j \in I_n$. We call the region

$$V(p_i) = \{\boldsymbol{x} \mid \|\boldsymbol{x} - \boldsymbol{x}_i\| \leq \|\boldsymbol{x} - \boldsymbol{x}_j\| \quad \text{for} j \neq i,\ j \in I_n\} \tag{2.1.8}$$

$$= \bigcap_{j \in I_n \setminus \{i\}} H(p_i, p_j) \tag{2.1.9}$$

the *m-dimensional ordinary Voronoi polyhedron* associated with p_i, and the set $\mathcal{V}(P) = \{V(p_1), \ldots, V(p_n)\}$ the *m-dimensional ordinary Voronoi diagram* generated by P, where $H(p_i, p_j)$ is given by equation (2.1.6) for $p_i, p_j \in \mathbb{R}^m$.

Note that when $\mathbb{R}^m$ is understood, we may simply call $\mathcal{V}(P)$ an *ordinary Voronoi diagram* or just a *Voronoi diagram*, and that Voronoi polyhedra (polygons) are sometimes called *Voronoi cells*.

For the three-dimensional Voronoi diagram, the boundaries of a Voronoi polyhedron consists of facets, which we call *Voronoi facets*. The boundaries of a Voronoi facet consist of line segments, half lines or infinite lines, which we call *Voronoi edges*. The boundaries of a Voronoi edge consist of points, which we call *Voronoi vertices*. Figure 2.1.5 shows a stereographic view of a three-dimensional Voronoi diagram obtained by Gen (1983) (see also Bowyer, 1981). In astronomy, realized Voronoi polyhedra in a three-dimensional space are sometimes called *Voronoi foams* (Icke and van der Weygaert, 1987). In winner-take-all type neural networks, the Voronoi polyhedron $V(p_i)$ is called the *receptive field* of a neural unit i with $\boldsymbol{x}_i$ being the synaptic weight vector of this neural unit (Martinetz and Schulten, 1994).

A visual presentation of an m-dimensional Voronoi diagram becomes difficult when $m \geq 4$. Formally, we call the boundaries of an m-dimensional

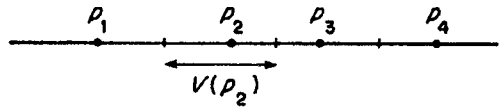

Figure 2.1.6 A Voronoi diagram on a line.

Voronoi polyhedron $(m-1)$-*dimensional Voronoi faces*; the boundaries of an $(m-1)$-dimensional Voronoi face $(m-2)$-*dimensional Voronoi faces* etc.; the boundaries of a three-dimensional Voronoi face *two-dimensional Voronoi faces* or simply *Voronoi faces*; the boundaries of a two-dimensional Voronoi face *one-dimensional Voronoi faces* or *Voronoi edges*; the boundaries of a one-dimensional Voronoi face *zero-dimensional Voronoi faces* or *Voronoi vertices*. An $(m-1)$-dimensional Voronoi face is also called a *Voronoi facet*.

Obviously we allow $m = 1$, a *one-dimensional Voronoi diagram*, or a *Voronoi diagram on a line* (Figure 2.1.6). In this case, a 'one-dimensional Voronoi polyhedron' is a half line or a line segment called a *Voronoi line*, and Voronoi vertices are end points of Voronoi lines. We easily notice that the boundary point between two adjacent Voronoi lines is the midpoint of the generator points of those Voronoi lines; the number of unbounded Voronoi lines is always two; the number of Voronoi lines adjacent to a Voronoi line is one or two. Because of these simple geometric properties, a Voronoi diagram on a line is often adopted in a simplified theoretical context to avoid complicated geometric arguments (for example, the original Hotelling model in Section 7.3). In this text we shall mainly treat a Voronoi diagram whose dimension is two or more.

In the above definitions, a space is represented by a continuous plane. This representation, however, may not be acceptable in some contexts, for instance raster image analysis. In such an analysis a space is represented by a set of square cells forming a grid lattice, and a geometrical figure is represented in terms of these cells. To be explicit, let $c_{ij} = \{(x, y) \mid i \le x \le i+1,\ j \le y \le j+1\}$, $i, j = \ldots, -n, \ldots, -1, 0, 1, \ldots, n, \ldots$. For a set of points representing a geometrical figure, G, we define $\mathrm{Im}(G) = \{c_{ij} \mid c_{ij} \cap G \neq \emptyset\}$, called the *image* of G. In terms of $\mathrm{Im}(G)$, we give the following definition (Dehne, 1989; Dehne *et al.*, 1991).

Definition V5 (a planar digitized Voronoi diagram) Let $\mathcal{V} = \{V(p_1), \ldots, V(p_n)\}$ be the Voronoi diagram defined in Definitions V1–V3. We call the set $\mathrm{Im}\mathcal{V} = \{\mathrm{Im}(V(p_1)), \ldots, \mathrm{Im}(V(p_n))\}$ the *(planar ordinary) digitized Voronoi diagram* of $\mathcal{V}$, $\mathrm{Im}(V(p_i))$ a *digitized Voronoi region*, and $\mathrm{Im}(\partial V(p_i))$ the *border* of a digitized Voronoi region $\mathrm{Im}(V(p_i))$.

An example is shown in Figure 2.1.7. Dehne (1989) shows a computational method for the planar ordinary digitized Voronoi diagram. Dehne (1989) also shows a computational method for a planar digitized Voronoi diagram generated by a set of objects with convex distance functions (see Section

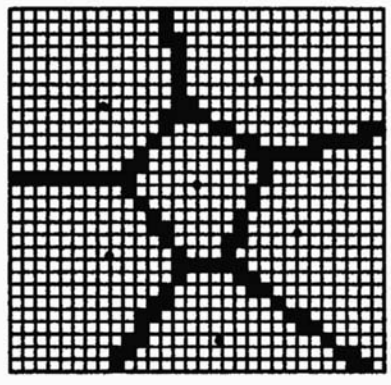

Figure 2.1.7 A planar ordinary digitized Voronoi diagram.

3.7). Embrechts and Roose (1996) develop a parallel algorithm using the Euclidean transformation. Also see Adamatzky (1994, 1996).

Alternatively we may define a Voronoi diagram by assigning cells to their nearest cells (Melkemi and Vandorpe, 1994; Watanabe and Murashima, 1996).

Definition V6 (a planar digital Voronoi diagram) Let $C = \{c_{ij}, i = 1, \ldots, n_h, j = 1, \ldots, n_v\}$ and $P_c = \{p_{c1}, \ldots, p_{cn}\}$ be a subset of C, where $2 \le n \le n_v n_h < \infty$, and $p_{ci} \neq p_{cj}$ for $i \neq j, i, j \in I_n$, and $d(c_{ij}, p_{ck})$ denotes the Euclidean distance between the centre of c_{ij} and that of p_{ck}. We call the region

$$\begin{aligned} V(p_{ci}) = \{c_{kl} \mid & d(c_{kl}, p_{ci}) < d(c_{kl}, p_{cj}) \quad \text{for } j \neq i; \\ & d(c_{kl}, p_{ci}) = d(c_{kl}, p_{cj}) < d(c_{kl}, p_{cm}) \\ & \text{for } i < j \neq m,\ k \in I_{n_h},\ l \in I_{n_v}\} \end{aligned} \tag{2.1.10}$$

the *digital Voronoi polygon* associated with p_{ci} and the set $\mathcal{V}(P_c) = \{V(p_{c1}), \ldots, V(p_{cn})\}$ the *digital Voronoi diagram* generated by P_c. Note that the second condition in equation (2.1.10) means that if a cell c_{kl} is equally distant from the generator cells p_{ci} and p_{cj}, we assign, for convenience, the cell c_{kl} to the generator that has a smaller index, i.e. p_{ci} where $i < j$ (not both as in the ordinary Voronoi diagram). Toriwaki and Yokoi (1988), Schwarzkopf (1989), Melter and Stojmenović (1995), and Watanabe and Murashima (1996) call the digital Voronoi diagram the *discrete Voronoi diagram*.

Recalling Definition V2, we notice that $V(p_i)$ is alternatively written in terms of a function $f_i(\boldsymbol{x}) = \|\boldsymbol{x} - \boldsymbol{x}_i\|$ as

$$V(p_i) = \{\boldsymbol{x} \mid f_i(\boldsymbol{x}) = \min_{j \in I_n} \{f_j(\boldsymbol{x})\}\}. \tag{2.1.11}$$

Geometrically, $z = f_i(\boldsymbol{x})$ shows the cone centred at $\boldsymbol{x}_i$ in the three-dimensional space $\{(x_1, x_2, z)\}$, and hence $z = f_{\min}(\boldsymbol{x}) = \min_{j \in I_n} \{f_j(\boldsymbol{x})\}$ shows the lower envelope of the n cones, $z = f_1(\boldsymbol{x}), \ldots, z = f_n(\boldsymbol{x})$. This envelope forms

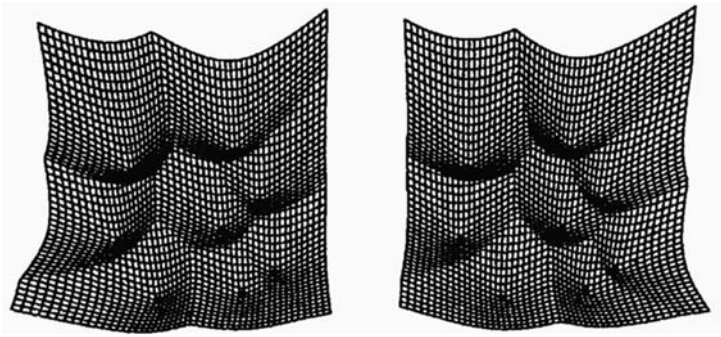

Figure 2.1.8 A Voronoi surface (look at the left-hand figure with the right eye and the right-hand figure with the left eye).

a surface, which we call the *Voronoi surface* of $\mathcal{V}$ (Huttenlocher *et al.*, 1993). An example is shown in Figure 2.1.8 (also see Figure 2 in Webster, 1998). Alternatively we may replace $f_i(\boldsymbol{x}) = \|\boldsymbol{x} - \boldsymbol{x}_i\|$ with $f_i(\boldsymbol{x}) = \|\boldsymbol{x} - \boldsymbol{x}_i\|^2$, and obtain another surface $z = f_{\min}(\boldsymbol{x})$. This surface is differentiable except at points on the boundaries $\cup_{i=1}^{n} \partial V(p_i)$. Siersma (1998) examines the differential topology of this surface through the Morse theory.

2.2 DEFINITIONS OF THE DELAUNAY TESSELLATION (TRIANGULATION)

In the same way that a planar graph has its dual graph, a Voronoi diagram has its 'dual tessellation', called a Delaunay tessellation. In this section we define a Delaunay tessellation, in particular a Delaunay triangulation.

We consider a Voronoi diagram in the Euclidean plane, and assume that generator points of the Voronoi diagram are not on the same line as in Figure 2.2.1(a). Since this assumption will be adopted often in this text, we shall refer to it as:

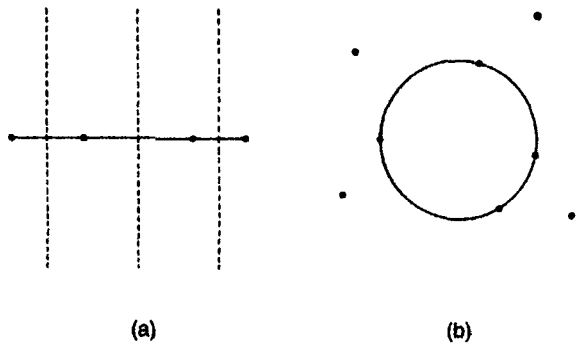

Figure 2.2.1 (a) Collinear generator points; (b) cocircular generator points.

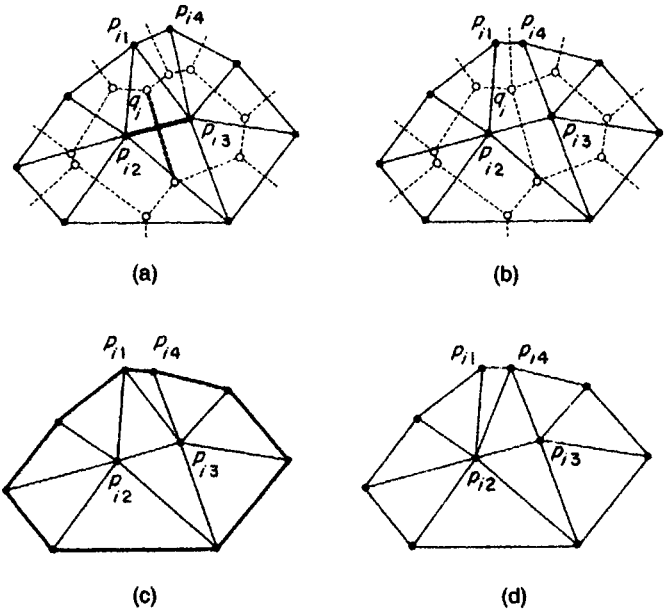

Figure 2.2.2 Voronoi diagrams (the broken lines) and triangulations (the solid lines): (a) a Delaunay triangulation; (b) a Delaunay pretriangulation; (c) a Delaunay triangulation obtained from (b); (d) another Delaunay triangulation obtained from (b).

Assumption D1 (the non-collinearity assumption) For a given set $P = \{p_1, \ldots, p_n\}$ of points, the points in P are not on the same line.

Note that Elbaz and Spehner (1990) show an approximation test for collinearity, which is useful in numerical computation with finite digits.

In addition to this assumption we assume that the number of points is three or more but finite. Note that the non-collinearity assumption implicitly implies $n \geq 3$, because two points are always on the same line. Also note that this assumption was not made in the preceding section, but it is made here because, as will be shown later, without these assumptions we cannot obtain a triangulation. Also note that we can obtain a Voronoi diagram even when $n = 2$ or when generator points are collinear (the broken lines in Figure 2.2.1(a)).

Under the non-collinearity assumption and $3 \leq n < \infty$, we now show how to obtain a Delaunay triangulation from a Voronoi diagram (the broken lines in Figure 2.2.2). First we choose a Voronoi edge in a Voronoi diagram (the heavy broken line in Figure 2.2.2(a)). This Voronoi edge is shared by two Voronoi polygons. We join the generator points (the filled circles) of these Voronoi polygons by a line segment (the heavy solid line in Figure 2.2.2(a)). We carry out this line generation with respect to all Voronoi edges in the Voronoi diagram. As a result, we obtain a second tessellation of the convex hull of the generator points (the solid lines in Figure 2.2.2(a)). In Figure

2.2.2(b) we have another tessellation of the convex hull of the generator points (the solid lines) obtained from another Voronoi diagram (the broken lines). These two tessellations are different in that the tessellation in panel (a) consists of only triangles, whereas the tessellation in panel (b) contains a quadrangle. We call the former tessellation a *Delaunay triangulation*. The latter is not a triangulation, but since it is to be triangulated, we call it a *Delaunay pretriangulation*. Inspecting the Voronoi diagram indicated by the broken lines in Figure 2.2.2(b), we notice that a Delaunay pretriangulation occurs when the Voronoi diagram is degenerate (this condition will be proved in Property V7 in Section 2.3).

A Delaunay pretriangulation has polygons having four or more vertices. We partition these non-triangular polygons into triangles by non-intersecting line segments joining the vertices. For example, we partition the quadrangle with vertices $p_{i1}, p_{i2}, p_{i3}, p_{i4}$ in Figure 2.2.2(b) by the line segment $\overline{p_{i1}p_{i3}}$. As a result, the Delaunay pretriangulation becomes a tessellation consisting of only triangles (Figure 2.2.2(c)). We also call this tessellation a *Delaunay triangulation* (and sometimes a *degenerate Delaunay triangulation* to distinguish it from the above Delaunay triangulation). We should note that, as can be seen in Figures 2.2.2(c) and 2.2.2(d), a Delaunay triangulation obtained from a Delaunay pretriangulation is not unique; the quadrangle $p_{i1}p_{i2}p_{i3}p_{i4}$ can be triangulated either by the line segment $\overline{p_{i1}p_{i3}}$ or the line segment $\overline{p_{i2}p_{i4}}$. Both triangulations are acceptable.

A Delaunay triangulation should consist of at least one triangle, and this condition is guaranteed by the non-collinearity assumption. If the non-collinearity assumption and $3 \leq n < \infty$ are not satisfied, as in Figure 2.2.1(a), the above procedure does not produce triangles but line segments, or triangles which degenerate into line segments. To sum up, we have the following definition.

Definition D1 (a Delaunay triangulation) Given a Voronoi diagram where generator points are not collinear and their number is three or more but finite, we join all pairs of generator points whose Voronoi polygons share the common Voronoi edge. As a result, we obtain a second tessellation. If this tessellation consists of only triangles, we call it a *Delaunay triangulation*. If not, we call it a *Delaunay pretriangulation*. For the Delaunay pretriangulation, we partition non-triangular polygons into triangles by non-intersecting line segments joining the vertices. As a result, the Delaunay pretriangulation becomes a triangulation. We also call it a *Delaunay triangulation*.

Note that in the same procedure in Definition D1, we can construct a diagram from a Voronoi diagram defined for a set of infinitely many points. We also call it a Delaunay triangulation, but such a Delaunay triangulation is treated only in Chapter 5 (where it is called an *infinite Delaunay triangulation*).

In Definition D1 we constructed a tessellation by generating line segments with respect to every Voronoi edge. Alternatively, we may construct a tessellation by generating line segments with respect to every Voronoi vertex.

Although a Delaunay triangulation can be obtained from a Voronoi diagram constructed by the former method as well as the latter method, we employ the latter method here because it will be easily extended to the definition in $\mathbb{R}^m$ (Definition D3).

We consider a Voronoi diagram $\mathcal{V}(p)$ generated by a set of distinct points $P = \{p_1, \ldots, p_n\}$ $(3 \le n < \infty)$ which satisfies the non-collinearity assumption. Consider a Voronoi vertex q_i and let $V(p_{i1}), \ldots, V(p_{ik_i})$ be the Voronoi polygons sharing the Voronoi vertex q_i. Note that the generator points $p_{i1}, \ldots, p_{ik_i}$ are indexed counterclockwise (or clockwise) around q_i (Figure 2.2.2(a)). For these generator points, we construct the polygon with line segments $\overline{p_{ij}p_{ij+1}}, j = 1, \ldots, k_i$ (p_{ik_i+1} is read as p_{i1}). If the resulting polygon is a triangle (such as $\Delta p_{i1}p_{i2}p_{i3}$ in Figure 2.2.2(a)), we leave it as it is. If it is not a triangle (such as the quadrangle $p_{i1}p_{i2}p_{i3}p_{i4}$ in Figure 2.2.2(b)), we partition the polygon into triangles by non-intersecting line segments joining the vertices (Figures 2.2.2(c) and 2.2.2(d)). In this manner we construct triangles with respect to all Voronoi vertices in $\mathcal{V}(P)$. As a result, we obtain the set of triangles that forms a tessellation of the convex hull CH(P) of P. We call this tessellation the *Delaunay triangulation* of CH(P) spanning P. Stated a little more mathematically, we have the following definition.

Definition D2 (a Delaunay triangulation) Let $\mathcal{V}(P)$ be a Voronoi diagram generated by a set of n distinct points $P = \{p_1, \ldots, p_n\} \subset \mathbb{R}^2$, $(3 \le n < \infty)$ that satisfies the non-collinearity assumption (D1); $Q = \{q_1, \ldots, q_{n_v}\}$ be the set of Voronoi vertices in $\mathcal{V}$; and $\boldsymbol{x}_{i1}, \ldots, \boldsymbol{x}_{ik_i}$ be the location vectors of the generator points whose Voronoi polygons share a vertex q_i. We define the set by

$$T_i = \left\{ \boldsymbol{x} \,\middle|\, \boldsymbol{x} = \sum_{j=1}^{k_i} \lambda_j \boldsymbol{x}_{ij}, \text{ where } \sum_{j=1}^{k_i} \lambda_j = 1, \lambda_j \ge 0, j \in I_{k_i} \right\} \tag{2.2.1}$$

(recall equation (1.3.19)) and let

$$\mathcal{D} = \{T_1, \ldots, T_{n_v}\}. \tag{2.2.2}$$

If $k_i = 3$ for all $i \in I_{n_v}$, we call the set $\mathcal{D}$ the *Delaunay triangulation* of CH(P) spanning P. If there exists at least one $k_i \ge 4$, we call the set $\mathcal{D}$ the *Delaunay pretriangulation* of CH(P) spanning P. We partition T_i having $k_i \ge 4$ into $k_i - 2$ triangles by non-intersecting line segments joining the vertices, and denote the resulting triangles by $T_{i1}, \ldots, T_{ik_i-2}$ (note that $T_{ik_i-2} = T_{i1} = T_i$ for $k_i = 3$). Let

$$\mathcal{D} = \{T_{11}, \ldots, T_{1k_1-2}, \ldots, T_{n_v1}, \ldots, T_{n_vk_{n_v}-2}\}. \tag{2.2.3}$$

We call the set $\mathcal{D}$ the *Delaunay triangulation* of CH(P) spanning P, and triangles in $\mathcal{D}$ *Delaunay triangles*.

As is seen in equation (2.2.1), a Delaunay triangle is defined as a closed set, and it contains the boundary consisting of line segments. We call these line segments *Delaunay edges*. Specifically, if a Delaunay edge is shared by

two Delaunay triangles, we call it an *internal Delaunay edge* (the light lines in Figure 2.2.2(c)); otherwise, we call it an *external Delaunay edge* (the heavy lines in Figure 2.2.2(c)). When $\mathcal{V}$ is non-degenerate, a Voronoi edge and a Delaunay edge are in one-to-one correspondence. Hence the number of Voronoi edges in $\mathcal{D}$ is the same as the number of Voronoi edges in $\mathcal{V}$. Unlike a Voronoi edge, a Delaunay edge is always finite. We call the end points of a Delaunay edge *Delaunay vertices*. Obviously, every Delaunay vertex is a generator of $\mathcal{V}(P)$, and hence the set of Delaunay vertices in $\mathcal{D}$ is given by P.

In Definitions D1 and D2 we defined a Delaunay triangulation using a Voronoi diagram. This does not imply that a Delaunay triangulation should always be defined with a Voronoi diagram. In fact, we shall show in Section 2.3 that a Delaunay triangulation can be defined without a Voronoi diagram. We can define a Delaunay triangulation once a set P of points is given. To indicate this property explicitly, we sometimes write $\mathcal{D}$ as $\mathcal{D}(P)$ in the same way that we write $\mathcal{V}$ as $\mathcal{V}(P)$.

Since triangulation is a two-dimensional geometric notion, a Delaunay triangulation is defined only in $\mathbb{R}^2$. We can, however, extend this notion (Definition D2) to the m-dimensional Euclidean space as follows.

Definition D3 (an *m*-dimensional Delaunay tessellation) Let $\mathcal{V}(P)$ be a Voronoi diagram generated by $P = \{p_1, \ldots, p_n\} \subset \mathbb{R}^m$ $(m+1 \leq n < \infty)$, where the generator points satisfy the non-collinearity assumption (D1); $Q = \{q_1, \ldots, q_{n_v}\}$ be the set of Voronoi vertices (0-faces) in $\mathcal{V}(P)$; $V(p_{i1}), \ldots, V(p_{ik_i})$ be Voronoi $(m-1)$-faces sharing q_i; and T_i be the m-dimensional convex hull spanning generator points $p_{i1}, \ldots, p_{ik_i}$. If $k_i = m + 1$ for all $i \in I_{n_v}$, the set $\mathcal{D}(\mathrm{P}) = \{T_1, \ldots, T_{n_v}\}$ consists of m-dimensional simplices. We call the set $\mathcal{D}(P)$ the *m-dimensional Delaunay tessellation* of $\mathrm{CH}(P)$ spanning P. If there exists at least one $k_i \geq m + 2$, we call the set $\mathcal{D}(P)$ the *m-dimensional Delaunay pretessellation* of $\mathrm{CH}(P)$ spanning P (note that the pretessellation is a tessellation). We partition T_i having $k_i \geq m + 2$ into $k_i - m$ simplices by non-intersecting hyperplanes passing through the vertices of T_i. Let $T_{i_1}, \ldots, T_{ik_i-m}$ be the resulting simplices $(T_{ik_i-m} = T_{i1} = T_i$ for $k_i = m+1)$, and $\mathcal{D}(\mathrm{P}) = \{T_{11}, \ldots, T_{1k_1-m}, \ldots, T_{n_v1}, \ldots, T_{n_vk_{n_v}-m}\}$. We call the set $\mathcal{D}(P)$ the *m-dimensional Delaunay tessellation* of $\mathrm{CH}(P)$ spanning P, and a simplex in $\mathcal{D}(P)$ an *m-dimensional Delaunay simplex*. When the notion of a simplical complex is the main concern, m-dimensional Delaunay tetrahedrization is sometimes called the *Delaunay simplical complex* (Edelsbrunner and Shah, 1994).

As defined in Definition D1 or D2, a two-dimensional Delaunay tessellation is called a *Delaunay triangulation*. A three-dimensional Delaunay tessellation is called a *Delaunay tetrahedrization*. Figure 2.2.3 shows a stereographic view of a Delaunay tetrahedrization. Higher dimensional $(m \geq 3)$ Delaunay tessellations have been investigated by many: Watson (1981), Bowyer (1981), Tanemura *et al.* (1983), Avis and Bhattacharya (1983), Field

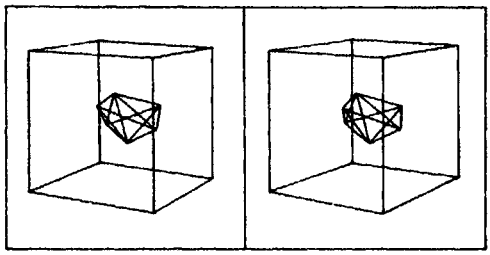

Figure 2.2.3 A stereographic view of a Delaunay tetrahedrization (view the left panel with the left eye and the right panel with the right eye, or use a stereographic viewer). (*Source*: Gen, 1983, p.78.)

(1986), Edelsbrunner *et al.* (1990a), Joe (1991a, 1993, 1995a), Dey *et al.* (1992b), Mohan and Lee (1993), Bertin *et al.* (1993), Teng *et al.* (1993), Rajan (1994), Weatherill and Hassan (1994), Borouchaki and Lo (1995), Lee and Jou (1995), Fang and Piegl (1995), Cignoni *et al.* (1995), Golias and Dutton (1997) and others. Escobar and Montenegro (1996) define a *'nearly' Delaunay tetrahedrization* considering round-off errors made by the computer when working with floating arithmetic. In general the round-off errors are problematic in practical computations. Dey *et al.* (1992b), and Jünger *et al.* (1991) discuss this problem in depth with respect to a Delaunay triangulation and Minkowski Voronoi diagrams (Section 3.7.1). We also discuss this problem in Chapter 4.

2.3 BASIC PROPERTIES OF THE VORONOI DIAGRAM

Having defined a Voronoi diagram in Section 2.1, we now wish to observe their geometric properties. We deal mainly with the properties of a planar Voronoi diagram, but some of them may be readily extended to an m-dimensional Voronoi diagram. (Note that in what follows, fairly technical or lengthy derivations are shown in **Proof** ... □. The reader who wishes to know the properties first may skip those derivations without losing the main stream.)

Although we have already stated in Definition V2 that the region $V(p_i)$ given by equation (2.1.1) is a polygon, this property is readily seen from Definition V3 which defines a Voronoi polygon in terms of half planes (equation (2.1.7)). Since a half plane is a convex set and the intersection of convex sets is a convex set (Section 1.3.1), a Voronoi polygon is a convex set. Since generator points are distinct, a Voronoi polygon is non-empty. Since every point in $\mathbb{R}^2$ is assigned to at least one of the generator points (Definition V1), the Voronoi polygons in $\mathcal{V}(P)$ are collectively exhaustive in $\mathbb{R}^2$. Moreover, noticing that Definition V3 implies $V(p_i) \subset H(p_i, p_j)$, $V(p_j) \subset H(p_j, p_i)$ and $[H(p_i, p_j) \setminus \partial H(p_i, p_j)] \cap [H(p_j, p_i) \setminus \partial H(p_j, p_i)] = \emptyset$, we understand that Voronoi polygons are mutually exclusive except for boundaries. These properties are quite obvious for an ordinary Voronoi diagram,

but some of them may not hold for generalized Voronoi diagrams (shown in Chapter 3). To draw attention to this contrast, we sum up these properties in Property V1.

Property V1 Let $P = \{p_1, \ldots, p_n\} \subset \mathbb{R}^2$ $(2 \leq n < \infty)$ be a set of distinct points. The set $V(p_i)$ defined by

$$V(p_i) = \{x \mid \|x - x_i\| \leq \|x - x_j\| \quad \text{for } j \neq i,\ j \in I_n\} \tag{2.3.1}$$

is a non-empty convex polygon, and $\mathcal{V}(P) = \{V(p_1), \ldots, V(p_n)\}$ satisfies

$$\bigcup_{i=1}^{n} V(p_i) = \mathbb{R}^2, \tag{2.3.2}$$

$$[V(p_i) \backslash \partial V(p_i)] \cap [V(p_j) \backslash \partial V(p_j)] = \varnothing,\ i \neq j,\ i, j \in I_n. \tag{2.3.3}$$

The Voronoi diagram $\mathcal{V}(P)$ is thus a unique tessellation of $\mathbb{R}^2$ for P.

It is straightforward to see that Property V1 also holds in $\mathbb{R}^m$ if a polygon is replaced by a polyhedron and $\mathbb{R}^2$ is replaced by $\mathbb{R}^m$. Since a Voronoi polyhedron is a convex set, a bounded Voronoi polyhedron is sometimes called a *Voronoi polytope*. Since Voronoi polygons cover the Euclidean plane, it is obvious that at least one Voronoi polygon is unbounded. From the assumption that $n \geq 2$, we have two or more Voronoi polygons, some of which may be bounded. When generator points are collinear, we readily notice from Figure 2.2.1(a) that all Voronoi polygons are unbounded. When generator points are non-collinear, we have Property V2.

Property V2 For a Voronoi diagram generated by a set of distinct points $P = \{p_1, \ldots, p_n\} \subset \mathbb{R}^2$ $(2 \leq n < \infty)$, a Voronoi polygon $V(p_i)$ is unbounded if and only if p_i is on the boundary of the convex hull of P, i.e. $p_i \in \partial \mathrm{CH}(P)$.

Proof Under the non-collinearity assumption, assume that some generator points are in the interior of $\mathrm{CH}(P)$. We shall show that a Voronoi polygon whose generator is an interior point of $\mathrm{CH}(P)$ is bounded. First, consider an interior generator point, p_i (p_i in Figure 2.3.1(a)). For p_i we can construct a triangle such that its vertices are generator points on the boundary of $\mathrm{CH}(P)$, say $p_{i1}, p_{i2}, p_{i3} \in P$, and it contains p_i in its interior (see Figure 2.3.1(a)). We next construct the triangle by the intersection of the half planes $H(p_i, p_{i1})$, $H(p_i, p_{i2})$ and $H(p_i, p_{i3})$ (the dash-dot lines in Figure 2.3.1(a)). Since p_i is an interior point of $\triangle p_{i1} p_{i2} p_{i3}$, this triangle is bounded and $H(p_i, p_{i1}) \cap H(p_i, p_{i2}) \cap H(p_i, p_{i3}) \supset \bigcap_{j \in I_n \backslash \{i\}}^{n} H(p_i, p_j) = V(p_i)$. The Voronoi polygon $V(p_i)$ is thus bounded.

Conversely, assume that the Voronoi polygon $V(p_i)$ is bounded by Voronoi edges $e(p_i, p_j)$ generated by p_i and p_j, $i \neq j$, $j \in J_i$, where J_i is the set of indices of Voronoi polygons adjacent to $V(p_i)$ (Figure 2.3.1(b)). It is then obvious that p_i is in the interior of $\mathrm{CH}(\{p_j, j \in J_i\})$ (the dash-dot lines in Figure

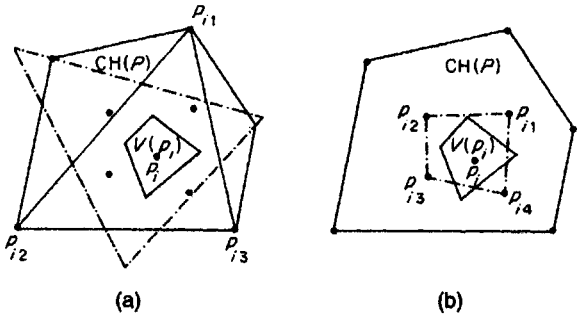

Figure 2.3.1 Illustration of the proof of Property V2.

2.3.1(b)). Since $\mathrm{CH}(\{p_j, j \in J_i\}) \subset \mathrm{CH}(P)$, p_i is not on the boundary of $\mathrm{CH}(P)$. When generator points are collinear, all generator points are on $\mathrm{CH}(P)$ which degenerates into a line segment, and all Voronoi polygons are unbounded. □

Note that almost in the same manner, we can prove that Property V2 holds for an m-dimensional Voronoi polyhedron.

When a Voronoi diagram $\mathcal{V}(P)$ is given, we can obtain the convex hull of P using Property V2; line segments joining generator points whose Voronoi polygons are unbounded and share the boundary give $\mathrm{CH}(P)$.

It follows from Property V2 that:

Property V3 For the Voronoi diagram generated by a set of distinct points $P = \{p_1, \ldots, p_n\}$ $(2 \leq n < \infty)$:

(i) Voronoi edges are infinite straight lines if and only if P is collinear.
(ii) A Voronoi edge $e(p_i, p_j)$ $(\neq \emptyset)$ is a half line if and only if P is non-collinear and p_i and p_j are consecutive generator points of the boundary of $\mathrm{CH}(P)$.
(iii) Suppose that p_i and p_j give a Voronoi edge $e(p_i, p_j)$. Then this edge is a finite line segment if and only if the line segment $\overline{p_i p_j}$ is not an edge of $\mathrm{CH}(P)$.

From Definition V3 we notice that Voronoi edges are parts of bisectors, but bisectors do not always generate Voronoi edges. The following property shows a sufficient condition for the generation of a Voronoi edge.

Property V4 The nearest generator point of p_i generates a Voronoi edge of $V(p_i)$.

Proof Let p_j be the nearest generator of p_i, and suppose that the bisector $b(p_i, p_j)$ does not generate a Voronoi edge. Let r_m be the midpoint of $\overline{p_i p_j}$ $(r_m \in b(p_i, p_j)$; Figure 2.3.2). Since $b(p_i, p_j)$ does not generate a Voronoi edge,

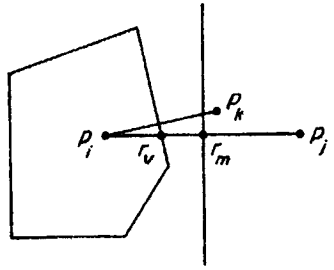

Figure 2.3.2 Illustration of the proof of Property V4.

r_m is outside of $V(p_i)$. Hence $\overline{r_m p_i}$ intersects a Voronoi edge, say $e(p_i, p_k)$, of $V(p_i)$, and let r_v be this intersection point. Since $\overline{p_i p_k}/2 \leq \overline{p_i r_v} < \overline{p_i r_m} = \overline{p_i p_j}/2$, we have $\overline{p_i p_k} < \overline{p_i p_j}$, but this contradicts that p_j is the nearest point of p_i. Thus, $b(p_i, p_j)$ generates the Voronoi edge $e(p_i, p_j)$. □

From Property V4, we readily notice Property V5.

Property V5 The nearest generator point from p_i exists in the generator points whose Voronoi polygons share the Voronoi edges of $V(p_i)$.

This property is useful in solving the following well-known problems (Shamos and Hoey, 1975; Bentley *et al.*, 1980).

Problem V1 (the closest pair problem) For a finite set P of distinct points, if the distance between $p_i \in P$ and $p_j \in P$ is the minimum among the distances between all possible pairs of points in P, we say that the pair $\{p_i, p_j\}$ is the *closest pair*. Given P, find the closest pair.

Problem V2 (the all nearest neighbour problem) Given a finite set P of distinct points, find the nearest neighbour point of p_i for every $p_i \in P$.

Property V5 suggests that when we want to solve the above problems, we need not compare all distances from p_i with the rest of the generator points; we just compare the distances from p_i with the generator points whose Voronoi polygons share the Voronoi edges of $V(p_i)$. Once Problem V2 is solved with this comparison, it is easy to find reciprocal pairs. A pair $\{p_i, p_j\}$ is a *reciprocal (nearest) pair* when p_i is the nearest neighbour point of p_j, and p_j is the nearest neighbour point of p_i. The closest pair is found in the reciprocal pairs.

Properties V4 and V5 are concerned with the nearest generator point from a generator point. The next property is concerned with the nearest generator point from an arbitrary point.

Property V6 The generator p_i is the nearest generator point from point p if and only if $V(p_i)$ contains p.

Although this property is quite obvious (almost the definition of a Voronoi polygon itself), we state it in the above because it is very useful in solving the following problem.

Problem V3 (the nearest-search problem) Given a finite set P of distinct points, find the nearest neighbour point among P from a given point p (p is not necessarily a point in P).

This problem is often referred to as the *post office problem* (Knuth, 1973). A naive method for solving Problem V3 is to find the minimum distance among n distances, $\{\|\boldsymbol{x} - \boldsymbol{x}_i\|, i \in I_n\}$. When we have only one probe point, this calculation is not so arduous. However, if the number of probe points becomes fairly large, the calculation with this naive method becomes time consuming. To unburden this computational load, Property V6 is useful. In general, when a tessellation is given, the problem of finding a region in which a given probe point is placed is called the *point-location problem*. Using efficient methods developed in computational geometry, such as the bucketing technique in Chapter 4 (or Mücke *et al.*, 1996), we can efficiently search to find in which Voronoi polygon a probe point exists. Once this polygon is known, say $V(p_i)$, then we immediately know from Property V6 that p_i is the nearest generator point.

In conjunction with Problem V3, we note the following problem (Dickerson and Drysdale, 1990; Dickerson *et al.*, 1992; Dickerson and Eppstein, 1996).

Problem V4 (the fixed-radius nearest neighbour search problem) Given a finite set P of distinct points on the plane and a given distance δ, find all pairs of p_i and p_j in P that satisfy $\|\boldsymbol{x}_i - \boldsymbol{x}_j\| \leq \delta$.

To solve this problem, we first construct the Delaunay triangulation spanning P. Second, we choose the Delaunay edges $\overline{p_i p_j}$ that satisfy $\|\boldsymbol{x}_i - \boldsymbol{x}_j\| \leq \delta$. The chosen edges form the graph $G(P_g, L_g)$, where P_g is the set of end points of the chosen edges and L_g is the set of the chosen open edges. Third, from each point $p_i \in P_g$, we do a depth-first search on $G(P_g, L_g)$, halting each branch of the search at the first point p_k such that $\|\boldsymbol{x}_i - \boldsymbol{x}_k\| \geq \delta$, and report all pairs $\{p_i, p_k\}$ with $\|\boldsymbol{x}_i - \boldsymbol{x}_k\| \leq \delta$ (Dickerson and Drysdale, 1990).

A Voronoi vertex also has interesting properties. Let $Q = \{q_1, \ldots q_n\}$ be the set of Voronoi vertices of $\mathcal{V}(P)$. Then we have the following property.

Property V7 For every Voronoi vertex, $q_i \in Q$, in a Voronoi diagram, there exists a unique circle C_i centred at q_i which passes through three or more generator points and contains no points in its interior. Under the non-degeneracy assumption, C_i passes through exactly three generator points.

Note that a circle which does not contain any points in its interior is called an *empty circle*; thus the circle C_i in Property V7 is an empty circle.

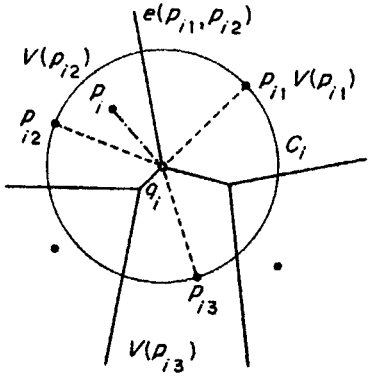

Figure 2.3.3 Illustration of the proof of Property V7.

Proof Since a Voronoi vertex q_i is shared by three or more Voronoi polygons, $V(p_{i1}), \ldots, V(p_{ik})$, $k \geq 3, p_{ij} \in P, j \in I_k$, where j is indexed counterclockwise (Figure 2.3.3), three or more Voronoi edges, $e(p_{i1}, p_{i2}), \ldots, e(p_{ik}, p_{i1})$, meet at q_i. Recalling that $e(p_{ij}, p_{ij+1})$ is contained in the bisector $b(p_{ij}, p_{ij+1})$, we see that the Voronoi vertex q_i is equally distant from p_{ij} and p_{ij+1}, i.e. $\overline{q_i p_{ij}} = \overline{q_i p_{ij+1}}$. Since this holds for $j \in I_k$ ($k+1$ is read as 1), we have $\overline{q_i p_{i1}} = \ldots = \overline{q_i p_{ik}}$ (the broken lines in Figure 2.3.3). The points $p_{i1}, \ldots, p_{ik}$ are hence on the same circle, which is denoted by C_i.

We next show that the circle C_i is an empty circle. Suppose that point $p_i \in P \setminus \{p_{i1}, \ldots, p_{ik}\}$ is inside C_i. Then $\overline{q_i p_i} < \overline{q_i p_{ij}}$ for $j = 1, \ldots, k$ (the dash-dot line in Figure 2.3.3), implying that q_i should be assigned to $V(p_i)$. This contradicts that q_i is shared only by $V(p_{i1}), \ldots, V(p_{ik})$. Hence C_i is an empty circle. □

From Property V7, the non-degeneracy assumption is equivalent to the following assumption.

Assumption V2 (the non-cocircularity assumption) Given a set of points $P = \{p_1, \ldots, p_n\} \subset \mathbb{R}^2$ ($4 \leq n < \infty$), there does not exist a circle, C, such that points $p_{i1}, \ldots, p_{ik} \in P$ ($k \geq 4$) are on C and all points in $P \setminus \{p_{i1}, \ldots, p_{ik}\}$ are outside C.

Note that Elbaz and Spehner (1990) show an approximation test for cocircularity.

This assumption can be extended to the assumption in $\mathbb{R}^m$ if we replace a circle with a (hyper)sphere and 4 with $m+2$. In this case, we may call the assumption the *non-cosphericity assumption*. In the literature of Poisson Voronoi diagrams (Chapter 5), the configuration of P satisfying this assumption and the non-collinearity assumption (D1) is referred to as the *general quadratic position* (Møller, 1994) (note that Huttenlocher *et al.*, 1992b, refer to the configuration of P satisfying only the non-cosphericity assumption as the *general position*).

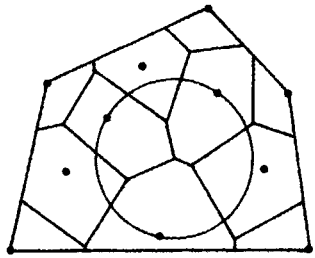

Figure 2.3.4 The largest empty circle whose centre is inside the convex hull of a set of points.

Immediately from Property V7, we obtain Property V8.

Property V8 The circle C_i in Property V7 is the largest empty circle among empty circles centred at the Voronoi vertex q_i.

Using this property with a slight modification, we can solve the following problem.

Problem V5 (the largest empty circle problem) Given a set P of distinct points, find the largest empty circle whose centre is in the convex hull of P.

Let Q' be the vertices of the Voronoi diagram $\mathcal{V}$ bounded by CH(P) (here Q' also includes the vertices formed at the points of the intersection between Voronoi edges and the boundary of the CH(P)), and C_i be the largest empty circle centred at $q_i \in Q'$. Then the largest circle among $\{C_i \mid q_i \in Q'\}$ gives the answer to Problem V5. An example is shown in Figure 2.3.4. This circle is useful to find the largest 'empty area' (an example is given in Section 7.3).

A Voronoi diagram has certain topological properties with respect to the number of Voronoi vertices, Voronoi edges and Voronoi polygons. To see them, we first induce a planar graph from a two-dimensional Voronoi diagram, $\mathcal{V}(P)$. Let $Q = \{q_1, \ldots, q_{n_v}\}$ be the set of Voronoi vertices and $E = \{e_1, \ldots, e_{n_e}\}$ be the set of Voronoi edges in $\mathcal{V}(P)$ in which the first n_c edges are infinite. Since infinite edges are not allowed in a geometric graph, a Voronoi diagram cannot be regarded as a geometric graph; we have to modify infinite Voronoi edges. To make this modification, we place a dummy point q_0 sufficiently far from CH(P). We cut every infinite Voronoi edge at a certain point, and join its end point and q_0 with a line segment (Figure 2.3.5). Let $e_{b1}, \ldots, e_{b\,n_c}$ be the edges obtained from $e_1, \ldots, e_{n_c}$ with this modification, and $E_b = [E \setminus \{e_1, \ldots, e_{n_c}\}] \cup \{e_{b1}, \ldots, e_{bn_c}\}$. Then, the pair of sets $Q_{+1} = Q \cup \{q_0\}$ and E_b actually forms a planar graph, $G(Q_{+1}, E_b)$. We call $G(Q_{+1}, E_b)$ the *Voronoi graph* induced from $\mathcal{V}(P)$. For a Voronoi graph, the Euler formula (equation (1.3.26)) holds, and hence we have the equation $(n_v + 1) - n_e + n = 2$ (n_r in equation (1.3.26) is n in $\mathcal{V}$), which is written as Property V9.

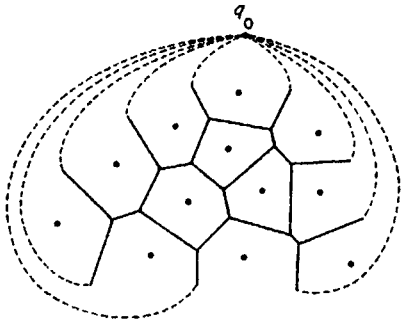

Figure 2.3.5 A Voronoi graph induced from a Voronoi diagram.

Property V9 Let n, n_e and n_v be the number of generator points, Voronoi edges and Voronoi vertices of a Voronoi diagram in $\mathbb{R}^2$, respectively ($2 \leq n < \infty$). Then

$$n_v - n_e + n = 1. \tag{2.3.4}$$

As an extension of this property, we obtain Property V10 from the Euler–Poincaré formula (equation (1.3.26)).

Property V10 Let n_k be the number of k-dimensional Voronoi faces in an m-dimensional Voronoi diagram. Then,

$$\sum_{k=0}^{m} (-1)^k n_k = (-1)^m. \tag{2.3.5}$$

Under the non-collinearity assumption and $3 \leq n < \infty$, every vertex in the Voronoi graph $G(Q_{+1}, E_b)$ has at least three edges. Hence the number of edges in $G(Q_{+1}, E_b)$ is not less than $3(n_v + 1)/2$ (the 2 in the denominator implies that every edge is counted twice), i.e.

$$n_e \geq \tfrac{3}{2}(n_v + 1). \tag{2.3.6}$$

Substituting this relation into equation (2.3.4), we obtain Property V11.

Property V11 Let n, n_e and n_v be the number of generator points, Voronoi edges and Voronoi vertices of a Voronoi diagram in $\mathbb{R}^2$, respectively, and assume that $3 \leq n < \infty$. Then

$$n_e \leq 3n - 6, \tag{2.3.7}$$

$$n_v \leq 2n - 5. \tag{2.3.8}$$

Although we derived this property under the non-collinearity assumption, Property V11 does not require it, because if generator points are collinear, then $n_v = 0$ and $n_e = n$, for which relations (2.3.7) and (2.3.8) hold for $n \geq 3$.

When a finite set P of generator points satisfies the non-collinearity assumption with $n \geq 3$, every bounded Voronoi polygon has at least three Voronoi edges, and every unbounded Voronoi polygon has at least two Voronoi edges. From these facts and recalling that the number of bounded Voronoi polygons is $n - n_c$ and that of unbounded Voronoi polygons is n_c,

we notice that the number of edges is not less than $[3(n - n_c) + 2n_c]/2$ (the 2 in the denominator implies that every edge is counted twice), i.e.

$$n_e \geq \frac{3(n - n_c) + 2n_c}{2}. \tag{2.3.9}$$

Substituting equation (2.3.4) into this relation, we obtain Property V12.

Property V12 Let n, n_e, n_v and n_c be the numbers of Voronoi polygons, Voronoi edges, Voronoi vertices and unbounded Voronoi polygons of a planar Voronoi diagram $\mathcal{V}(P)$, respectively, where $3 \leq n < \infty$ and P satisfies the non-collinearity assumption. Then the following relations hold:

$$n_v \geq \tfrac{1}{2}(n - n_c) + 1, \tag{2.3.10}$$

$$n_e \leq 3n_v - n_c - 3. \tag{2.3.11}$$

A Voronoi polygon is given by the intersection of $n-1$ half planes (equation 2.1.9)). A Voronoi polygon thus has $n-1$ Voronoi edges at the maximum. At the minimum when generator points are collinear (Figure 2.2.1(a)), the leftmost and the rightmost Voronoi polygons have only one Voronoi edge. So, what is the average number of Voronoi edges of a Voronoi polygon? From relation (2.3.7) and the fact that every Voronoi edge is shared by exactly two Voronoi polygons, we notice that the average number of Voronoi edges per Voronoi polygon is less than or equal to $2(3n - 6)/n$ (also see Table 5.5.1 and equation (5.5.6)). We hence obtain Property V13.

Property V13 The average number of Voronoi edges per Voronoi polygon does not exceed six.

Relation (2.3.8) shows that the maximum possible number of Voronoi vertices in a two-dimensional Voronoi diagram is $2n - 5$. For an m-dimensional Voronoi diagram, we have the following property.

Property V14 The maximum number, $n_{max}(i, m)$, of i-dimensional Voronoi faces of an m-dimensional Voronoi diagram generated by n distinct generator points is given by:

for $n \leq m + 1$,

$$n_{max}(i, m) = \binom{n}{m + 1 - i}; \tag{2.3.12}$$

for $1 \leq m+1 \leq n$,

$$n_{max}(i, m) = \begin{cases} C(m - i, m + 1) - 1, & i = 0, \\ C(m - i, m + 1), & 0 < i \leq m, \end{cases} \tag{2.3.13}$$

where

$$C(j, m+1)=\begin{cases}\sum_{i=1}^{s} \frac{n}{i}\binom{n-i-1}{i-1}\binom{i}{j-i+1}, & m+1=2s, \\ \sum_{i=1}^{s} \frac{j+2}{i+1}\binom{n-i-1}{i}\binom{i+1}{j-i+1}, & m=2s.\end{cases} \tag{2.3.14}$$

The proof of this property is shown in Seidel (1991) (also see Klee, 1980). This property is closely related to *Crum's problem*: what is the maximum number of non-overlapping convex polyhedra such that any pair of them has a common boundary of positive area? (Dewdney and Vranch, 1977.)

When a generator set is given, we can of course construct Voronoi edges. Conversely, when Voronoi edges are given without generator points, can we determine the locations of generator points? This problem is referred to as the *generator recognition problem* or the problem of *inverting the Voronoi diagram* (Adamatzky, 1993).

Problem V6 (the generator recognition problem) Provided that the Voronoi edges of a non-degenerate Voronoi diagram $\mathcal{V}(P)$ are given, recover the locations of generator points P.

Note that this problem can be extended to generalized Voronoi diagrams (Chapter 3; see Ash and Bolker, 1985), and degenerated cases are discussed in depth in Section 2.6.

To consider this problem, see Figure 2.3.6. Let q_i be a Voronoi vertex, p_{i1}, p_{i2}, p_{i3} be generator points whose Voronoi polygons share q_i, and q_{i1}, q_{i2}, q_{i3} be Voronoi vertices of the Voronoi edges incident to q_i. From Property V7, q_i is the centre of the circle that passes through p_{i1}, p_{i2}, p_{i3}. Since the Voronoi edges $e(p_{i1}, p_{i2})$, $e(p_{i2}, p_{i3})$ and $e(p_{i3}, p_{i1})$ perpendicularly bisect the Voronoi edges $\overline{q_{i2}q_i}$, $\overline{q_{i3}q_i}$, and $\overline{q_{i1}q_i}$, respectively, we have the equations $\angle p_{i1}\, q_i\, q_{i1} = \angle p_{i3}\, q_i\, q_{i1} = \alpha_i$, $\angle p_{i1}\, q_i\, q_{i2} = \angle p_{i2}\, q_i\, q_{i2} = \beta_i$, $\angle p_{i2}\, q_i\, q_{i3} = \angle p_{i3}\, q_i\, q_{i3} = \gamma_i$. Hence

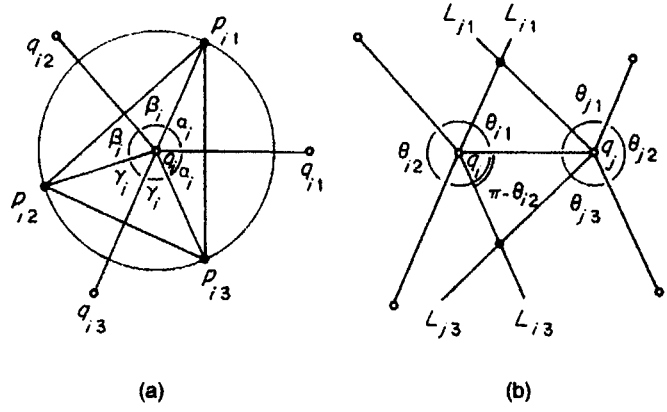

Figure 2.3.6 Recognition of generator points from Voronoi edges.

$2\alpha_i + 2\beta_i + 2\beta_i = 2\pi$, i.e. $\alpha_i = \pi - \beta_i - \gamma_i = \pi - \angle q_{i2}\, q_i\, q_{i3}$. From this equation, we obtain Property V15.

Property V15 Let $\overline{q_i q_j}$ be a Voronoi edge in a non-degenerate Voronoi diagram, and θ_{ik} and θ_{jk}, $k = 1, 2, 3$, be acute angles at q_i and q_j, respectively, where k is indexed counterclockwise from $\overline{q_i q_j}$ at q_i and clockwise at q_j (Figure 2.3.6(b)). Let $L_{ik}\,(L_{jk})$ be the half line radiating from $q_i\,(q_j)$ with angle $\pi - \theta_{i2}(\pi - \theta_{j2})$ with $\overline{q_i q_j}$ in the sector of $\theta_{ik}(\theta_{jk})$, $k = 1, 3$. Then the intersection point made by L_{i1} and L_{j1}, and that by L_{i3} and L_{j3} give the generator points of the Voronoi diagram sharing $\overline{q_i q_j}$.

This property can be developed into a more general property with which we can examine whether or not a given planar tessellation, $\mathcal{S} = \{S_1, \ldots, S_n\}$, is a Voronoi diagram. Suppose that the tessellation $\mathcal{S}$ consists of convex polygons and every vertex has exactly three edges. Let $q_{i1}, \ldots, q_{ik_i}$ be the vertices of a polygon S_i indexed counterclockwise. Let p_{ij} be the intersection point in S_i obtained through the same procedure stated in Property V15, where $\overline{q_i q_j}$ is replaced by $\overline{q_{ij} q_{ij+1}}$, $j = 1, \ldots, k_i$ (k_i+1 should be read as 1). Then we have the following property.

Property V16 A planar tessellation consisting of convex polygons whose vertices are all degree three is a Voronoi diagram if and only if $p_{i1} = p_{i2} = \ldots = p_{ik_i}$ holds for $i \in I_{n_v}$, where p_{ij} is defined in the above.

The proof of this property is provided by Ash and Bolker (1985). Degenerated cases are shown in Section 2.6.

A closely related problem to Problem V6 was raised by Heath and Kasif (1993). Consider a planar tessellation $\mathcal{T}$ consisting of k regions and a planar Voronoi diagram $\mathcal{V}$ generated by a finite set P of n distinct points (Figure 2.3.7). We say that $\mathcal{V}$ is *finer* than $\mathcal{T}$ if every region in $\mathcal{T}$ is partitioned into one or more regions of $\mathcal{V}$, or every edge which forms part of the boundary of $\mathcal{T}$ is covered by a union of Voronoi edges of $\mathcal{V}$ (Heath and Kasif, 1993)

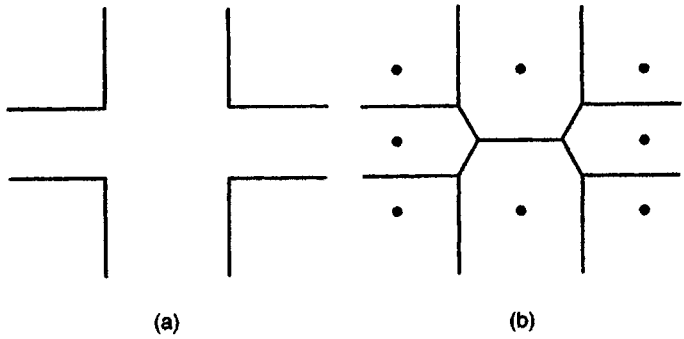

Figure 2.3.7 (a) A tessellation $\mathcal{T}$, and (b) a Voronoi diagram $\mathcal{V}$ that is finer than $\mathcal{T}$.

(obviously, $k \leq n$). We call the set P a *Voronoi cover* of $\mathcal{T}$ or, more specifically, *n-Voronoi cover* if $\mathcal{V}$ is finer than $\mathcal{T}$.

Problem V7 (the Voronoi cover problem) For a given tessellation $\mathcal{T}$ consisting of k regions and an integer n ($k \leq n$), is there a Voronoi cover $P = \{p_1, \ldots, p_n\}$ of $\mathcal{T}$ that contains no more than n points? If there is, find the locations of such generator points P.

Note that if $k = n$, the Voronoi cover problem is equivalent to the generator recognition problem (Problem V6). Heath and Kasif (1993) show that this problem is NP-hard (Section 1.3.4).

A planar Voronoi diagram is of course defined in $\mathbb{R}^2$, but interestingly we can construct this Voronoi diagram through a polyhedron in $\mathbb{R}^3$. This construction uses a transformation from a point in $\mathbb{R}^2$ to a point in $\mathbb{R}^3$, which is illustrated in Figure 2.3.8. Let p_i be a point on the x–y plane with coordinates (x_i, y_i). We lift this point vertically by height $z_i = x_i^2 + y_i^2$, and denote the lift-up point by p_i^*. The coordinates of p_i^* are given by $(x_i, y_i, x_i^2 + y_i^2)$. Recalling that the set $A = \{(x, y, z) \mid z = x^2 + y^2\}$ represents the paraboloid of the revolution along the z-axis, we notice that the point p_i^* is on the paraboloid A. Thus the above transformation is to lift a point p_i on the x–y plane vertically to the point p_i^* on the paraboloid A. We call this transformation the *lift-up transformation*; that is, we call the transformation from (x_i, y_i) to (x_i, y_i, z_i) by $z_i = x_i^2 + y_i^2$ the *lift-up transformation* from p_i to p_i^*, and call p_i^* the *lift-up* of p_i. For a set $P = \{p_1, \ldots, p_n\}$ of points, we also say that $P^* = \{p_1^*, \ldots, p_n^*\}$ is the *lift-up* of P.

For a given finite generator set P on the x–y plane, let P^* be the lift-up of P, and A_i be the plane tangential to the paraboloid A at p_i^* (Figure 2.3.9). Then the plane A_i is given by

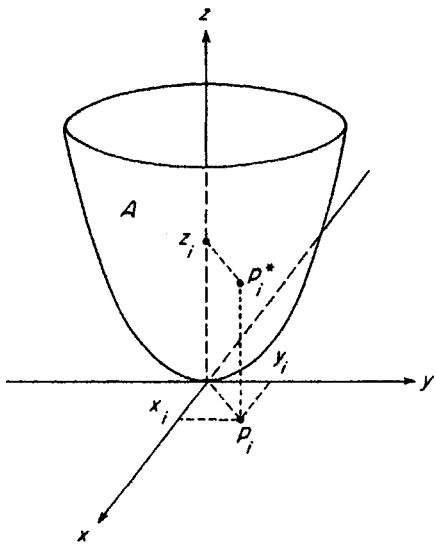

Figure 2.3.8 The lift-up transformation (p_i^* is the lift-up of p_i).

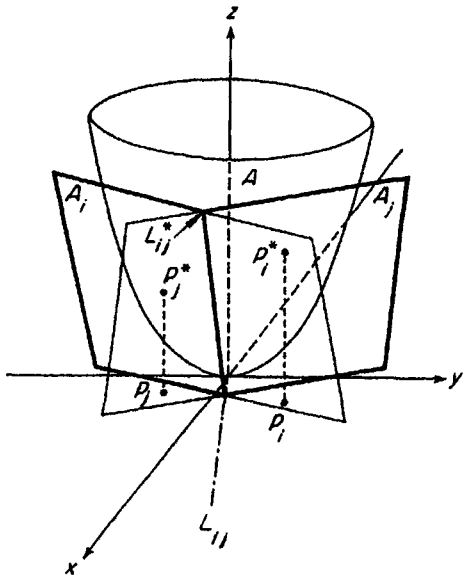

Figure 2.3.9 The construction of a planar Voronoi diagram through a polyhedron in $\mathbb{R}^3$.

$$z = 2x_i x + 2y_i y - (x_i^2 + y_i^2). \tag{2.3.15}$$

Notice that p_i^* is on the plane A_i and the points of P^*, other than p_i^*, are all above the plane A_i.

We next consider the intersection of two planes A_i and A_j, $i \neq j$ (Figure 2.3.9). Obviously this intersection, denoted by L_{ij}^*, is a line in $\mathbb{R}^3$. We project the line L_j^* on the x–y plane orthographically, and let L_{ij} be the projected line (the dash-dot line in Figure 2.3.9). The line L_{ij} is algebraically obtained by eliminating z from the equations of (2.3.15) for i and j. As a result, we obtain

$$2(x_i - x_j)x + 2(y_i - y_j)y - (x_i^2 + y_i^2 - x_j^2 - y_j^2) = 0. \tag{2.3.16}$$

This equation represents the line perpendicularly bisecting $\overline{p_i p_j}$, namely the bisector $b(p_i, p_j)$ between p_i and p_j.

The plane A_i divides $\mathbb{R}^3$ into two half spaces. Let H_i be the half space given by the region above the plane A_i with the boundary A_i, i.e.

$$H_i = \{(x, y, z) \mid z \geq 2x_i x + 2y_i y - (x_i^2 + y_i^2)\}. \tag{2.3.17}$$

For two half spaces H_i and H_j $(i \neq j)$, we construct the intersection $H_i \cap H_j$ (the heavy solid lines in Figure 2.3.9), which forms a polyhedron in $\mathbb{R}^3$. Since the orthographic projection of the edge of the polyhedron $H_i \cap H_j$ onto the x–y plane is the bisector between p_i and p_j, the orthographic projection of the facet of $H_i \cap H_j$ containing A_i onto the x–y plane gives the half plane $H(p_i, p_j)$. From this property we understand that the orthographic projection of the surface of the polyhedron given by $\cap_{i=1}^n H_i$ onto the x–y plane gives $\mathcal{V}(P)$. To sum up, we obtain the following property.

Property V17 The Voronoi diagram $\mathcal{V}(P)$ is obtained as the orthographic projection of the facets of the polyhedron made by the intersection of all upper half spaces $H_i, i \in I_n$, onto the x–y plane, where the upper half space H_i is the region above the plane tangential to the paraboloid at the lift-up point of the generator p_i.

We note that a planar Voronoi diagram can also be obtained through the inversion transformation in $\mathbb{R}^3$, which will be referred to in Section 2.4 (Property D7), and that the Delaunay triangulation obtained through the lift-up transformation is linked to a certain matroid, called the *Delaunay oriented matroid* (Santos, 1996).

2.4 BASIC PROPERTIES OF THE DELAUNAY TRIANGULATION

Corresponding to Property V1 of a Voronoi diagram, we first state the following basic property which is almost obvious from Definition D2.

Property D1 The set T_i defined by equation (2.2.1) is a unique non-empty polygon, and the set $\mathcal{D}(P) = \{T_1, \ldots, T_{n_v}\}$ given by equation (2.2.2) satisfies

$$\bigcup_{i=1}^{n_v} T_i = \mathrm{CH}(P), \tag{2.4.1}$$

$$[T_i \backslash \partial T_i] \cap [T_j \backslash \partial T_j] = \varnothing, \quad i \neq j,\ i, j \in I_{n_v}. \tag{2.4.2}$$

Hence the set $\mathcal{D}(P)$ forms a unique tessellation spanning P. If P satisfies the non-cocircularity assumption, $\mathcal{D}(P)$ is a Delaunay triangulation; otherwise, $\mathcal{D}(P)$ is a Delaunay pretriangulation. A Delaunay triangulation obtained from the Delaunay pretriangulation through the procedure mentioned in Definition D2 is not unique.

Although implicitly stated in equation (2.4.1) (and the heavy lines in Figure 2.2.2(c)), it follows from Definition D1 and Property V2 that:

Property D2 The external Delaunay edges in $\mathcal{D}(P)$ constitute the boundary of the convex hull of P.

Thus the Delaunay triangulation spanning P is a triangulation of $\mathrm{CH}(P)$ spanning P. Since $\mathrm{CH}(P)$ is bounded, all Delaunay triangles and Delaunay edges are finite. This property is in contrast to Properties V2 and V3 of a Voronoi diagram.

In Properties V4–V6 we showed the properties concerning the nearest neighbour point in a Voronoi diagram. To find a similar property for a Delaunay triangulation, let us inspect the Delaunay triangulations in Figure

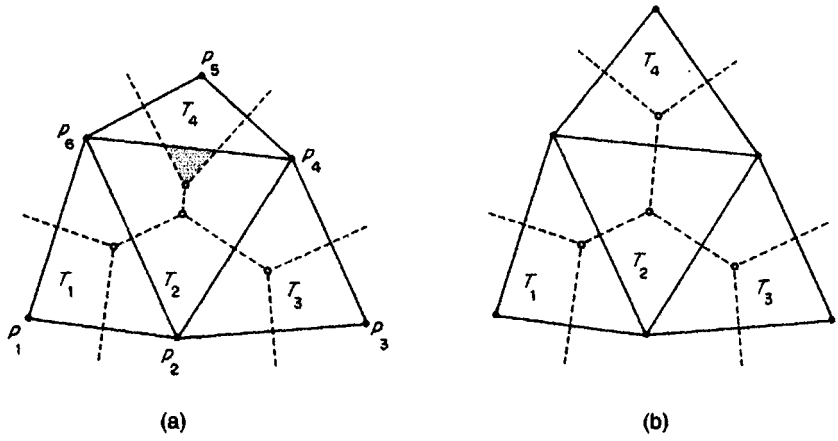

Figure 2.4.1 Delaunay triangulations: (a) is not a Pitteway triangulation, while (b) is a Pitteway triangulation.

2.4.1, where the unfilled circles, the broken lines and the solid lines represent Voronoi vertices, Voronoi edges and the Delaunay triangulation spanning six generator points $p_1, p_2, \ldots, p_6$, respectively. In observing the Delaunay triangles T_1, T_3, T_4 in panel (a), we notice that the nearest generator from any point in a triangle is one of the three vertices of the triangle, because the whole triangle is covered by the three Voronoi polygons whose generator points are the vertices of the triangle. On the other hand, the nearest generator from some points in T_2 (points in the shaded area) is a generator other than the three vertices of T_2, because T_2 is not exhaustively covered by the three Voronoi polygons whose generator points are the vertices of T_2. If a triangulation consists of only the former type triangles, such as in Figure 2.4.1(b), we call the triangulation a *Pitteway triangulation*. More generally, for a triangulation $\mathcal{T}(P)$ of CH(P) spanning P, if for any point P in CH(P) the closest generator point from p is one of the three vertices of the triangle containing p, we call the triangulation $\mathcal{T}(P)$ a *Pitteway triangulation* spanning P (cf. McLain, 1976). The triangulation in Figure 2.4.1(b) is a Pitteway triangulation.

Between a Delaunay triangulation and a Pitteway triangulation, we have the following relationship.

Property D3 (the Pitteway triangulation theorem) The Delaunay triangulation spanning P is a Pitteway triangulation spanning P if and only if every internal Delaunay edge crosses the associated Voronoi edge of the Voronoi diagram generated by P.

Proof First, assume that $\mathcal{D}(P)$ is a Pitteway triangulation spanning P. Then, any Delaunay triangle is covered by the three Voronoi polygons whose generator points are the vertices of the triangle. Let $\overline{p_i p_j}$ be an internal

Delaunay edge shared by Delaunay triangles $\Delta p_i p_j p_k$ and $\Delta p_i p_j p_l$. Assume, contrary to the property, that $\overline{p_i p_j}$ does not cross the associated Voronoi edge. This means that if the four generator points p_i, p_j, p_k and p_l are not cocircular, the Voronoi vertices generated by p_i, p_j, p_k and by p_i, p_j, p_l are both on the same side of $\overline{p_i p_j}$. If the four generator points are cocircular, the Voronoi vertex shared by $V(p_i)$, $V(p_j)$, $V(p_k)$ and $V(p_l)$ (in other words, the length-zero Voronoi edge associated with the Delaunay edge $\overline{p_i p_j}$) is not on $\overline{p_i p_j}$. Hence the midpoint of $\overline{p_i p_j}$ belongs to $V(p_k)$ or $V(p_l)$ but not to the both, which contradicts that $\mathcal{T}(P)$ is a Pitteway triangulation. Thus, any internal Delaunay edge crosses the associated Voronoi edge.

Assume next that any internal Delaunay edge crosses the associated Voronoi edge. Let p_i, p_j and p_k be the three vertices forming a Delaunay triangle. The proof varies according to which edges are internal edges among $\overline{p_i p_j}$, $\overline{p_j p_k}$ and $\overline{p_k p_i}$.

Case 1. Suppose that $\overline{p_i p_j}$, $\overline{p_j p_k}$ and $\overline{p_k p_i}$ are all internal edges (such as T_2 in Figure 2.4.1(b)). Then, because of the above assumption, the triangle contains the Voronoi vertex generated by p_i, p_j and p_k, but does not contain any other Voronoi vertex. Since the line segment connecting the generator p and a point on the boundary of $V(p)$ belongs to $V(p)$, the triangle is covered by $V(p_i)$, $V(p_j)$ and $V(p_k)$.

Case 2. Suppose that $\overline{p_i p_j}$, $\overline{p_j p_k}$ and $\overline{p_k p_i}$ are all external Delaunay edges. This implies that there are exactly three generator points in P, and hence the triangle (actually the whole plane) is covered by $V(p_i)$, $V(p_j)$ and $V(p_k)$.

Case 3. Suppose that one edge, say $\overline{p_i p_j}$, is an external Delaunay edge while the other two edges are internal. Then, the Voronoi vertex generated by p_i, p_j and p_k is either in the triangle or on the side opposite to the triangle with respect to $\overline{p_i p_j}$. In the former case, the external Delaunay edge $\overline{p_i p_j}$ also crosses the associated Voronoi edge, and hence the triangle is covered by $V(p_i)$, $V(p_j)$ and $V(p_k)$, as we saw in Case 1. In the latter case, the triangle contains no Voronoi vertex, and the Voronoi edge generated by p_i and p_k crosses both $\overline{p_j p_k}$ and $\overline{p_i p_j}$; the Voronoi edge generated by p_j and p_k crosses both $\overline{p_i p_k}$ and $\overline{p_i p_j}$. No other Voronoi edge traverses the triangle. This means that the triangle is covered by the three Voronoi polygons generated by its vertices.

Case 4. Suppose that two edges, say $\overline{p_i p_j}$ and $\overline{p_j p_k}$, are external edges and the other is an internal edge (such as T_1 in Figure 2.4.1(b)). Then, the Voronoi vertex generated by p_i, p_j and p_k is either in the triangle or on the side opposite to the triangle with respect to one of the external edges. In both cases the configuration is the same as in Case 3, and hence the triangle is covered by the three Voronoi polygons generated by its vertices. □

Property D3 gives the necessary and sufficient condition for $\mathcal{D}(P)$ to be a Pitteway triangulation. The next question is: If the point set P admits a Pitteway triangulation, does it necessarily coincide with $\mathcal{D}(P)$? The answer is 'no'. A counterexample is shown in Figure 2.4.2, where P consists of four points forming a rhombus; (a) is $\mathcal{D}(P)$ whereas (b) is not. However, both (a)

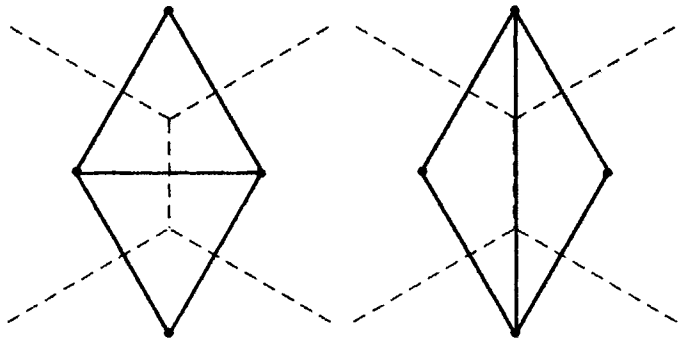

Figure 2.4.2 Two Pitteway triangulations spanning four points forming a rhombus (the solid lines) and Voronoi diagrams (the broken lines): (a) is the Delaunay triangulation while (b) is not.

and (b) are Pitteway triangulations. Thus, a Pitteway triangulation spanning P, if it exists, is not necessarily unique, and does not necessarily coincide with $\mathcal{D}(P)$.

As we observed in Definitions D1 and D2, we have nice relationships between $\mathcal{V}(P)$ and $\mathcal{D}(P)$ that share the same point set P. First, from Definition D1, the Delaunay vertices of $\mathcal{D}(P)$ are the generator points of $\mathcal{V}(P)$; conversely, the generator points of $\mathcal{V}(P)$ are the Delaunay vertices of $\mathcal{D}(P)$. Second, from Property V7, the Voronoi vertices of $\mathcal{V}(P)$ are the circumcentres of Delaunay triangles in $\mathcal{D}(P)$; conversely, the circumcentres of Delaunay triangles in $\mathcal{D}(P)$ are the Voronoi vertices in $\mathcal{V}(P)$. Lastly, the number of Delaunay edges of $\mathcal{D}(P)$ is greater than or equal to that of Voronoi edges (recall a Delaunay pretriangulation); under the non-degeneracy assumption, both numbers are the same. To sum up, we have the following property.

Property D4 For the Voronoi diagram $\mathcal{V}(P)$ generated by a finite set P of distinct points, and the Delaunay triangulation spanning P, let Q and Q_d be the set of Voronoi vertices and that of Delaunay vertices, respectively; E and E_d be the set of Voronoi edges and that of Delaunay edges, respectively; C_d be the set of circumcentres of Delaunay triangles. Then,

(i) $Q_d = P$;
(ii) $C_d = Q$;
(iii) $|E_d| \geq |E|$; $|E_d| = |E|$ if and only if $\mathcal{V}(P)$ is non-degenerate, where $|E|$ indicates the number of elements in the set E.

From Property D4 and Property V7, all Delaunay triangles have the next property which corresponds to Property V8.

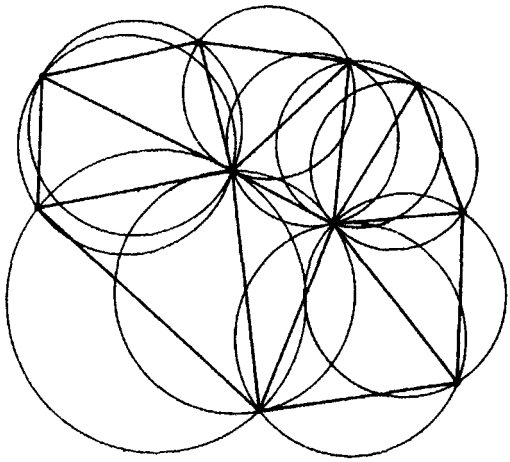

Figure 2.4.3 Empty circumcircles of Delaunay triangles (i.e. Delaunay circles) in a Delaunay triangulation.

Property D5 All circumcircles of Delaunay triangles are empty circles.

Note that the circumcircle of a Delaunay triangle is sometimes called a *Delaunay circle* and points on a Delaunay circle are called *natural neighbours* (Watson, 1985). An example is shown in Figure 2.4.3. The notion of a Delaunay circle can be extended in $\mathbb{R}^3$, and we call the circumsphere of a Delaunay tetrahedron a *Delaunay sphere*. Using Property D5, we can solve the largest empty circle problem (Problem V5) (a slight modification is necessary, as we remarked below Property V8).

Having observed Figure 2.4.3, the reader may question whether or not the converse relation in Property D5 holds; that is, if the circumcircles of all triangles in a triangulation are empty circles, then the triangulation is a Delaunay triangulation. To answer this question, we first introduce the following criterion.

The empty circumcircle criterion Given a triangulation of $\mathrm{CH}(P)$ spanning a finite set P of distinct points, if the circumcircle of a triangle in the triangulation is an empty circle, we say that the triangle satisfies the *empty circumcircle criterion.*

With this criterion, we can now show Property D6.

Property D6 (the empty circumcircle theorem) Every triangle in a triangulation spanning a finite set P of distinct points satisfies the empty circumcircle criterion if and only if the triangulation is the Delaunay triangulation spanning P.

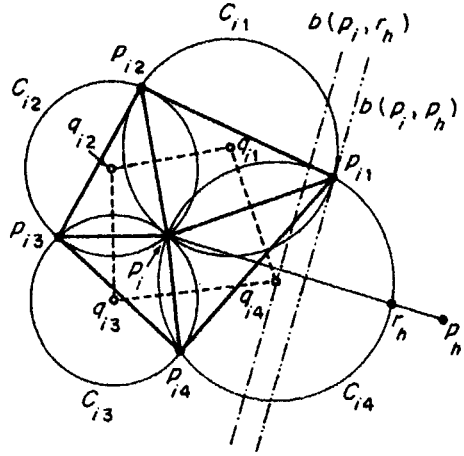

Figure 2.4.4 Illustration of the proof that a triangulation in which every triangle satisfies the empty circumcircle criterion is a Delaunay triangulation.

Proof Since we have already obtained Property D5, what is left is to prove that a triangulation in which every triangle satisfies the empty circumcircle criterion is a Delaunay triangulation.

Consider triangles sharing a point $p_i \in P$ in a triangulation $\mathcal{T}$ spanning P (Figure 2.4.4). Let $p_{i1}, \ldots, p_{ik}$ be the vertices of these triangles where the points are indexed counterclockwise, and $q_{i1}, \ldots, q_{ik}$ be the centres of the circumcircles, $C_{i1}, \ldots, C_{ik}$, of triangles $\Delta p_i p_{i1} p_{i2}, \ldots, \Delta p_i p_{ik} p_{i1}$ (the heavy solid lines in Figure 2.4.4). Since $\overline{p_i p_{ij}}$ is orthogonal to $\overline{q_{ij} q_{ij-1}}$, $j = 1, \ldots, k$ (0 is read as k), the polygon with vertices $q_{i1}, \ldots, q_{ik}$ is given by $\bigcap_{j=1}^{k} H(p_i, p_{ij})$ (the broken lines in Figure 2.4.4). From the assumption, all points of P other than $p_i, p_{ij}, j = 1, \ldots, k$, are outside the circumcircles $C_{i1}, \ldots, C_{ik}$. We take a point, say p_h, from $P \setminus \{p_i, p_{ij}, \ldots, p_{ik}\}$, and draw the line segment $\overline{p_i p_h}$. Then $\overline{p_i p_h}$ intersects the arc of the circumcircle on the boundary of $\mathrm{CH}(\bigcup_{j=1}^{k} C_{ij})$, say the arc $p_{ij} p_{ij+1}$ of C_{ij} ($j + 1 = 5$ is read as 1). Let r_h be this intersection point. Then the boundary of $H(p_i, r_h)$ (the dash-dot line in Figure 2.4.4) passes through q_{ij} because r_h is on the circumcircle, and $\bigcap_{j=1}^{k} H(p_i, p_{ij}) \subset H(p_i, r_h) \subset H(p_i, p_h)$. This relation holds for all p_h in $P \setminus \{p_i, p_{ij}, \ldots, p_{ik}\}$. Therefore

$$\bigcap_{j=1}^{k} H(p_i, p_{ik}) = \bigcap_{j \in I_n \setminus \{i\}} H(p_i, p_j) = V(p_i). \tag{2.4.3}$$

Thus the polygon with $q_{i1}, \ldots, q_{ik}$ is the Voronoi polygon of p_i. If we carry out the above procedure for every p_i in P, we obtain $\mathcal{V}(P)$. Since $\mathcal{T}$ is the same as the Delaunay triangulation obtained from $\mathcal{V}(P)$ (Definition D2), the given triangulation is the Delaunay triangulation spanning P. □

A Delaunay triangulation is of course a tessellation in $\mathbb{R}^2$, but like Property V17 we can also construct a Delaunay triangulation through a polyhedron in $\mathbb{R}^3$. Here we show two methods: one using the inversion transformation (to be defined below), and one using the lift-up transformation adopted in

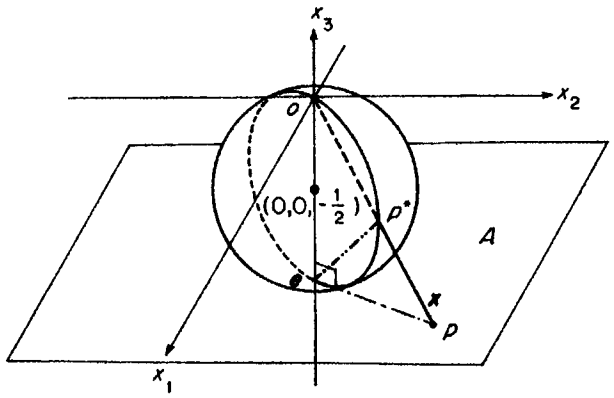

Figure 2.4.5 The inversion transformation.

Property V17. The *inversion transformation* with the inversion centre at the origin o and the inversion radius 1 is defined by

$$F(\boldsymbol{x}) = \frac{\boldsymbol{x}}{\|\boldsymbol{x}\|^2}, \quad \boldsymbol{x} \in \mathbb{R}^m \tag{2.4.4}$$

(Dodge, 1972, Chapter 5). This function has the property that $\|F(\boldsymbol{x})\| = 1/\|\boldsymbol{x}\|$, that is, the direction of the vector $F(\boldsymbol{x})$ is the same as that of the vector $\boldsymbol{x}$; the length of the vector $F(\boldsymbol{x})$ is the inverse of the length of the vector $\boldsymbol{x}$. We now consider the three-dimensional Euclidean space $\mathbb{R}^3$ with the Cartesian coordinate system (x_1, x_2, x_3), and let A be the plane parallel to the x_1–x_2 plane passing through the point $(0, 0, -1)$ whose location vector is given by $\boldsymbol{e}$ (see Figure 2.4.5). Suppose that p is on the plane A and $\boldsymbol{x}$ is the location vector of p. Then the vectors $\boldsymbol{e}$ and $\boldsymbol{x}-\boldsymbol{e}$ are orthogonal (observe that the x_3-axis and the dash-dot line in Figure 2.4.5 are orthogonal) which is mathematically written as $\boldsymbol{e}^{\mathrm{T}}(\boldsymbol{x} - \boldsymbol{e}) = 0$ or $\boldsymbol{e}^{\mathrm{T}}\boldsymbol{x} = 1$. Let $\boldsymbol{x}^* = F(\boldsymbol{x}) = \boldsymbol{x}/\|\boldsymbol{x}\|^2$. Then $\boldsymbol{x}^{*\mathrm{T}}(\boldsymbol{x}^* - \boldsymbol{e}) = (\boldsymbol{x}^{\mathrm{T}}/\|\boldsymbol{x}\|^2)(\boldsymbol{x}/\|\boldsymbol{x}\|^2 - \boldsymbol{e}) = (1/\|\boldsymbol{x}\|^2)(1 - \boldsymbol{x}^{\mathrm{T}}\boldsymbol{e}) = 0$, showing that the vectors $\boldsymbol{x}^*$ and $\boldsymbol{x}^*-\boldsymbol{e}$ are orthogonal (observe that the heavy broken line and the dash-dot-dot line in Figure 2.4.5 are orthogonal). This means that the point p^* indicated by the location vector $\boldsymbol{x}^*$ is on the circle centred at $(0, 0, -1/2)$ with radius 1/2 (see the great circle in Figure 2.4.5). Since this property holds for any point on the plane A, the set $S = \{\boldsymbol{x}^* | \boldsymbol{x}^* = F(\boldsymbol{x}), \boldsymbol{x} \in A\}$ forms a sphere without the point o. Thus, the inversion transformation of equation (2.4.4) maps the plane A onto $S\backslash\{o\}$. Stated more specifically, the image of a point p on the plane A under the inversion transformation is the point p^* given by the intersection point of the sphere S and the line joining the point p and the origin o (Figure 2.4.5). This mapping is indicated by $p^* = F(p)$.

The inversion transformation is a one-to-one function, and hence the inverse function F^{-1} exists. To obtain F^{-1} explicitly, we solve $\boldsymbol{x}^* = \boldsymbol{x}/\|\boldsymbol{x}\|$ with respect to $\boldsymbol{x}$ using the property $\|\boldsymbol{x}^*\| = 1/\|\boldsymbol{x}\|$. As a result, we get

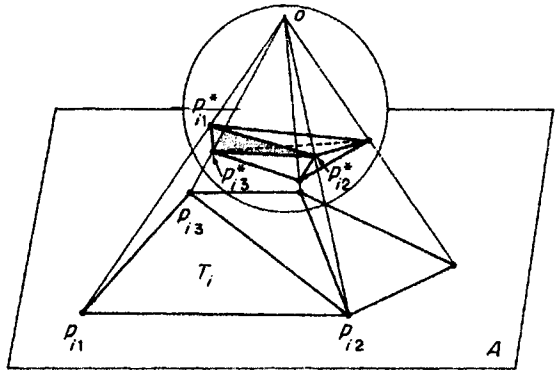

Figure 2.4.6 A Delaunay triangulation obtained through the inversion transformation.

$$F^{-1}(x^*) = \frac{x^*}{\|x^*\|^2} \tag{2.4.5}$$

We notice from equations (2.4.4) and (2.4.6) that $F^{-1} = F$. The inverse inversion transformation (i.e. the inversion transformation) maps $S\backslash\{o\}$ onto the plane A.

Using the inversion transformation, we now construct a triangulation according to the following procedure (Brown, 1979).

In $\mathbb{R}^3$ with the Cartesian coordinates (x_1, x_2, x_3) we consider the plane A which is parallel to the x_1–x_2 plane passing through $(0, 0, -1)$, and place a set of n distinct points $P = \{p_1, \ldots, p_n\}$ $(3 \le n < \infty)$ on A, where P satisfies the non-collinearity assumption (this assumption can be easily relaxed). Let $P^* = \{p_1^*, \ldots, p_n^*\} = \{F(p_1), \ldots, F(p_n)\}$, where F is given by equation (2.4.4) $(m = 3)$ (the filled circles on the sphere in Figure 2.4.6). Then, CH(P^*) (the polyhedron in Figure 2.4.6) consists of triangular faces $T_i^*, i \in I_t$. These triangles can be classified into 'near-side' triangles and 'far-side' triangles. A *near-side triangle* T_i^* is a triangle that satisfies the condition that CH(P^*) and the origin are in the same half space produced by the plane containing T_i^* (the shaded face in Figure 2.4.6). We reindex T_i^* so that the first n_v triangles are near-side triangles. Let $p_{ij}^*, j = 1, 2, 3$, be vertices of a near-side triangle $T_i^*, i \in I_{n_v}$, where $j = 1, 2, 3$ are indexed counterclockwise on the surface of CH(P^*), and let $p_{ij} = F^{-1}(p_{ij}^*), j = 1, 2, 3$. On the plane A, we construct the triangle by $\overline{p_{ij}p_{ij+1}}, j = 1, 2, 3$ (where 4 is read as 1), and denote it by T_i. Then the set $\mathcal{T}(P) = \{T_1, \ldots, T_{n_v}\}$ gives a triangulation of CH(P) spanning P. We now demonstrate that this triangulation satisfies the next property.

Property D7 The triangulation obtained through the above inversion transformation procedure is a Delaunay triangulation.

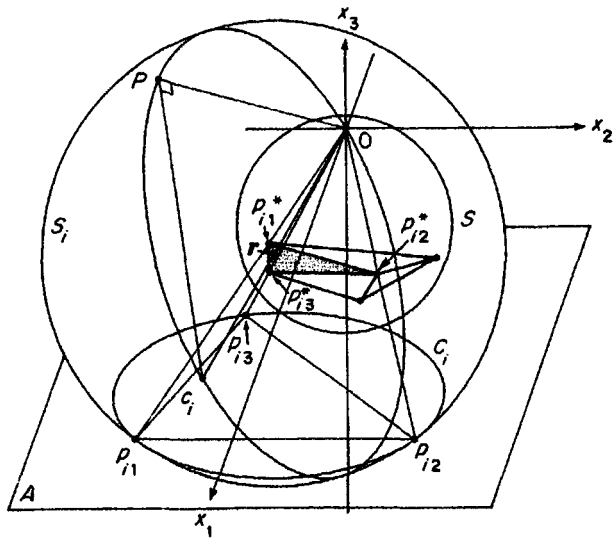

Figure 2.4.7 Illustration of the proof of Property D7.

Proof Let $x^*_{ij} = F(x_{ij}) = x_{ij}/\|x_{ij}\|^2$, $j = 1, 2, 3$, be the location vectors of the vertices $p^*_{i1}, p^*_{i2}, p^*_{i3}$ of a near-side triangular face T_i^* (the shaded face in Figure 2.4.7) of $\mathrm{CH}(P^*)$, where $P^* = \{p^*_1, \ldots, p^*_n\}$, $p^*_i = F(p_i)$, $p^*_{ij} = F^*(p_{ij})$, $p_{ij} \in P$ and x_{ij} is the location vector of p_{ij}. Let A_i^* be the plane containing the face T_i^*, i.e.

$$A_i^* = \{z^* \mid \lambda_1 x^*_{i1} + \lambda_2 x^*_{i2} + \lambda_3 x^*_{i3}, \text{ where } \lambda_1 + \lambda_2 + \lambda_3 = 1\}$$

$$= \left\{ z^* \mid z^* = \lambda_1 \frac{x_{i1}}{\|x_{i1}\|^2} + \lambda_2 \frac{x_{i2}}{\|x_{i2}\|^2} + \lambda_3 \frac{x_{i3}}{\|x_{i3}\|^2}, \text{ where } \lambda_1 + \lambda_2 + \lambda_3 = 1 \right\}. \quad (2.4.6)$$

Let S_i be the sphere passing through points $p_{i1}, p_{i2}, p_{i3}, o$; r be the location vector of the centre of the sphere S_i; and c_i be the point indicated by $2r$. If a point p (indicated by the location vector x) is on S_i, points o, c_i, p are on the great circle of S_i (the great circle in Figure 2.4.7) whose diameter is given by the line segment joining o and c_i, and so $\angle opc_i = \pi/2$, i.e. the vectors x and $x - 2r$ are orthogonal. Thus S_i is represented by the set of points

$$S_i = \{x \mid x^{\mathrm{T}}(x - 2r) = 0, x \in \mathbb{R}^3\}. \quad (2.4.7)$$

Since points p_{i1}, p_{i2}, p_{i3} are on S_i, the equation $x_{ij}^{\mathrm{T}}(x_{ij} - 2r) = 0$, i.e. $x_{ij}^{\mathrm{T}} x_{ij} = 2 x_{ij}^{\mathrm{T}} r$, holds for $j = 1, 2, 3$.

We now prove that points on the plane A_i^* are mapped on the sphere S through the (inverse) inversion transformation, i.e. we prove $S_i = \{z \mid z = F^{-1}(z^*), z^* \in A_i^*\}$. From $F^{-1}(z^*) = z^*/\|z^*\|^2$ and equation (2.4.6), we obtain:

$$F^{-1}(z^*)^{\mathrm{T}}(F^{-1}(z^*)-2r)=\frac{z^{*\mathrm{T}}}{\|z\|^2}\left(\frac{z^{*\mathrm{T}}}{\|z\|^2}-2r\right)$$
$$=\frac{z}{\|z^*\|^2}\left(1-\sum_{j=1}^{3}\frac{2\lambda_j x_{ij}^{\mathrm{T}} r}{\|x_{ij}\|^2}\right). \tag{2.4.8}$$

Upon substituting $x_{ij}^{\mathrm{T}}x_{ij} = 2x_{ij}^{\mathrm{T}}r$ into this equation, we obtain:

$$F^{-1}(z^*)^{\mathrm{T}}(F^{-1}(z^*)-2r)=\frac{1}{\|z^*\|^2}(1-\lambda_1-\lambda_2-\lambda_3)=0. \tag{2.4.9}$$

Thus $F^{-1}(z^*)$ satisfies the equation in equation (2.4.7), showing that the plane A_i^* is mapped onto S_i, and that the closed half space, H^*, produced by A_i^* which contains the origin is mapped onto the space outside the sphere S_i (recall that the distance is reversed by the inversion transformation of equation (2.4.4)). The intersection of S_i with the plane parallel to the x_1–x_2 plane passing through $(0, 0, -1)$ is the circle C_i passing through points p_{i1}, p_{i2}, p_{i3}. Obviously the circle C_i is the circumcircle of the triangle T_i. Since all points in P^* are in H^*, all points in $P = F^{-1}(P^*)$ are on or outside C_i, indicating that the circumcircle C_i is an empty circle. Thus the set $\{T_1, \ldots, T_{n_v}\}$ of triangles forms a triangulation in which circumcircles of the triangles are all empty circles. From the empty circumcircle theorem (Property D6), we notice that this triangulation is the Delaunay triangulation spanning P. □

In Definition D2 we remarked that $\mathcal{D}$ was not necessarily defined with $\mathcal{V}$. In fact, Property D7 shows that once a set of points P is given, we can define $\mathcal{D}$ as the triangulation obtained from the above procedure (which does not require a Voronoi diagram). We can also use Property D7 to give a definition of $\mathcal{V}$ alternative to Definition V1 or V2. When $\mathcal{D}$ is given, it is straightforward

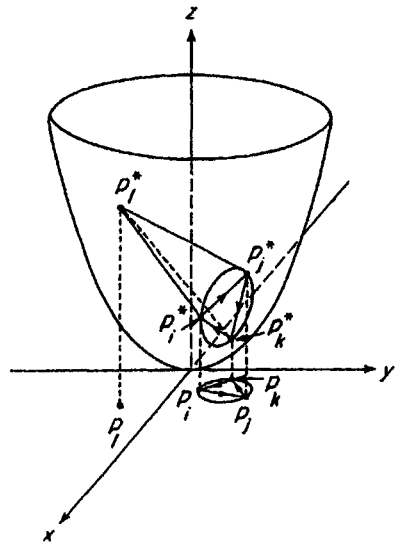

Figure 2.4.8 A Delaunay triangulation obtained through the lift-up transformation.

to construct $\mathcal{V}$ by inverting the procedure mentioned in Definition D1. Thus we may define $\mathcal{V}$ via $\mathcal{D}$ obtained from the inversion transformation procedure. We also note that we can construct $\mathcal{V}$ directly through the inversion transformation. We leave it as an exercise.

In Property D7 we obtained the Delaunay triangulation $\mathcal{D}(P)$ from the convex hull of $P^* = F(P)$ in $\mathbb{R}^3$ through the inversion transformation F. This method can be extended to $\mathbb{R}^m$. We can construct an m-dimensional Delaunay tessellation $\mathcal{D}(P)$ or an m-dimensional Voronoi diagram $\mathcal{V}(P)$ from the convex hull of $F(P)$ in $\mathbb{R}^m$ through the inversion transformation (Brown, 1979, 1980).

We next show another correspondence between a Delaunay triangulation and a convex hull in $\mathbb{R}^3$ (Edelsbrunner and Seidel, 1986; O'Rourke *et al.*, 1986; Edelsbrunner, 1987; Agarwal *et al.*, 1989a).

Let P^* be the lift-up of $P = \{p_1, \ldots, p_n\}$ (where $p_i \in \mathbb{R}^2$) and $\mathrm{CH}(P^*)$ be the convex hull of P^*. A facet of $\mathrm{CH}(P^*)$ is called a *lower facet* if the plane containing the facet passes through or below any point in P^*. The surface formed by all the lower facets of $\mathrm{CH}(P^*)$ is called the *lower boundary* of $\mathrm{CH}(P^*)$.

Suppose without loss of generality that three points p_i, p_j, p_k are placed on the x–y plane so that the cycle p_i, p_j, p_k, p_i has a counterclockwise direction when it is viewed from a point far above the x–y plane (see Figure 2.4.8). Let

$$H(p_i,p_j,p_k,p) \simeq \begin{vmatrix} 1 & x_i & y_i & x_i^2+y_i^2 \\ 1 & x_j & y_j & x_j^2+y_j^2 \\ 1 & x_k & y_k & x_k^2+y_k^2 \\ 1 & x & y & x^2+y^2 \end{vmatrix}. \tag{2.4.10}$$

It is left as an exercise to see that the circle passing through p_i, p_j, p_k is represented by $H(p_i, p_j, p_k, p) = 0$, and that this circle is an empty circle if and only if $H(p_i, p_j, p_k, p_l) \geq 0$ for any point $p_l \in \mathrm{P} \setminus \{p_i, p_j, p_k\}$. In this connection, recall that the three points p_i, p_j, p_k form a Delaunay triangle if and only if the circle passing through these points is an empty circle (Property D6).

$H(p_i, p_j, p_k, p)$ gives another implication. The value of $H(p_i, p_j, p_k, p)/6$ can be interpreted as the signed volume of the tetrahedron with vertices p_i, p_j, p_k, p. Since we choose p_i, p_j, p_k so that the cycle p_i, p_j, p_k, p_i has a counterclockwise direction, the volume of the tetrahedron is positive if and only if p_l^* is above the plane containing p_i^*, p_j^*, p_k^* (see Figure 2.4.8). This means that p_i, p_j and p_k form a Delaunay triangle if and only if p_i^*, p_j^* and p_k^* give a facet of the lower boundary of $\mathrm{CH}(P^*)$. Thus we obtain the following property.

Property D8 The Delaunay triangulation $\mathcal{D}(P)$ is obtained as the orthographic projection of the lower boundary of $\mathrm{CH}(P^*)$ onto the x–y plane, where P^* is the lift-up of P.

This property gives an interesting implication to the interpolation problem (Chapter 6). Suppose that we are given the height $z_i = x_i^2 + y_i^2$ at each site $p_i = (x_i, y_i)$, and that we want to interpolate these data by a collection of triangles whose vertices are the given points $p_1^*, \ldots, p_n^*$, where p_i^* is the lift-up of p_i. Every triangulation spanning P gives such an interpolation, but among them, $\mathcal{D}(P)$ is the only one that gives the surface of interpolation convex downward. Recall that the points in P^* lie on the paraboloid of revolution (Figure 2.4.8), which is convex downward. It is hence desirable that the interpolant is also convex downward. This requirement is satisfied only by $\mathcal{D}(P)$. Since this property is a distinct property, we state it as Property D9.

Property D9 The Delaunay triangulation spanning a finite set P of distinct points is the only triangulation $\mathcal{T}(P)$ spanning P such that the lift-up transformation of $\mathcal{T}(P)$ gives a surface convex downward.

Property D9 gives a justification for the use of a Delaunay triangulation as a tool for interpolation. Applications of Voronoi diagrams and Delaunay triangulations to interpolation are discussed in detail in Chapter 6.

Unlike a Voronoi diagram, a Delaunay pretriangulation or a Delaunay triangulation has edges of finite length. Thus we can regard a Delaunay pretriangulation or a Delaunay triangulation as a geometric graph. This graph is a connected planar graph consisting of the set of Delaunay vertices, P, and the set of Delaunay edges, E_d. We call this graph the *Delaunay graph* of $\mathcal{D}(P)$ and denote it by $G(P, E_d)$. It is easy to see from Definition D2 that the Voronoi graph $G(Q_{+1}, E_d)$ and the Delaunay graph $G(P, E_d)$ have the following relation.

Property D10 The Delaunay graph $G(P, E_d)$ is the dual graph of the Voronoi graph $G(Q_{+1}, E_d)$.

Because of this property, we sometimes say that the Delaunay triangulation is the *dual tessellation* of the Voronoi diagram. Alternatively, we can view the duality between a Voronoi diagram and a Delaunay triangulation in terms of Legendre dual functions (Chynoweth and Sewell, 1990; Chynoweth, 1996). In Section 2.3 (Figure 2.3.9) we constructed a Voronoi diagram through the polyhedron consisting of planes tangential to the paraboloid at the lift-up points of the generator points. Earlier in this section (Figure 2.4.8) we constructed a Delaunay triangulation through the convex hull of the lift-up points of the same generator points. The relationship between the polyhedron and the convex hull forms Legendre dual functions (a precise and general definition of the Legendre dual functions is found in Chapter 2 of Sewell, 1987). Chynoweth (1996) calls this relationship the *generalized Voronoi/Delaunay duality*.

Recalling Definitions V3 and D1, we notice that a Voronoi edge and its corresponding Delaunay edge are orthogonal under the non-degeneracy

assumption. When two geometric figures form the primal–dual graphs, and their corresponding edges are orthogonal, these two figures are called *reciprocal figures* (Maxwell, 1864). The Voronoi diagram generated by P and the Delaunay triangulation spanning P are hence reciprocal figures. This property is strongly related to the realizability of polyhedra from a Delaunay triangulation and a Voronoi diagram (Properties D8 and V17). The relation between realizability and reciprocity is discussed in depth by Sugihara (1986). Note that the topological stability of a Delauany graph with respect to the location of nodes is examined by Abellanas *et al.* (1994).

From Properties D4 and D10 we can obtain a few relationships among the numbers of Delaunay triangles, Delaunay edges, external Delaunay edges and Delaunay vertices, denoted by n_v, n_e, n_c and n, respectively (equivalently n_c is the number of unbounded Voronoi polygons in $\mathcal{V}(P)$). First, since the Delaunay graph is a planar graph, Euler's formula (equation (1.3.26)) holds, i.e. $n - n_e + (n_v + 1) = 2$, which is equivalent to Property V9. Second, more generally, for an m-dimensional Delaunay tessellation, the Euler–Poincaré formula (equation (1.3.27)) holds, which corresponds to Property V10. Third, since every internal edge is shared by two Delaunay triangles and every external edge belongs to only one Delaunay triangle, the number of Delaunay edges is given by

$$n_e = \tfrac{1}{2}(3n_v + n_c) \tag{2.4.11}$$

Upon substituting equation (2.4.11) into $n - n_e + n_v = 1$, we have the following property.

Property D11 For the Delaunay triangulation $\mathcal{D}(P)$ spanning a finite set P of distinct points, which satisfies the non-cocircularity assumption, let n_e be the number of Voronoi or Delaunay edges, n_v be the number of the triangles in $\mathcal{D}(P)$ and n_c be the number of the vertices on the boundary of $\mathrm{CH}(P)$. Then, the following equations hold:

$$n_v = 2n - n_c - 2, \tag{2.4.12}$$

$$n_e = 3n - n_c - 3. \tag{2.4.13}$$

Recalling Property D4, we notice that the above equations hold for a non-degenerate $\mathcal{V}(P)$, where n_e, n_v and n_c are the number of Voronoi edges, Voronoi vertices and unbounded Voronoi polygons, respectively.

For the non-degenerate Delaunay tetrahedrization spanning a finite set P of n distinct points, the Euler–Poincaré equation, $n_0 - n_1 + n_2 - n_3 = 1$, holds, where n_i is the number of ith dimensional faces, or more specifically, n_0, n_1, n_2,and n_3 are the number of vertices, edges, triangular faces, and tetrahedra, respectively. Since the vertices are points in P, we have $n_0 = n$. Since every tetrahedron is bounded by four triangular faces and every triangular face bounds at most two tetrahedra, we have $2n_3 \leq n_2$. Substituting this relation and $n_0 = n$ into $n_0 - n_1 + n_2 - n_3 = 1$, we obtain the following property (Chazelle *et al.*, 1990).

Property D12 For the Delaunay tetrahedrization $\mathfrak{D}(P)$ spanning a finite set P of n distinct points satisfying the non-cosphericity assumption, the following relations hold:

$$n_3 \leq n_1 - n + 1, \tag{2.4.14}$$

$$n_2 \leq 2n_1 - 2n + 2. \tag{2.4.15}$$

These relations imply that n_1 is a good measure of the combinatorial complexity of $\mathfrak{D}(P)$. Chazelle *et al.* (1990) call it the *size* of $\mathfrak{D}(P)$. The maximum size of $\mathfrak{D}(P)$ is $\binom{n}{k}$. Chazelle *et al.* (1990) show that no matter how badly P is distributed, there is always a small set, A, of points such that $\mathfrak{D}(P \cup A)$ has the size at most $O(n^{3/2} \log^3 n)$. Bern *et al.* (1990) give an algorithm that adds a set A of $O(n)$ new points such that $\mathfrak{D}(P \cup A)$ has size $O(n)$.

For a Delaunay vertex p_i of the m-dimensional Delaunay tessellation, consider Delaunay spheres $B_{i1}, \ldots, B_{ik_i}$ incident to p_i. Bern *et al.* (1991) call the boundary of $B_{i1} \cup \ldots \cup B_{ik_i}$ the *Delaunay surface* of p_i. They show that the $(m-1)$-dimensional volume of the Delaunay surface is of order $O(r^{m-1})$, where r is the maximum radius of the balls $B_{i1}, \ldots, B_{ik_i}$ (Lemma 7 in Bern *et al.*, 1991).

In the same way that a Delaunay triangulation can be regarded as a geometric graph, any triangulation can be regarded as a geometric graph with the vertices and edges of the triangles. Figure 2.4.9(a) shows an example in which the geometric graph $G(P, L)$ consists of a set $P = \{p_0, p_1, \ldots, p_4, p_1', \ldots, p_4'\}$ of nine points and a set $L = \{L_1, \ldots, L_8, L_1', \ldots, L_8'\}$ of 16 line segments (they are labelled as in Figure 2.4.9(a)). We now ask whether or not there exists a non-degenerate Delaunay triangulation whose geometric graph is isomorphic to the geometric graph $G(P, L)$ in Figure 2.4.9(a). More generally, we ask whether or not there exists a non-degenerate Delaunay triangulation whose geometric graph is isomorphic to the geometric graph of a given triangulation.

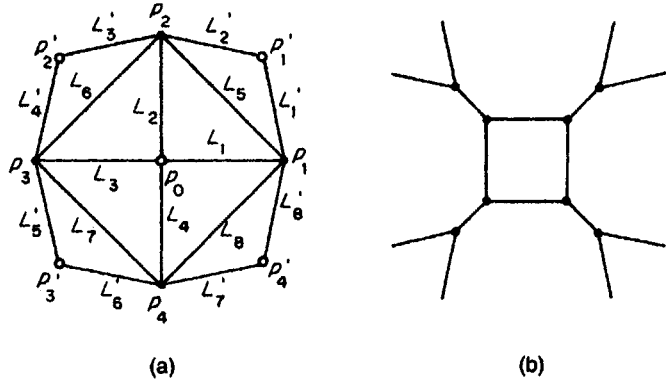

Figure 2.4.9 (a) A triangulation whose geometric graph is not isomorphic to any non-degenerate Delaunay triangulation, and (b) its dual diagram whose geometric graph is not isomorphic to any non-degenerate Voronoi diagram.

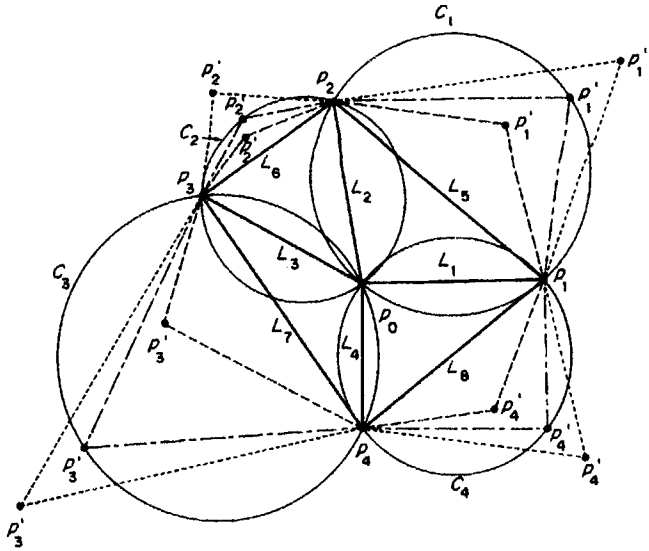

Figure 2.4.10 Three triangulations (the solid lines with the broken lines, the dash-dot lines, or the dot lines).

To answer the first question we construct a geometric subgraph, $G_s(P_s, L_s)$, consisting of $P_s = \{p_0, p_1, \ldots, p_4\}$ and $L_s = \{L_1, \ldots, L_8\}$ in such a way that $L_5, \ldots, L_8$ and $p_1, \ldots, p_4$ form an arbitrary convex quadrangle and the point p_0 is placed in its interior (Figure 2.4.10). Obviously the subgraph $G_s(P_s, L_s)$ is isomorphic to the corresponding subgraph in Figure 2.4.9(a). We next add four points $p_1', \ldots, p_4'$ and eight line segments $L_1, \ldots, L_8$ to $G_s(P_s, L_s)$ so that the resulting geometric graph is isomorphic to the geometric graph $G(P, L)$ in Figure 2.4.9(a). The number of such geometric graphs is infinitely many. To examine which geometric graph is a Delaunay triangulation, we construct the circle C_i which passes through p_0, p_i, p_{i+1} for $i = 1, \ldots, 4$ (p_5 is read as p_1), and consider the following three possible cases relative to the circle C_i.

First, suppose that we place p_i' in the region encircled by $\overline{p_i p_{i+1}}$, and the arc from p_i to p_{i+1} of C_i that does not contain p_0, and let $L'_{2i-1} = \overline{p_i p_i'}$, $L'_{2i} = \overline{p_i' p_{i+1}}$, $i = 1, \ldots, 4$ (the broken lines in Figure 2.4.10). Then $\triangle p_i p_i' p_{i+1}$ does not satisfy the empty circle criterion. Thus, the resulting triangulation is not a Delaunay triangulation.

Second, suppose that p_i is on the arc of C_i from p_j to p_{i+1} that does not contain p_o (the dash-dot lines in Figure 2.4.10). Then the triangles in the resulting triangulation satisfy the empty circle criterion. If the octagon with vertices $p_1, p_1', \ldots, p_4, p_4'$ is convex, this triangulation is a Delaunay triangulation. At first glance the convexity is not satisfied in general, but it may be satisfied in a special case. To examine the convexity, we construct a triangulation by adding $p_1', \ldots, p_4', L_1', \ldots, L_4'$ in the following way.

Choose a point p_1' on C_1 such that p_o and p_1' are on mutually opposite sides of the line $\overline{p_1 p_2}$ (Figure 2.4.11). For $i = 2, \ldots, 4$, let p_i' be the point

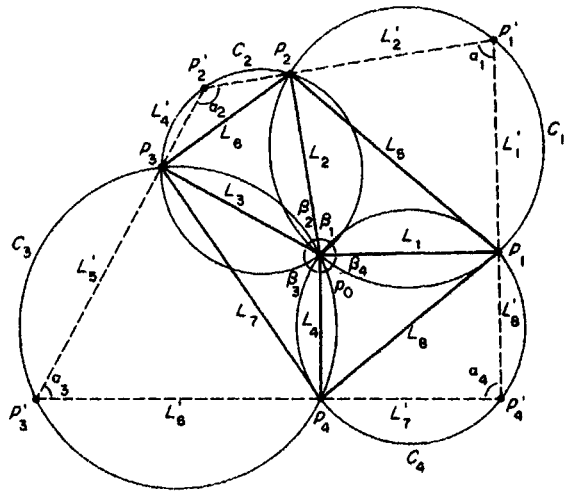

Figure 2.4.11 The degenerate Delaunay triangulation isomorphic to the geometric graph in Figure 2.4.9(a).

(other than p_i) of intersection between C_i and the line $\overline{p'_{i-1}p_i}$ (the broken lines), $i = 2, \ldots, 4$. We now show that p_1 is on the line $\overline{p_1'p_4'}$. Let $\alpha_i = \angle p_i p_i' p_{i+1}$ and $\beta = \angle p_i p_o p_{i+1}$ for $i = 1, \ldots, 4$, where $p_5 = p_1$. Since p_o, p_i, p_i', p_{i+1} are on C_i, we get $\alpha_i + \beta_i = \pi$ for $i = 1, \ldots, 4$. Substituting these equations into $\beta_1 + \ldots + \beta_4 = 2\pi$, we obtain $\alpha_1 + \ldots + \alpha_4 = 2\pi$. On the other hand, the sum of the inner angles of the pentagon with vertices $p_1', p_2', \ldots, p_5', p_1$ is 3π, i.e. $\alpha_1 + \ldots + \alpha_4 + \angle p_4' p_1 p_1' = 3\pi$. From these equations we have the equation $\angle p_4' p_1 p_1' = \pi$. Hence p_1, p_1' and p_4' are on the same line (note that this property can be easily generalized for m-gons $p_1, \ldots, p_m$ and $p_1', \ldots, p_m'$ obtained in the same manner). Thus the polygon with vertices $p_1, p_1', p_2, p_2', \ldots, p_4, p_4'$ is a convex quadrangle. Since the triangulation in Figure 2.4.11 is a triangulation spanning the convex quadrangle $p_1', \ldots, p_4'$ and every triangle satisfies the empty circle criterion, the triangulation in Figure 2.4.11 is a Delaunay triangulation. The graph $G(P, L)$ in Figure 2.4.9(a) is hence isomorphic to the Delaunay triangulation in Figure 2.4.11. However, the Delaunay triangulation is degenerate because every circle C_i has four points in P on it.

Last, suppose that p_i is placed outside C_i in such a way that the geometric graph of the resulting triangulation is isomorphic to the geometric graph $G(P, L)$ (the dot lines in Figure 2.4.10). In this case every triangle in the triangulation satisfies the empty circle criterion, but using the triangulation in Figure 2.4.11 we can show that the octagon with vertices $p_1, p_1', \ldots, p_4, p_4'$ cannot be convex.

To sum up, we come to the conclusion that there does not exist a non-degenerate Delaunay triangulation whose geometric graph is isomorphic to the geometric graph of the triangulation in Figure 2.4.9(a). This conclusion

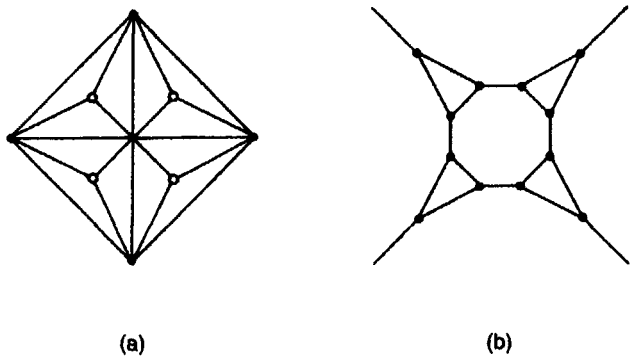

Figure 2.4.12 (a) A triangulation whose geometric graph is not isomorphic to any Delaunay triangulation, and (b) its dual diagram whose geometric graph is not isomorphic to any Voronoi diagram.

in turn implies that the diagram shown in Figure 2.4.9(b), which is the dual of the diagram in Figure 2.4.9(a), is not isomorphic to any non-degenerate Voronoi diagram. Similarly, using the triangulation shown in Figure 2.4.11, we can show that there does not exist a Delaunay triangulation whose geometric graph is isomorphic to the geometric graph shown in Figure 2.4.12(a). Consequently, the diagram shown in Figure 2.4.12(b), which is the dual of the diagram shown in Figure 2.4.12(a), is not isomorphic to any Voronoi diagram.

Dillencourt (1990a,b) investigated these unrealizability properties more generally, and showed the following two properties.

Property D13 A triangulation $\mathcal{T}$ spanning P is not isomorphic to a non-degenerate Delaunay triangulation if there exists a subset $P' \subset P$ such that the subgraph of $\mathcal{T}$ induced by the vertex set $P \backslash P'$ contains more than $|P|$ connected components (where $|P|$ indicates the number of points in P).

Property D14 A triangulation $\mathcal{T}$ spanning P is not isomorphic to a Delaunay triangulation if there exists a subset $P' \subset P$ such that the subgraph of $\mathcal{T}$ induced by the vertex set $P \backslash P'$ contains more than $|P| - 2$ connected components that do not contain any vertex on the boundary of $\mathcal{T}$.

The proofs are provided by Dillencourt (1990a).

We can recognize the unrealizability of the triangulation in Figure 2.4.9(a) by Property D13. Indeed, if we remove the four vertices represented by the filled circles, we obtain five connected components, each consisting of an isolated vertex represented by an unfilled circle. We can also recognize the unrealizability of the triangulation in Figure 2.4.12(a) by Property D14. If we remove the five vertices represented by the filled circles, we obtain four connected components each of which consists of an isolated vertex (represented by an unfilled circle) that is not on the boundary of the triangulation.

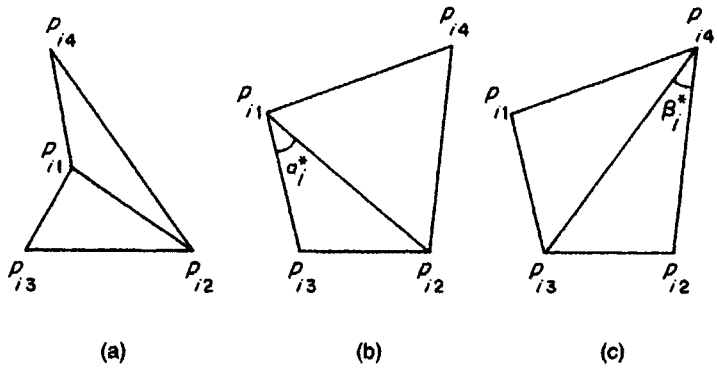

Figure 2.4.13 The local max-min angle criterion.

Properties D12 and D13 present only the sufficient conditions for a triangulation not to be isomorphic to a Delaunay triangulation. Characterization of the necessary and sufficient conditions in combinatorial terms, however, is still an open problem (Dillencourt, 1990a,b).

For a given finite set P of distinct points we have many possible triangulations of CH(P) spanning P. In some applications we want to choose a triangulation in which triangles are as closely equiangular as possible (practical examples will be shown in Chapter 6). One of the criteria is to choose a triangulation in which the minimum angle in each triangle is as large as possible. To state this criterion more explicitly, let us consider an internal edge $\overline{p_{i1}p_{i2}}$ in a triangulation $\mathcal{T}$, and let $\Delta p_{i1}p_{i2}p_{i3}$ and $\Delta p_{i1}p_{i2}p_{i4}$ be triangles sharing the edge $\overline{p_{i1}p_{i2}}$ (Figure 2.4.13(a), (b)). The quadrangle $p_{i1}p_{i3}p_{i2}p_{i4}$ may be non-convex (Figure 2.4.13(a)) or convex (Figure 2.4.13(b)). If it is convex and it does not degenerate into a triangle (p_{i1} is on $\overline{p_{i3}p_{i4}}$ or p_{i2} is on $\overline{p_{i3}p_{i4}}$), we have another possible triangulation, i.e. $\Delta p_{i1}p_{i3}p_{i4}$ and $\Delta p_{i2}p_{i3}p_{i4}$ (Figure 2.4.13(c)). We are concerned with which triangulation is locally better ('locally' in the sense that a triangulation is made in a local area, i.e. the quadrangle $p_{i1}p_{i3}p_{i2}p_{i4}$). In the triangulation in panel (b), the minimum angle among the six angles in $\Delta p_{i1}p_{i2}p_{i3}$ and $\Delta p_{i1}p_{i2}p_{i4}$ is $\angle p_{i2}p_{i1}p_{i3} = \alpha_i^*$. In the triangulation in panel (c), the minimum angle among the six angles in $\Delta p_{i1}p_{i3}p_{i4}$ and $\Delta p_{i2}p_{i3}p_{i4}$ is $\angle p_{i2}p_{i4}p_{i3} = \beta_i^*$. Comparing α_i^* and β_i^* in Figures 2.4.13(b) and 2.4.13(c), we notice that $\alpha_i^* > \beta_i^*$, or $\alpha_i^* = \max\{\alpha_i^*, \beta_i^*\}$. We may thus conclude that the triangulation in panel (b) is locally better than that in panel (c), because the minimum angle is maximized in the triangulation in panel (b). This criterion may be written generally as follows.

The local max-min angle criterion For a triangulation $\mathcal{T}$ of CH(P) spanning P, let $\overline{p_{i1}p_{i2}}$ be an internal edge in CH(P), and $\Delta p_{i1}p_{i2}p_{i3}$ and $\Delta p_{i1}p_{i2}p_{i4}$ be two triangles sharing the edge $\overline{p_{i1}p_{i2}}$. For the convex quadrangle $p_{i1}p_{i3}p_{i2}p_{i4}$ which does not degenerate into a triangle, let $\alpha_{ij}, j \in I_6$, be the

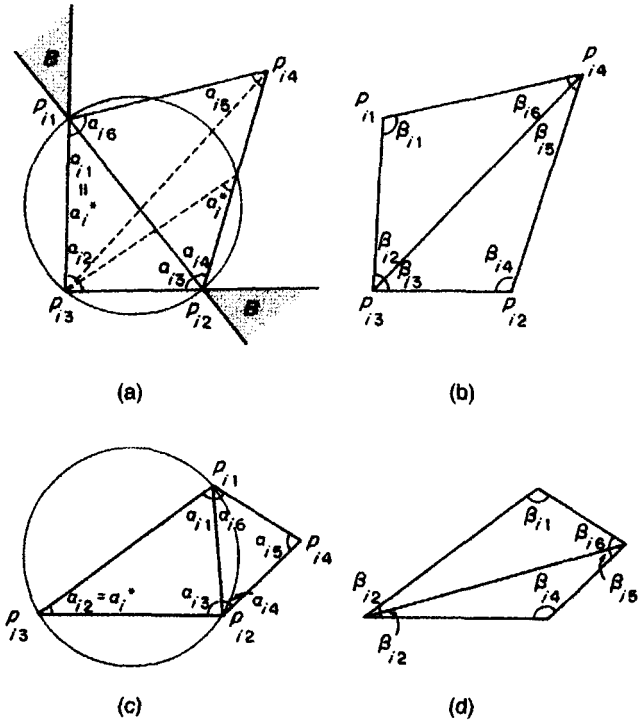

Figure 2.4.14 Conditions for the local max-min angle criterion.

six angles in $\Delta p_{i1}p_{i2}p_{i3}$ and $\Delta p_{i1}p_{i2}p_{i4}$; and $\beta_{ij}, j \in I_6$, be the six angles in $\Delta p_{i1}p_{i3}p_{i4}$ and $\Delta p_{i2}p_{i3}p_{i4}$. If the quadrangle $p_{i1}p_{i3}p_{i2}p_{i4}$ is non-convex or it degenerates into a triangle, or if it is a convex quadrangle which does not degenerate into a triangle and the relation

$$\min_j\{\alpha_{ij}, j \in I_6\} \geq \min_j\{\beta_{ij}, j \in I_6\} \tag{2.4.16}$$

holds, then we say that the edge $\overline{p_{i1}p_{i2}}$ satisfies the *local max-min angle criterion.*

In Figure 2.4.13 the edge $\overline{p_{i1}p_{i2}}$ in panels (a) and (b) satisfies the local max-min angle criterion, but the edge $\overline{p_{i3}p_{i4}}$ in panel (c) does not.

At first glance the practical operation in equation (2.4.16) (measuring angles and finding the minimum angles among them) appears a little complicated. In practice, we do not carry out such an operation but use the following relation.

Let $\alpha_i^* = \min_j \{\alpha_{ij}, j \in I_6\}$, and suppose, without loss of generality, that α_i^* is one of the angles of $\Delta p_{i1}p_{i2}p_{i3}$. Let C_i be the circumcircle of $\Delta p_{i1}p_{i2}p_{i3}$; H be the open half plane made by the line containing $\overline{p_{i1}p_{i2}}$ that does not contain $\Delta p_{i1}p_{i2}p_{i3}$; and B be the region indicated by the shaded region

(including the boundary) in Figure 2.4.14(a). Obviously, p_{i4} is in H. The quadrangle $p_{i1}p_{i2}p_{i3}p_{i4}$ may be convex or non-convex. If p_{i4} is in B, the quadrangle $p_{i1}p_{i2}p_{i3}p_{i4}$ is non-convex or it degenerates into a triangle ($\triangle p_{i4}p_{i2}p_{i3}$). The quadrangle $p_{i1}p_{i2}p_{i3}p_{i4}$ is a convex quadrangle which does not degenerate into a triangle if $p_{i4} \in H \setminus B$. Now suppose that p_{i4} is in $H \setminus [B \cup CH(C_i)]$ and the minimum angle α_i^* is either $\angle p_{i3}p_{i1}p_{i2}$ (Figure 2.4.14(a)) or $\angle p_{i3}p_{i2}p_{i1}$. Let $\triangle p_{i1}p_{i3}p_{i4}$ and $\triangle p_{i2}p_{i3}p_{i4}$ be triangles constituting another triangulation of the quadrangle $p_{i1}p_{i2}p_{i3}p_{i4}$, and $\beta_{ij}, j \in I_6$, be angles of those triangles indicated in Figure 2.4.14(b). Using the theorem of equiangles on a circle (see the two α_i^*'s in Figure 2.4.14(a)), we notice that $\alpha_i^* = \min_j \{\alpha_{ij}, j \in I_6\} = \alpha_{i1}$ (or α_{i3}) $> \beta_{i5}$ (or β_{i6}) $\geq \min_j \{\beta_{ij}, j \in I_6\} = \beta_i^*$. If the minimum angle α_i^* is $\angle p_{i1}p_{i3}p_{i2}$ as in Figure 2.4.14(c), $\alpha_i^* = \min_j \{\alpha_{ij}, j \in I_6\} = \alpha_{i2} > \beta_{i2} \geq \min_j \{\beta_{ij}, j \in I_6\} = \beta_i^*$. Therefore the edge $\overline{p_{i1}p_{i2}}$ satisfies the local max-min angle criterion. Almost in the same manner, we can show that if $p_{i4} \in H \cap C_i$, then $\alpha_i^* = \beta_i^*$ holds, and if $p_{i4} \in H \cap [CH(C_i) \setminus C_i]$, then $\alpha_i^* < \beta_i^*$ holds. Therefore we obtain the following relations:

$$\begin{aligned}
&\min_j\{\alpha_{ij}, j \in I_6\} > \min_j\{\beta_{ij}, j \in I_6\} \quad \text{if } p_{i4} \text{ is outside } C_i, \\
&\min_j\{\alpha_{ij}, j \in I_6\} = \min_j\{\beta_{ij}, j \in I_6\} \quad \text{if } p_{i4} \text{ is on } C_i, \\
&\min_j\{\alpha_{ij}, j \in I_6\} < \min_j\{\beta_{ij}, j \in I_6\} \quad \text{if } p_{i4} \text{ is inside } C_i
\end{aligned} \tag{2.4.17}$$

(Lawson, 1977; Kishimoto, 1978; Sibson, 1978; Lee and Schachter, 1980; Lee and Lin, 1986). Note that the choice of a triangle from the two triangles $\triangle p_{i1}p_{i2}p_{i3}$ and $\triangle p_{i1}p_{i2}p_{i3}$ does not affect the result (it is an exercise of elementary geometry to prove that the circumcircle of $\triangle p_{i1}p_{i2}p_{i3}$ does not contain p_{i4} if and only if the circumcircle of $\triangle p_{i1}p_{i2}p_{i4}$ does not contain p_{i3}). Using relation (2.4.17), we can prove the following property.

Property D15 (the local max-min angle theorem) Let $P = \{p_1, \ldots, p_n\} \subset \mathbb{R}^2$ ($3 \leq n < \infty$) be a finite set of distinct points satisfying the non-cocircularity assumption, and $\mathcal{T}$ be a triangulation of $CH(P)$ spanning P. Every internal edge in $\mathcal{T}(P)$ satisfies the local max-min criterion if and only if $\mathcal{T}(P)$ is the Delaunay triangulation spanning P.

Proof From relation (2.4.17) it is obvious that if $\mathcal{T}(P)$ is $\mathcal{D}(P)$, every internal edge satisfies the local max-min criterion, because if the circumcircle of $\triangle p_{i1}p_{i2}p_{i3}$ is an empty circle, p_{i4} is outside of the circumcircle. We shall prove that if every internal edge in $\mathcal{T}(P)$ satisfies the local max-min angle criterion, $\mathcal{T}(P)$ is $\mathcal{D}(P)$. Since the edge $\overline{p_{i1}p_{i2}}$ satisfies the local max-min angle criterion, p_{i4} is outside C_i. What is left to prove is that all other vertices of the triangles are outside C_i (Figure 2.4.15). Since the edges $\overline{p_{i2}p_{i4}}$ and $\overline{p_{i1}p_{i4}}$ satisfy the local max-min angle criterion, there are no points in the horizontally and vertically hatched regions in Figure 2.4.15. Similarly, since the edges $\overline{p_{i1}p_{i3}}$ and $\overline{p_{i2}p_{i3}}$ satisfy the local max-min angle criterion, there are no points in the diagonally hatched regions. Obviously there are no points

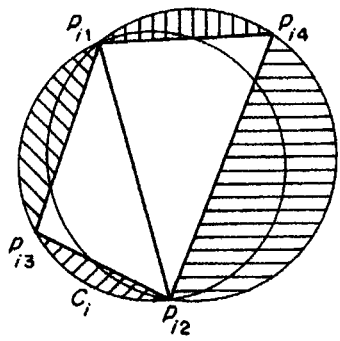

Figure 2.4.15 Illustration of the proof of Property D14.

in $\Delta p_{i1}p_{i2}p_{i3}$ and $\Delta p_{i1}p_{i2}p_{i4}$. Therefore there are no points in the circumcircle of $\Delta p_{i1}p_{i2}p_{i3}$. Applying the same procedure to every triangle, we can prove that every circumcircle is an empty circle. From the empty circumcircle theorem (Property D6), we see that the triangulation spanning P is $\mathcal{D}(P)$. □

Having understood Property D15 in theory, let us now consider a practical method for finding a triangulation satisfying the condition in Property D15 with an example shown in Figure 2.4.16.

We first construct an arbitrary triangulation of $\mathrm{CH}(P)$ spanning P, which is indicated by the continuous lines in Figure 2.4.16(a). Let E be the set of edges in this triangulation. We choose an edge, say $\overline{p_3p_5}$ (the heavy continuous lines in Figure 2.4.16(a)), from $E\backslash\partial\mathrm{CH}(P)$ and examine if this edge satisfies the local max-min angle criterion. Since $\alpha^* > \beta^*$ in Figure 2.4.16(a), the edge satisfies it. We next choose another edge, $\overline{p_2p_5}$ (the heavy continuous line segment in Figure 2.4.16(b)), from $E\backslash\mathrm{CH}(P)$, and examine if this edge satisfies the local max-min angle criterion. Since $\alpha^* < \beta^*$ in Figure 2.4.16(b), the edge does not satisfy it. In this case we swap $\overline{p_2p_5}$ (the heavy continuous line in Figure 2.4.16(b)) for $\overline{p_1p_3}$ (the broken line in Figure 2.4.16(b)), and replace E with $(E\setminus\{\overline{p_3p_5}\})\cup\{\overline{p_1p_4}\}$. We next choose an edge, say $\overline{p_3p_5}$ (the heavy continuous line in Figure 2.4.16(c)), from $E\backslash\mathrm{CH}(P)$. Since $\alpha^* < \beta^*$ in Figure 2.4.16(c), we swap $\overline{p_3p_5}$ (the heavy line in Figure 2.4.16(c)) for $\overline{p_1p_4}$ (the broken line in Figure 2.4.16(c)), and replace E with $(E\setminus\{\overline{p_3p_5}\})\cup\{\overline{p_1p_4}\}$. We continue this procedure until we do not have to swap any edge in E. In the example of Figure 2.4.16(d), both internal edges satisfy the local max-min angle criterion, and so we stop. From Property D15, we notice that this triangulation is $\mathcal{D}(P)$.

We now state the above procedure in a general form as follows.

The swapping procedure Let $P = \{p_1, \ldots, p_n\} \subset \mathbb{R}^2$ $(3 \le n < \infty)$ be a finite set of n distinct points satisfying the non-cocircularity assumption.

Step 0. Construct an arbitrary triangulation of $\mathrm{CH}(P)$ spanning P, and let E be the set of edges in the triangulation.

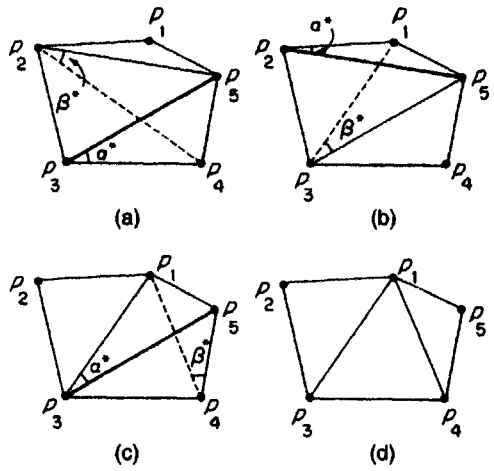

Figure 2.4.16 The swapping procedure.

Step 1. If all the edges in E satisfy the local max-min angle criterion, report E and stop; otherwise go to Step 2.

Step 2. Choose and delete from E an edge e that does not satisfy the local max-min angle criterion, and add to E the other diagonal edge of the quadrangle formed by the two triangles containing e, and go to Step 1.

We call this procedure the *swapping procedure*. Note that the above procedure is alternatively called the *local(ly) optimal procedure* in Lee and Schachter (1980), the *locally equiangular triangulation* in Sibson (1978), and the *Delaunay diagonal flips* in Fortune (1993).

The process of the swapping procedure can be easily understood by the lift-up transformation (Edelsbrunner, 1988). As shown in Figure 2.4.17, let $\mathcal{T} = \{T_1, \ldots, T_n\}$ be an arbitrary triangulation spanning P, and let $\mathcal{T}^* = \{T_1^*, \ldots, T_n^*\}$ be the surface formed by the collection of triangles obtained from $\mathcal{T}$ by the lift-up transformation (T_i^* is the lift-up of T_i). As we saw in Property D9, if $\mathcal{T}$ is not a Delaunay triangulation, the surface $\mathcal{T}^*$ is not convex downward. Let T_i^* and T_j^* be two triangles in $\mathcal{T}^*$ such that the triangles share the edge $\overline{p_i^* p_j^*}$ and they bend downward along the edge $\overline{p_i^* p_j^*}$ as in Figure 2.4.17(a). Such triangles make the surface $\mathcal{T}^*$ non-convex.

Let p_i, p_j, p_k be the vertices of T_i, and p_i, p_j, p_l be the vertices of the triangle T_j. Let T_i' and T_j' be two triangles created by swapping the edge $\overline{p_i p_j}$ with the other diagonal edge $\overline{p_k p_l}$. By this swapping, we get a new pair of triangles $T_i^{*\prime}$ and $T_j^{*\prime}$ in $\mathbb{R}^3$ that bend upward along the edge $\overline{p_k^* p_l^*}$, as in Figure 2.4.17(b). Such triangles contribute to the convex surface $\mathcal{T}^*$. It is easy to see that by this swapping the edge shared by the resulting triangles satisfies the local max-min angle criterion. Hence swapping an edge according to the local max-min angle criterion corresponds to the procedure for

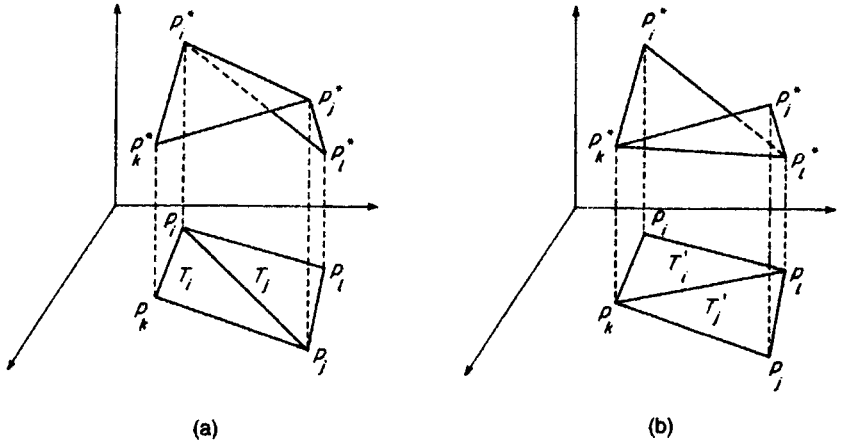

Figure 2.4.17 Two triangles: (a) bending downward along the common edge and (b) those bending upward along the common edge.

changing the surface from $\mathcal{T}^*$ to $\mathcal{T}^{*\prime}$ by replacing two upper facets of the tetrahedron having the vertices $p_i^*, p_j^*, p_k^*, p_l^*$ with two lower facets. Intuitively, this procedure corresponds to gluing the tetrahedron onto the surface $\mathcal{T}^*$ from below; the new lower surface gives $\mathcal{T}^{*\prime}$. We apply this replacement to any edge on the surface $\mathcal{T}^*$. Consequently, the swapping procedure terminates only when the lift-up surface $\mathcal{T}^*$ becomes convex downward. From this property and Property D9 we obtain the following property.

Property D16 The swapping procedure based upon the local max-min angle criterion always terminates with a Delaunay triangulation.

We know that the number of tetrahedra in the three-dimensional tessellation spanning n points is of order n^2 (Edelsbrunner, 1987). Consequently, a Delaunay triangulation is obtained from any initial triangulation by at most of order n^2 repetitions of the swappings.

We may extend the idea of the swapping procedure to the construction of a Delaunay tetrahedrization in $\mathbb{R}^3$. Joe (1989, 1991a) develops this extension and calls the procedure the *local transformation procedure* in which faces are swapped according to a certain criterion. It is shown by Joe (1991a) that the local transformation procedure can be used to construct a Delaunay tetrahedrization under a certain condition.

A Delaunay triangulation satisfies a little stronger property than Property D16. Let $\alpha_i^*(\mathcal{T}_j)$ be the minimum angle in a triangle $T_i, i \in I_{n_v}$, in a triangulation $\mathcal{T}_j$ of CH(P) spanning P. We reindex $\alpha_1^*(\mathcal{T}_j), \ldots, \alpha_{n_v}^*(\mathcal{T}_j)$ as $\alpha_{(1)}^*(\mathcal{T}_j), \ldots, \alpha_{(n_v)}^*(\mathcal{T}_j)$, where $(\alpha_{(1)}^*(\mathcal{T}_j) \leq \ldots \leq \alpha_{(n_v)}^*(\mathcal{T}_j)$, and call $\boldsymbol{a}(\mathcal{T}_j)^{\mathrm{T}} = (\alpha_{(1)}^*(\mathcal{T}_j), \ldots, \alpha_{(n_v)}^*(\mathcal{T}_j))$ the *ordered minimum angle vector* of $\mathcal{T}_j$ or briefly the *angle vector* of $\mathcal{T}_j$. For two angle vectors $\boldsymbol{a}(\mathcal{T}_1)$ and $\boldsymbol{a}(\mathcal{T}_2)$, if there exists $k \leq n_v$ such that

$$\begin{aligned} &\alpha^*_{(i)}(\mathcal{T}_1) = \alpha^*_{(i)}(\mathcal{T}_2), \quad i = 1, \ldots, k-1, \\ &\alpha^*_{(k)}(\mathcal{T}_1) < \alpha^*_{(k)}(\mathcal{T}_2), \end{aligned} \tag{2.4.18}$$

we say that $\mathcal{T}_2$ is *lexicographically greater* than $\mathcal{T}_1$, and denote this relation by $\mathcal{T}_1 \preccurlyeq \mathcal{T}_2$. In terms of this relation, we can now state the following property.

Property D17 (the lexicographically maximum triangulation theorem) A triangulation spanning a finite set P of distinct points is lexicographically maximum with respect to the ordered minimum angle vector if and only if the triangulation is the Delaunay triangulation spanning P.

Proof Suppose that an edge is swapped according to the local max-min angle procedure, and the triangulation changes from $\mathcal{T}_1$ to $\mathcal{T}_2$. By this swapping, suppose that two triangles sharing the edge, say T_1 and T_2 in $\mathcal{T}_1$, change into T_1^* and T_2^* in $\mathcal{T}_2$ (the other triangles remain the same), and that $\alpha_1^*(\mathcal{T}_1)$ and $\alpha_2^*(\mathcal{T}_1)$ are $\alpha^*_{(k)}(\mathcal{T}_1)$ and $\alpha^*_{(h)}(\mathcal{T}_1)$ in the ordered minimum angle vector $\boldsymbol{a}(\mathcal{T}_1)$, $k < h$. Since the edge is swapped according to the local max-min angle procedure, the relation

$$\min\{\alpha_1^*(\mathcal{T}_1), \alpha_2^*(\mathcal{T}_1)\} < \min\{\alpha_1^*(\mathcal{T}_2), \alpha_2^*(\mathcal{T}_2)\} \tag{2.4.19}$$

holds (recall relation (2.4.17)), where $\alpha_i^*(\mathcal{T}_2)$ is the minimum angle in the triangle T_i', $i = 1, 2$. Hence $\alpha^*_{(i)}(\mathcal{T}_2) = \alpha^*_{(i)}(\mathcal{T}_1)$, $i = 1, \ldots, k-1$, and $\alpha^*_{(k)}(\mathcal{T}_1) < \alpha^*_{(k)}(\mathcal{T}_2)$, from which we obtain $\mathcal{T}_1 \preccurlyeq \mathcal{T}_2$. Whenever an edge is swapped, the new triangulation becomes lexicographically greater than the old triangulation. Moreover, Property D16 shows that the swapping procedure always terminates with $\mathcal{D}(P)$ for any initial triangulation. Therefore $\mathcal{D}(P)$ is lexicographically maximum. □

As is shown in Property D17, $\mathcal{D}(P)$ is the triangulation with the lexicographically largest angle vector. This intuitively means that $\mathcal{D}(P)$ avoids thin and elongated triangles as much as possible. Noticing this property, we might expect that the length of the shortest path on $\mathcal{D}(P)$ between two points in P is a good approximation to the Euclidean distance. This expectation is indeed true. To be precise, let $D(p_i, p_j)$ be the length of the shortest chain connecting p_i and p_j composed of Delaunay edges in $\mathcal{D}(P)$, where the length of a Delaunay edge is the Euclidean distance between the two endpoints of the edge and the length of the chain is the sum of the length of the edges on the chain. Then the following property holds.

Property D18 For any p_i and p_j in a finite set $P = \{p_1, \ldots, p_n\}$ of distinct points,

$$D(p_i, p_j) \leq c\, d(p_i, p_j) \tag{2.4.20}$$

holds, where $d(p_i, p_j)$ is the Euclidean distance between p_i and p_j, and $c = 2\pi/(3\cos(\pi/6)) \approx 2.42$.

This is proved by Keil and Gutwin (1989); a little weaker result, where $c = (1 + \sqrt{5})\,\pi/2 \approx 5.08$, is proved by Dobkin *et al.* (1990).

Recall that for n points there are $O(n^2)$ pairs of points whereas there are only $O(n)$ edges in $\mathfrak{D}(P)$. Hence, the network composed of $O(n^2)$ direct routes between points and the points of their intersection can be efficiently approximated by the Delaunay triangulation, which requires only $O(n)$ storage.

Having noticed that $\mathfrak{D}(P)$ satisfies the optimal criteria shown in Properties D14, D15 and D16, we might expect that $\mathfrak{D}(P)$ satisfies more optimal criteria. We refer to two notable criteria for optimal triangulations (a general review is provided by Tan, 1996).

The minimax length criterion For a given finite set P of distinct points, if a triangulation spanning P minimizes the length of its longest edge, we say that the triangulation satisfies the *minimax length criterion*, and call the triangulation satisfying the minimax criterion the *minimax length triangulation*.

The minimum weight (minimum length) criterion For a given finite set P of distinct points, if a triangulation spanning P minimizes the total length of its edges, we say that the triangulation satisfies the *minimum weight (minimum length) criterion*, and call the triangulation satisfying the minimum weight criterion the *minimum weight (minimum length) triangulation*.

It is shown that $\mathfrak{D}(P)$ neither satisfies the minimax length criterion (Edelsbrunner and Tan, 1993) nor the minimum weight criterion (Lloyd, 1977; Kirkpatrick, 1980). In comparison with $\mathfrak{D}(P)$, Edelsbrunner and Tan (1993) and Levcopoulos and Lingas (1989, 1992) examine the lower bound for the minimax triangulation; Manacher and Zobrist (1979), Kirkpatrick (1980) and Levcopoulos and Krznaric (1996) examine that for the minimum weight triangulation.

We also note a few more optimal triangulations. A *minimum energy triangulation* is a triangulation for which the finite element solution has the minimum energy. Rippa and Schiff (1990) show that the Delaunay triangulation is a minimum energy triangulation for the energy functional associated with the non-homogeneous Laplace equation (the proof is given by Rippa and Schiff, 1990; see also Corollary 3.3 in Rees and Morton, 1991). Rippa (1990, Theorem 2.1) shows that the Delaunay triangulation is a 'minimum roughness triangulation' (also see Power, 1992, and Section 2.6). Rajan (1994) shows that the maximum min-containment radius of the Delaunay triangulation of a point set is less than or equal to the maxmum min-containment radius of any other triangulation of the point set (Theorem 2); the weighted sum of squares of the edge lengths is the smallest for a Delaunay triangulation (Theorem 4).

Noticing that Manacher and Zobrist (1979), Kirkpatrick (1980) and Levcopoulos and Krznaric (1996) tend to avoid thin and elongated triangles as much as possible (Property D17), we might expect that a Delaunay tetrahedrization also has a similar property. This expectation is not always true.

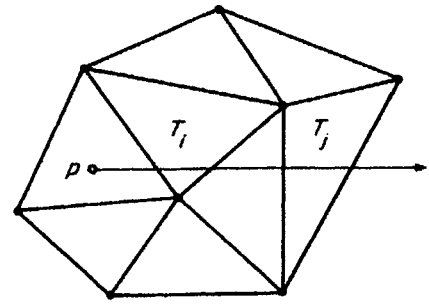

Figure 2.4.18 Monotonicity with respect to ray shooting.

Joe (1991a) reports that a Delaunay tetrahedrization tends to contain poorly shaped sliver tetrahedra with four nearly co-planar vertices lying near an equator of the circumsphere (see Figure 2.8 in Ruppert, 1995). To avoid poorly shaped sliver tetrahedra, Joe (1995a) proposes an alternative method for constructing a tetrahedrization using 'combined local transformations' (see Section 6.5.2).

The Delaunay triangulation has an interesting monotonicity property with respect to ray shooting. To illustrate it, let us consider a triangulation spanning P, and let p be a point in $\mathbb{R}^2$. For any triangles T_i and T_j in $\mathcal{T}$, we write $T_i \leqslant_p T_j$ if there exists a ray starting at p such that a traveller traversing along the ray from p passes through T_i and T_j in this order (Figure 2.4.18). If there is no cyclic sequence $(T_1, T_2, \ldots, T_k, T_1)$ of triangles satisfying $T_1 \leqslant_p T_2 \leqslant_p \ldots \leqslant_p T_k \leqslant_p T_1$, $k \geq 2$, we say that $\mathcal{T}$ is *monotone with respect to ray shooting* at p. If $\mathcal{T}$ is monotone with respect to ray shooting at any point in $\mathbb{R}^2$, we say that $\mathcal{T}$ is *ray-shoot monotone.*

The ray-shoot monotonicity is not necessarily satisfied by any triangulation. A counterexample is shown in Figure 2.4.19. For the ray r_1, $T_1 \leqslant_p T_2$ holds; for the ray r_2, $T_2 \leqslant_p T_3$ holds; for the ray r_3, $T_3 \leqslant_p T_1$ holds. Thus $T_1 \leqslant_p T_2 \leqslant_p T_3 \leqslant_p T_1$, showing that the triangulation in Figure 2.4.19 is not monotone with respect to ray shooting at p. The Delaunay triangulation, however, has the following property.

Property D19 The Delaunay triangulation is ray-shoot monotone.

To show the outline of the proof, let p be any point in $\mathbb{R}^2$. For convenience, we transform the (x, y) coordinate system in such a way that p is at the origin, and construct the lower boundary of the convex hull of the lift-up of P, i.e. $\mathrm{CH}(P^*)$. For a Delaunay triangle T_i in $\mathbb{R}^2$, let T_i^* be the corresponding triangular facet on the boundary of $\mathrm{CH}(P^*)$, and α_i be the z coordinate of the intersection point between the z-axis and the plane containing T_i^* (see Figure 2.4.20). Using the value of α_i, we define a binary relation, $<_p$: $T_i <_p T_j$ if and only if $\alpha_i \leq \alpha_j$. The binary relation $<_p$ gives a total order in the set of Delaunay triangles in $\mathcal{D}(P)$.

Next consider a ray in $\mathbb{R}^2$ starting at the origin and passing through T_i and T_j in this order. Since the lower boundary of $\mathrm{CH}(P^*)$ lies on the paraboloid

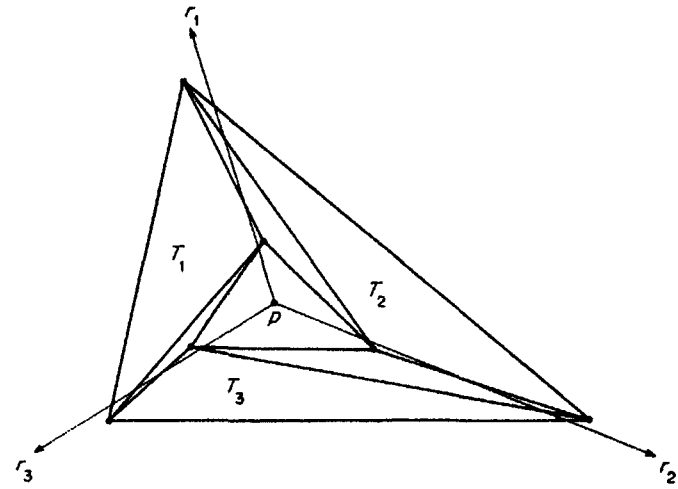

Figure 2.4.19 A triangulation not satisfying ray-shoot monotonicity.

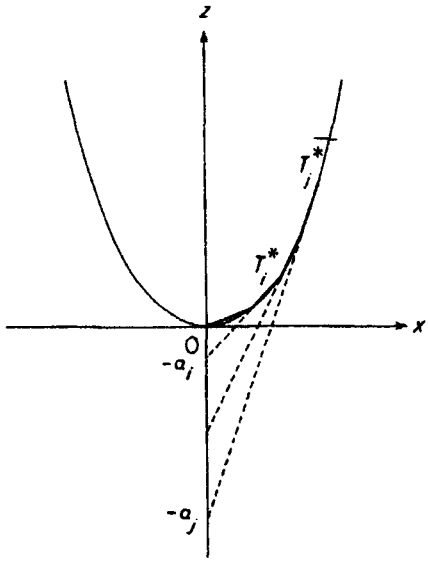

Figure 2.4.20 Monotonicity and order.

of revolution with the bottom at (0, 0, 0), the plane containing T_i^* cuts the z-axis at the higher point than the plane containing T_j^*, as shown in Figure 2.4.20. Thus, $T_i \leq_p T_j$ implies $T_i <_p T_j$. Since $<_p$ is a total order, we notice that $\mathcal{T}(P)$ is monotone with respect to ray shooting at p. This property holds for an arbitrary point p, and hence we obtain Property D19.

The ray-shoot property is a useful property when we consider problems related to visibility (De Floriani, 1989b), and ordering multivariate data (see Section 6.6).

2.5 GRAPHS RELATED TO THE DELAUNAY TRIANGULATION

As we mentioned in Section 2.4 (Property D10), the Delaunay triangulation $\mathcal{D}(P)$ spanning P can be regarded as the connected geometric graph that consists of the set of nodes given by P and the set of links given by the edges E_d of the Delaunay triangles. We call this graph a *Delaunay graph* and denote it by $G(P, E_d)$. The graph $G(P, E_d)$ contains many subgraphs. Among them, notable subgraphs are the Gabriel graph, the relative neighbourhood graph, the Euclidean minimum spanning tree and the nearest neighbour graph. In this section we show the definitions of these graphs together with their geometric properties. Note that we assume throughout this section that P satisfies the non-cocircularity assumption, so that $G(P, E_d)$ is defined uniquely for the set P of points.

First of all we notice from Property D2 that the boundary $\partial\mathrm{CH}(P)$ of the convex hull $\mathrm{CH}(P)$ is a subgraph of $G(P, E_d)$. Figure 2.5.1 represents an example, where (a) shows a Delaunay triangulation for 12 points and (b) shows $\partial\mathrm{CH}(P)$ of the same points.

In Property D6 we characterized $\mathcal{D}(P)$ or $G(P, E_d)$ in terms of an empty circle. Similarly, we can characterize a subgraph of $G(P, E_d)$, called the Gabriel graph, in terms of another type of empty circle. The *Gabriel graph*, denoted by $\mathrm{GG}(P)$, of P is defined by the graph in which $\overline{p_i p_j}$ is an edge of $\mathrm{GG}(P)$ if and only if the circle having $\overline{p_i p_j}$ as a diameter is an empty circle, that is, if and only if it contains no point of P in its interior (Gabriel and Sokal, 1969). Figure 2.5.1(c) presents the Gabriel graph for the same set of points as in (a). If $\overline{p_i p_j}$ is an edge of the Gabriel graph, p_i and p_j are said to be *Gabriel neighbours* of each other. Obviously, an edge of $\mathrm{GG}(P)$ is a Delaunay edge of $G(P, E_d)$. It should be noted, however, that a Delaunay edge of $G(P, E_d)$ is not necessarily an edge of $\mathrm{GG}(P)$.

To derive a necessary and sufficient condition for an edge of $\mathrm{GG}(P)$ to be a Delaunay edge, let $\overline{p_i p_j}$ be an edge of $\mathrm{GG}(P)$, and C be the circle with diameter $\overline{p_i p_j}$, as shown in Figure 2.5.2. Let C' be the empty circle that passes through p_i, p_j and one more point, say p_k, in P. Since C' contains no point of P in its interior, the centre of C' is a Voronoi vertex shared by the Voronoi polygons of p_i, p_j and p_k (Property V7). Let C'' be the empty circle passing through p_i, p_j and one more point other than p_k, say p_l, such that the centre of C' is on the other side of $\overline{p_i p_j}$ (see Figure 2.5.2). Then, the centre of C'' is also a Voronoi vertex, and the line segments connecting the centre of C' and that of C'' is a Voronoi edge shared by the two Voronoi polygons $V(p_i)$ and $V(p_j)$. Since the centres of C' and C'' are both on the perpendicular bisector of $\overline{p_i p_j}$, the line segment $\overline{p_i p_j}$ crosses the Voronoi edge shared by $V(p_i)$ and $V(p_j)$. In the above argument we implicitly assume that both C' and C'' exist. If C' or C'' does not exist (which happens when p_i and p_j are consecutive vertices on the boundary of the convex hull of P), we can consider that the centre of C' or C'' is at infinity, and hence the above property still holds. Thus we get the next property.

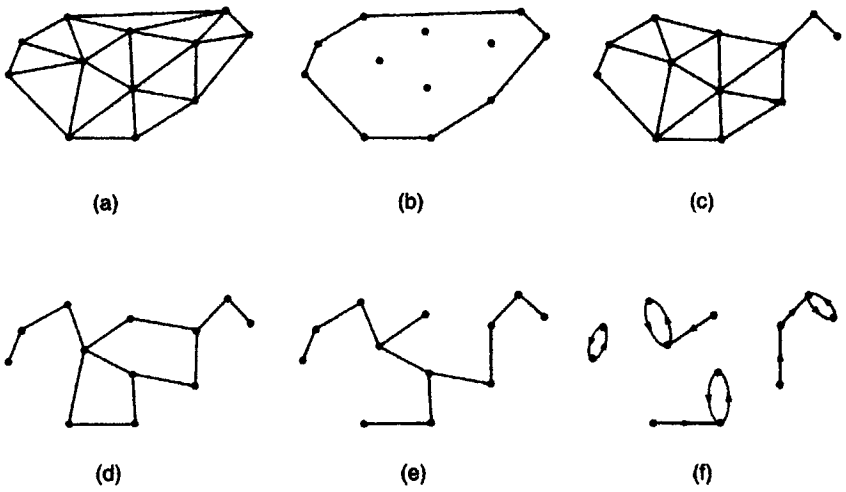

Figure 2.5.1 Graphs related to the Delaunay triangulation: (a) Delaunay triangulation; (b) convex hull; (c) Gabriel graph; (d) relative neighbourhood graph; (e) Euclidean minimum spanning tree; (f) nearest neighbourhood graph.

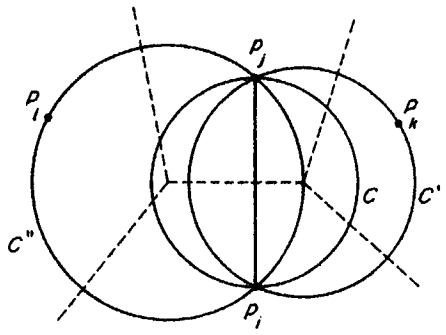

Figure 2.5.2 An edge of a Gabriel graph.

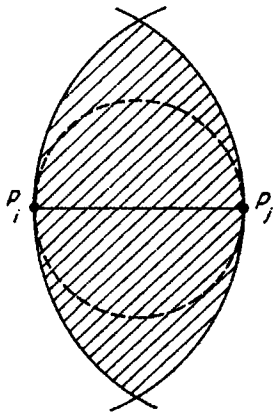

Figure 2.5.3 An edge of a relative neighbourhood graph.

Property D20 $\overline{p_i p_j}$ is an edge of GG(P) if and only if $\overline{p_i p_j}$ is a Delaunay edge of $G(P, E_d)$ and $\overline{p_i p_j}$ crosses the corresponding Voronoi edge.

Note that the condition stated in Property D19 is similar to the condition imposed on each interior edge of the Pitteway triangulation (recall Property D3). Actually in the Pitteway triangulation, every edge is an edge of GG(P). Hence we get the next property.

Property D21 If the Delaunay triangulation $\mathfrak{D}(P)$ is a Pitteway triangulation, GG(P) is exactly the same as $G(P, E_d)$.

We can use GG(P) in defining adjacency in point patterns (Gabriel and Sokal, 1969; Matula and Sokal, 1980; Urquhart, 1982).

As is illustrated in Figure 2.5.3, the Gabriel graph is defined with the empty circle indicated by the broken lines. Modifying this empty circle, we may define a subgraph of $G(P, E_d)$, called the relative neighbourhood graph, with an 'empty spindle', indicated by the shaded area in Figure 2.5.3. To be precise, the *relative neighbourhood graph*, denoted by RNG(P), is defined as a geometric graph in which RNG(P) has an edge between p_i and p_j if and only if

$$d(p_i, p_j) \leq \min_{k(\neq i,j)} \max\{d(p_i, p_k), d(p_j, p_k)\} \tag{2.5.1}$$

(Toussaint, 1980a; Supowit, 1983; Urquhart, 1982). In other words, $\overline{p_i p_j}$ is an edge of RNG(P) if and only if there is no other point of P in the interior of the intersection of the disk with the centre at p_i and the radius $d(p_i, p_j)$ and the disk with the centre at p_j and the same radius (i.e. the open region represented by the shaded area in Figure 2.5.3). This region contains the interior of the circle (represented by the dashed line in Figure 2.5.3) having $\overline{p_i p_j}$ as a diameter, and hence we get the next property.

Property D22 An edge of RNG(P) is an edge of GG(P).

Figure 2.5.1(d) represents the relative neighbourhood graph for the same set of points as in (a). We can use RNG(P) as well as GG(P) for the analysis of point patterns (Toussaint, 1980a; Urquhart, 1982; Lefkovitch, 1984, 1985, 1987; Ichino and Sklansky, 1985; Dearholt *et al.*, 1988).

The subgraphs of the graph $G(P, E_d)$ include tree graphs. One of the most frequently referred to tree graphs is the Euclidean minimum spanning tree. The *Euclidean minimum spanning tree*, denoted by EMST(P), is defined as the tree having a vertex set P in which the sum of the Euclidean length of all the edges attains the minimum over all trees having the vertex set P. Regarding the relationship between an edge of EMST(P) and that of RNG(P), we can show the following property.

Property D23 An edge of EMST(P) is an edge of RNG(P).

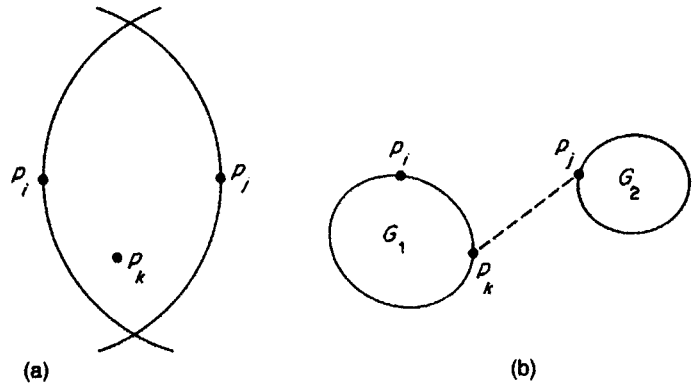

Figure 2.5.4 An edge in the EMST(P).

To prove this property, assume, contrary to Property D23, that $\overline{p_i p_j}$ is an edge of EMST(P) but that there is a point, say p_k, in the intersection of the two disks with radius $d(p_i, p_j)$ centred at p_i and p_j, as shown in Figure 2.5.4(a). If we remove the edge $\overline{p_i p_j}$ from EMST(P), the tree is divided into two subtrees, G_1 and G_2; one contains p_i and the other contains p_j. Without loss of generality, suppose that G_1 contains p_i and p_k and G_2 contains p_j. Then we can obtain a new tree G' from G_1 and G_2 by adding a new edge $\overline{p_j p_k}$, as shown in Figure 2.5.4(b). Since $d(p_j, p_k) < d(p_i, p_j)$, the total length of the edges in G' is smaller than the total length of the edges in EMST(P), which is a contradiction. Thus, we get Property D23.

Figure 2.5.1(e) represents the Euclidean minimum spanning tree for the same set of points as in (a).

Minimum-cost spanning trees, EMST(P) in particular, have many applications such as clustering (Gower and Ross, 1969; Rohlb, 1973; Friedman and Rafsky, 1979, 1981; Johnson, 1967; Kayser *et al.*, 1992; Martinetz *et al.*, 1990; McIntosh, 1988), pattern recognition (Osteen and Lin, 1974), natural pattern analysis (Billia *et al.*, 1991; Bhavsar and Line, 1988; Dussert *et al.*, 1986), biological pattern analysis (Dussert *et al.*, 1987; Kayser and Stute, 1989; Choi *et al.*, 1995) and approximation algorithms for the travelling salesman problem (Rosenkrantz *et al.*, 1977).

The geometric subgraphs of $\mathfrak{D}(P)$ discussed above are all non-directed graphs. If we introduce a direction in a subgraph of $G(P, E_d)$, we can define a directed subgraph, called the nearest neighbour graph. The *nearest neighbour graph*, denoted by NNG(P), is defined as the directed graph having a vertex set P such that $\overrightarrow{p_i p_j}$ is an edge of NNG(P) if and only if

$$d(p_i, p_j) = \min_{k\,(\neq i)} d(p_i, p_k).$$

In other words, $\overrightarrow{p_i p_j}$ is an edge of NNG(P) if and only if p_j is the nearest neighbour of p_i. Note that the nearest neighbour relation is not symmetric; p_j being the nearest neighbour of p_i does not necessarily imply that p_i is the nearest

neighbour of p_j. Every point has its nearest neighbour unless P consists of only one point. However, the nearest neighbour is not necessarily unique; there may be two or more points whose distances from p_i attain the minimum. Hence, in general, every vertex in NNG(P) has one or more edges going out from that vertex. The next property follows directly from the definition.

Property D24 If $\overrightarrow{p_ip_j}$ is an edge of NNG(P), then $\overline{p_ip_j}$ is an edge of RNG(P).

Furthermore, we may derive a little stronger property than Property D24.

Property D25 If $\overrightarrow{p_ip_j}$ is an edge of NNG(P) and there is no other edge in NNG(P) that has the same initial vertex p_i, then $\overline{p_ip_j}$ is an edge of EMST(P).

To prove this property, assume, contrary to Property D25, that (p_i, p_j) is an edge of NNG(P) but $\overline{p_ip_j}$ is not an edge of EMST(P). If we add an edge $\overline{p_ip_j}$ to EMST(P), the resulting graph has exactly one cycle, and $\overline{p_ip_j}$ belongs to this cycle. Let $\overline{p_ip_k}$ be the other edge that is on this cycle and that has p_i as one of the terminal points. Let G be the graph obtained from EMST(P) by replacing the edge $\overline{p_ip_k}$ with the edge $\overline{p_ip_j}$. Then G is a spanning tree. Moreover, since $\overrightarrow{p_ip_j}$ is the only edge starting at p_i in NNG(P), $\overline{p_ip_j}$ is shorter than $\overline{p_ip_k}$. Hence, the total length of the edges in G is smaller than that in EMST(P), which is a contradiction. Thus we get Property D25.

Property D25 implies that if no two pairs of points in P have the same distance, NNG(P) is a subgraph of the directed graph that is obtained from EMST(P) by replacing each edge with two parallel edges having opposite directions. Figure 2.5.1(f) represents the nearest neighbour graph for the same set of points as in (a). NNG(P) can be applied to geographic analysis (Kolars and Nystuen, 1974). The properties of NNG(P) are studied by Saaty (1970) and Pielou (1977).

For a set P of points in the plane, we have considered six graphs $G(P, E_d)$, ∂CH(P), GG(P), RNG(P), EMST(P) and NNG(P). The relations of the first five undirected graphs are shown in Figure 2.5.5, where the lower graph is a subgraph of the upper graph. These relations come from Properties D2 and D20–D25. ∂CH(P) is a subgraph of $G(P, E_d)$ (Property D2). EMST(P) is a subgraph of RNG(P) (Property D23). RNG(P) is a subgraph of GG(P)

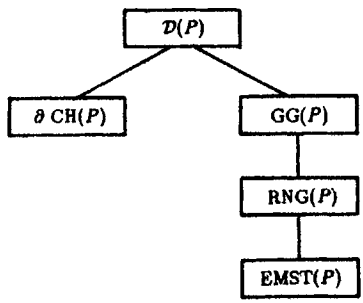

Figure 2.5.5 Relations among the Delaunay triangulation and the related graphs.

(Property D22). GG(P) is a subgraph of $G(P, E_d)$ (Property D20). NNG(P) is a subgraph of the directed graph obtained from RNG(P) by replacing each edge with two parallel edges having opposite directions (Property D24). If no two pairs of points in P have the same distance, NNG(P) is a subgraph of the directed graph obtained from EMST(P) by replacing each edge with two parallel edges having opposite directions (Property D25). In particular, $\overrightarrow{p_ip_j}$ or $\overrightarrow{p_ip_j}$ can be a candidate for an edge of these graphs only when $\overline{p_ip_j}$ is a Delaunay edge. As we will see in Chapter 4, $G(P, E_d)$ can be constructed efficiently. Hence, the above relationships give us methods for constructing these graphs through $G(P, E_d)$; we first construct $G(P, E_d)$ and next delete superfluous edges from $G(P, E_d)$.

The construction of ∂CH(P) from $G(P, E_d)$ is straightforward; indeed, what we have to do is simply gather the outermost Delaunay edges in $G(P, E_d)$. The construction of GG(P) from $G(P, E_d)$ is likewise straightforward, because whether or not a Delaunay edge is an edge of GG(P) can be checked locally according to Property D20. Similarly, the construction of NNG(P) from $G(P, E_d)$ is straightforward; all we have to do is to select, for each point in P, the shortest Delaunay edge incident to the point. The construction of RNG(P) and EMST(P) requires a more global check. See Toussaint (1980a) and Supowit (1983) for the construction of RNG(P). Prim (1957) showed some principles for finding the minimum-cost spanning tree, and those principles were used in many algorithms proposed thereafter. An efficient algorithm for finding the minimum-cost spanning tree for a planar graph is known (Cheriton and Tarjan, 1976). Since $G(P, E_d)$ is a planar graph, this algorithm can be used for finding EMST(P) from $G(P, E_d)$.

Historically there is another graph that was believed to be a subgraph of the Delaunay graph. For a vertex set P, a route visiting all the vertices in P exactly once and returning to the start vertex is called a *Hamilton cycle*. A minimum length Hamilton cycle for P is called a Euclidean travelling salesman cycle for P. It was once conjectured that every Delaunay diagram for P has a Euclidean travelling salesman cycle for P (Shamos, 1978). However, this conjecture was refuted by Kantabutra (1983); actually he found a Delaunay diagram that does not have even a Hamilton cycle. While Kantabutra's counterexample is a degenerate Delaunay diagram, Dillencourt (1987a) found a non-degenerate Delaunay diagram that does not have a Hamilton cycle. He also showed that it is very hard to judge whether or not a given Delaunay diagram has a Hamilton cycle (Dillencourt, 1996a). Cimikowski (1990) found a subclass of the Delaunay diagrams that have Hamilton cycles.

The graphs considered in this section are all defined on the basis of proximity relations. Hence these graphs are called *proximity graphs*. The graph theoretical properties of the proximity graphs together with their construction algorithms are studied by Devroye (1988), Jaromczyk and Kowaluk (1987), Katajainen (1988), Katajainen and Nevalainen (1986) and Chang *et al.* (1992).

The proximity graphs have many applications in engineering, particularly to morphological problems. For example, Radke (1988) applied the proximity

graphs to point pattern analysis; the proximity graphs define structures among unstructured collections of points that are useful for pattern recognition. Toussaint (1988) used these proximity graphs together with another proximity graph called a 'sphere-of-influence graph' for constructing a so-called primal sketch to capture the low-level perceptual structure of visual scenes consisting of dot patterns. Tüceryan and Chorzempa (1991) studied the stability of the proximity graphs against noise points in the context of line extraction using Hough transformation, and observed that the Delaunay triangulation is more stable than other types of proximity graphs. Toriwaki and Yokoi (1988) applied the Delaunay triangulation and the Gabriel graph to the recognition of the structure of texture in digital images, and showed that they are useful for the decomposition of images into meaningful regions. ElGindy and Toussaint (1988) applied the relative neighbourhood graph to the decomposition of polygons into perceptually meaningful points. Beasley and Goffinet (1994) used the Delaunay triangulation for finding the Euclidean minimum Steiner tree. Dickerson and Drysdale (1991) used the Delaunay triangulation to enumerate k smallest distances. Other applications can also be found in a survey by Jaromczyk and Toussaint (1992).

The proximity graphs have been generalized in many directions. O'Rourke (1982) studied the proximity graphs with respect to L_1 and L_∞ norms. The relative neighbourhood graph is generalized to 'k-relative neighbourhood graphs', in which two points are connected by an edge if and only if the spindle in Figure 2.5.3 contains less than k points (Su and Chang, 1991b; Chang *et al.*, 1990b, 1992). The Gabriel graph can be generalized to the 'k-Gabriel graph' similarly (Su and Chang, 1990). Proximity graphs with constraints are also defined; they admit an inclusion relationship similar to Figure 2.5.5 (Su and Chang, 1991a; Jennings and Lingas, 1992); refer to the next chapter for the constrained Delaunay triangulation. The proximity graphs are also defined and studied in higher dimensional spaces (Agarwal *et al.*, 1990b; Jaromczyk and Kowaluk, 1991; Agarwal and Matousek, 1992; Smith *et al.*, 1995).

2.6 RECOGNITION OF VORONOI DIAGRAMS

Sometimes we want to judge whether a given diagram is a Voronoi/Delaunay diagram or not. Here we consider methods for this judgement.

The problems can be divided into three types. The first type, given a diagram actually drawn in the plane, is to judge whether it is a Voronoi/Delaunay diagram. This problem is called the *geometric recognition problem*. The second type, given a graph embedded in the plane, is to judge whether it is isomorphic to a Voronoi/Delaunay diagram. This problem is called the *combinatorial recognition problem*. The third type, given a diagram drawn in the plane, is to find the Voronoi/Delaunay diagram that is closest to the given diagram. This problem is called the *approximation problem*.

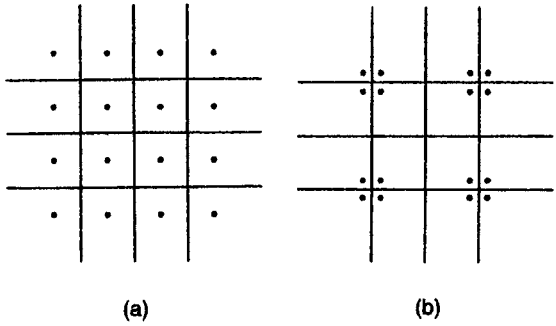

Figure 2.6.1 Voronoi diagram whose generators are not unique.

In this section we consider the first and second types of problems. The approximation problem will be considered in Section 9.5.

2.6.1 The geometric approach

As before, let $P = \{p_1, p_2, \ldots, p_n\}$ be a set of n points in the plane. Suppose that we are given a triangulation $\mathcal{T}$ with the vertex set P. The first problem we consider is the following.

Problem V8 Given a triangulation $\mathcal{T}$ with the vertex set P, judge whether $\mathcal{T}$ is the Delaunay diagram for P.

This problem can be solved easily. What we have to do is to check whether the circumcircle of each triangle in $\mathcal{T}$ is an empty circle. $\mathcal{T}$ is the Delaunay diagram if and only if all the circumcircles are empty circles. Recall Property D5 in Section 2.4.

Next, suppose that we are given a partition Q of the plane into n convex polygons $q_1, q_2, \ldots, q_n$ and their boundaries. We are interested in judging whether Q is the Voronoi diagram for some set P of n points. Thus the problem is as follows.

Problem V9 Given a partition Q of the plane into n convex polygons, judge whether Q is the Voronoi diagram for some P.

This problem is less trivial because we have to search for the locations of the generators. Suppose that Q is the Voronoi diagram, and that the location of any one generator, say p_i, is known. Then, we can find the locations of the neighbouring generators uniquely, because they are the mirror images of p_i with respect to the mirrors at the Voronoi edges on the boundary of $V(p_i)$. The locations of their neighbours are determined in a similar way. In this way, starting with p_i, we can locate all the generators from neighbour to neighbour.

Keeping this fact in mind, let us first consider the case where Q has at least one edge, say e, both end vertices of which are incident to exactly three edges (including e). Then, Property V15 tells us the unique locations of the generators on both sides of e. Consequently, we can locate all the generators by taking the mirror images with respect to other edges. Let the resultant set of generators be P. We construct the Voronoi diagram $\mathcal{V}(P)$ and compare it with Q. We can judge that Q is the Voronoi diagram if $Q = \mathcal{V}(P)$, and Q is not otherwise. This direction of analysis was given by Loeb (1976), Stoyan and Stoyan (1980) and Ash and Bolker (1985); see also Problem V6, Property V15 and Property V16.

Next, let us consider the case where there is no edge both end vertices of which are incident to exactly three edges. In this case, even if Q is the correct Voronoi diagram, the locations of the generators are not necessarily unique. An example is shown in Figure 2.6.1; the generators in (a) are different from those in (b), but both sets of generators give the same Voronoi diagram.

Hartvigsen (1992) solved Problem V9 by reducing it to the satisfiability of a system of linear equations and linear inequalities in the following way.

Let $\boldsymbol{x}^{\mathrm{T}} = (x_1, y_1, x_2, y_2, \ldots, x_n, y_n)$ be the $2n$-dimensional unknown vector. We search for the locations $(x_1, y_1), (x_2, y_2), \ldots, (x_n, y_n)$ of n generators whose Voronoi diagram coincides with Q. The generators should satisfy the following conditions.

(1) Each generator should be in the associated Voronoi region.
(2) An edge in Q should be on the perpendicular bisector of the two side generators.

Let e be an edge of Q shared by two polygons q_i and q_j. Without loss of generality, we assume that the line containing e does not contain the origin of the coordinate system. Then, the line containing e can be expressed by the equation

$$ax + by = 1. \tag{2.6.1}$$

Suppose that q_i and the origin lie in the same side of e. Then we get

$$ax_i + by_i > 0 \quad \text{and} \quad ax_j + by_j < 0. \tag{2.6.2}$$

We obtain similar inequalities for each edge of Q. Collecting them all, we get the system of linear inequalities. Let us denote this system by

$$A\boldsymbol{x} > 0. \tag{2.6.3}$$

This is the mathematical expression of condition (1).

Next, let us consider condition (2). The line containing e should contain the midpoint of (x_i, y_i) and (x_j, y_j). Hence we get

$$a\frac{x_i + x_j}{2} + b\frac{y_i + y_j}{2} = 1. \tag{2.6.4}$$

Furthermore, since the line connecting (x_i, y_i) and (x_j, y_j) should be perpendicular to e, we get

$$a(y_i - y_j) - b(x_i - x_j) = 0. \tag{2.6.5}$$

Note that the above two equations are linear in the unknown coordinates.

We get similar equations for each edge. Collecting them all, we obtain a system of linear equations, which we denote by

$$Bx = c. \tag{2.6.6}$$

This system of equations represents condition (2). We now state the following theorem.

Theorem V1 (Hartvigsen, 1992) The partition Q of the plane is the Voronoi diagram if and only if the system of equations (2.6.6) and inequalities (2.6.5) has a solution.

The satisfiability of the system of linear equations and inequalities can be checked by the linear programming techniques. Hence, if the vertices and the edges of Q are represented by rational numbers, Problem V9 can be solved in time represented by a polynomial function of n (Khachian, 1979, 1980).

Usually the given diagram contains numerical errors in the coordinates of the vertices, and hence equations (2.6.6) do not hold strictly. Evans and Jones (1987) proposed to

$$\text{minimize } \|Bx - c\|^2$$

instead of searching for the exact solution of equations (2.6.6).

The above theorem was generalized to the n-dimensional space by Hartvigsen (1992). Aurenhammer (1987b) also gave another method for recognizing the Voronoi diagram in the n-dimensional space; he also studied the recognition of a weighted Voronoi diagram.

2.6.2 The combinatorial approach

Suppose that G is a simple, connected, and planar graph embedded in the plane, where the graph G being simple means that G has no self-loop or no parallel edges, and hence any cycle of G contains at least three edges. In this subsection we assume that every vertex in G is incident to three or more edges. Let $V = \{v_1, v_2, \ldots, v_n\}$ be the set of vertices of G, and let E be the set of edges of G. The edges of G divide the plane into connected regions. These regions are called *cells* generated by the embedded graph G. The outermost cell is unbounded while the other cells are bounded. The bounded cells are called *inner cells*. We call the embedded graph G a *triangulation graph* if all the inner cells are bounded by exactly three edges.

Let G be a triangulation graph, and C be the set of all the cycles of G that bound the inner cells counterclockwise. We represent this triangulation graph by $G(V, E, C)$. When we write $G(V, E, C)$, we concentrate our

attention on the combinatorial structure of the embedded graph; we do not care about the actual locations at which the vertices are placed.

For a triangulation graph $G(V, E, C)$, let ψ be a mapping from V to $\mathbb{R}^2$ such that $\psi(v_i) \neq \psi(v_j)$ whenever $i \neq j$. Placing the vertices v_i of G at $\psi(v_i)$ and representing the edges of G by the straight line segments connecting the two terminal vertices, we get a diagram. If this diagram realizes the triangulation graph G (i.e. both if no edges intersect except at the end points, and if the set of all the cycles that bound the inner cells coincides with C), then this diagram is called a *triangulation* and is denoted by $\mathcal{T} = (G, \psi)$ or $\mathcal{T} = (V, E, C, \psi)$.

Triangulation $\mathcal{T} = (V, E, C, \psi)$ is a Delaunay triangulation if

1. the boundary of the outermost cell forms a convex polygon, and
2. the circumcircle of each inner cell (i.e. triangle) does not contain a vertex in its interior.

The triangulation graph $G(V, E, C)$ is called a *Delaunay-triangulation-realizable graph* (*DT-realizable graph* for short) if there is a mapping ψ such that $\mathcal{T} = (G, \psi)$ is a Delaunay triangulation.

The triangulation graph $G(V, E, C)$ is called a *non-degenerate DT-realizable graph* if there exists a mapping ψ such that $\mathcal{T} = (G, \psi)$ is a non-degenerate Delaunay triangulation.

The graph G is said to be 2-*connected* if deletion of any one vertex and all the edges incident to it from G does not make the resultant graph disconnected. The Delaunay triangulation gives a 2-connected graph. Hereafter we assume that G is 2-connected. The problem we consider is the following.

Problem V10 Given a triangulation graph $G(V,E,C)$, judge whether G is a (non-degenerate) DT-realizable graph.

As we have already seen, Property D13 gives a sufficient condition for G to be a non-degenerate DT-realizable graph, and Property D14 gives a sufficient condition for G to be a DT-realizable graph (Dillencourt, 1990a,b). On the other hand, Hodgson *et al.* (1992) gave a necessary and sufficient condition for a graph to be the vertex-edge graph of a convex polyhedron with all the vertices on a common sphere. As we have seen in Property D7, the Delaunay triangulation and a convex polyhedron inscribed in a sphere have a one-to-one correspondence through the inversion transformation. Hence, Hodgson *et al.*'s result (1992) together with Property D7 gives a solution of Problem V10.

Hiroshima and Sugihara (1994, 1996) also gave a necessary and sufficient condition for G to be a DT-realizable graph. Their condition is represented by a system of linear equations and linear inequalities. Hence, Problem V10 can be solved by linear programming techniques. They assigned variables to the angles of all the triangles, and formulated the condition in the following way.

For the triangulation graph $G(V,E,C)$, let the elements of C be $c_1, c_2, \ldots, c_{|C|}$. Each cycle c_i has three vertices; we assign three variables x_{3i-2}, x_{3i-1}

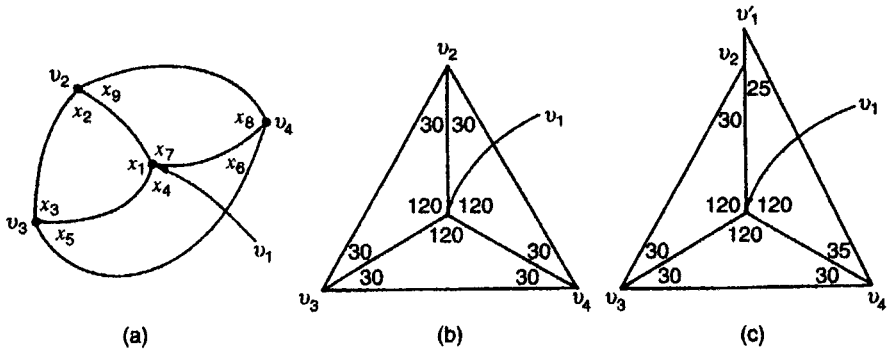

Figure 2.6.2 Triangulation graph and angle variables.

and x_{3i}, one to each vertex of c_i. We interpret these variables as angles at the corresponding corners of the triangle. So let us call these variables *angle variables*. In total we have $3|C|$ angle variables, each corresponding to a corner of a triangle. For the triangulation graph in Figure 2.6.2(a), for example, we assign nine angle variables $x_1, x_2, \ldots, x_9$ as shown in this figure.

We call a vertex of G an *outer vertex* if it is on the boundary of the outermost cell, and an *inner vertex* otherwise. Similarly, we call an edge of G an *outer edge* if it is on the boundary of the outermost cell, and an *inner edge* otherwise.

For a given triangulation graph $G(V,E,C)$, we generate the following five types of constraints; they should be satisfied if G is realized as a Delaunay triangulation.

(C1) For each cycle in C, the sum of the associated three angle variables is equal to 180.
(C2) For each inner vertex, the sum of all the associated angle variables is equal to 360.
(C3) For each outer vertex, the sum of all the associated angle variables is equal to or less than 180.
(C4) For each inner edge, the sum of the associated pair of facing angle variables (i.e. the angle variables corresponding to the vertices that are on the same cycle as, but are not incident to, the inner edge) is equal to or less than 180.
(C5) Each angle variable is positive.

Let us denote by $S(G)$ the system consisting of all the constraints.

For example, for the triangulation graph in Figure 2.6.2(a), (C1) implies

$$x_1 + x_2 + x_3 = 180, \quad x_4 + x_5 + x_6 = 180, \quad x_7 + x_8 + x_9 = 180. \tag{2.6.7}$$

(C2) implies

$$x_1 + x_4 + x_7 = 360. \tag{2.6.8}$$

(C3) implies

$$x_3 + x_5 \leq 180, \quad x_6 + x_8 \leq 180, \quad x_9 + x_2 \leq 180. \tag{2.6.9}$$

(C4) implies

$$x_2 + x_6 \leq 180, \quad x_5 + x_9 \leq 180, \quad x_3 + x_8 \leq 180. \tag{2.6.10}$$

(C5) implies

$$x_1 > 0, x_2 > 0, \ldots, x_9 > 0. \tag{2.6.11}$$

Thus $S(G)$ consists of four equations, six improper inequalities and nine proper inequalities.

For any Delaunay triangulation $\mathcal{T} = (G, \psi)$, the realized values of the angle variables (measured in degrees) satisfy the constraints. Indeed, (C1), (C2) and (C5) are satisfied by any triangulation, whereas (C3) means that the outermost cycle of $\mathcal{T}$ forms a convex polygon, and (C4) means that the circumcircle of any triangle is an empty circle. An example of a Delaunay triangulation realizing the graph in Figure 2.6.2(a) is shown in Figure 2.6.2(b).

However, the converse is not true. That is, the values of the angle variables that satisfy all the constraints in $S(G)$ do not necessarily correspond to a Delaunay triangulation. For example, for the graph G in Figure 2.6.2(a), the angle values

$$x_1 = x_4 = x_7 = 120, \quad x_2 = x_3 = x_5 = x_6 = 30,$$
$$x_8 = 35, x_9 = 25$$

satisfy $S(G)$, but they do not correspond to a triangulation; if we try to draw the diagram using these angle values, we come across inconsistency, as shown in Figure 2.6.2(c). Indeed, we can choose the size of the first triangle $\Delta v_1 v_2 v_3$ arbitrarily, but next we must glue the second triangle $\Delta v_1 v_3 v_4$ along the edge $\overline{v_1 v_3}$, and finally glue the third triangle $\Delta v_1 v_4 v_2$ along the edge $\overline{v_1 v_4}$, ending up with an inconsistent position of the vertex v_2. In order to avoid such inconsistency we need still more constraints.

Let x_i, x_j and x_k be three angle variables corresponding to the three vertices v_α, v_β and v_γ, counterclockwise in this order, of a cell. Then, we say that x_j is *cc-facing* (meaning 'facing counterclockwise') around v_α, and x_k is *c-facing* (meaning 'facing clockwise') around v_α. In Figure 2.6.2(a), x_2, x_5 and x_8 are cc-facing around v_1, while x_3, x_9 and x_6 are c-facing around v_1.

For two mutually adjacent vertices v_i and v_j, there is a unique angle variable x_k such that x_k is cc-facing around v_i and c-facing around v_j. We denote the angle variable x_k by μ_{ij}. For the triangulation graph in Figure 2.6.2(a), $\mu_{12} = x_8$ because x_8 is the unique angle variable that is cc-facing around v_1 and c-facing around v_2. Note that $\mu_{ij} \neq \mu_{ji}$. In Figure 2.6.2(a), $\mu_{21} = x_3, \mu_{32} = x_1$ and μ_{23} is undefined.

Suppose that v_i is an inner vertex of G. Let $d(i)$ denote the number of edges incident to v_i, let $\phi_1^{(i)}, \phi_2^{(i)}, \ldots, \phi_{d(i)}^{(i)}$ be the cc-facing angle variables around v_i, and let $\theta_1^{(i)}, \theta_2^{(i)}, \ldots, \theta_{d(i)}^{(i)}$ be the c-facing angle variables around v_i. Furthermore, we define

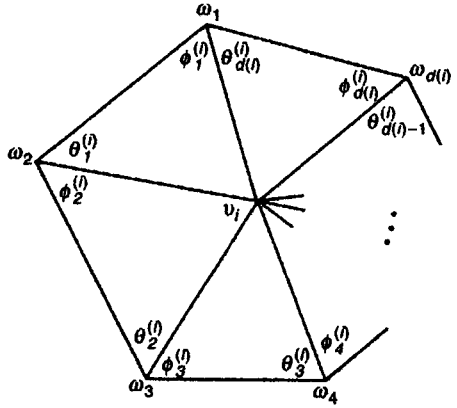

Figure 2.6.3 Angles cc-facing and c-facing around the vertex v_i.

$$F(v_i) = \frac{\sin\phi_1^{(i)} \sin\phi_2^{(i)} \ldots \sin\phi_{d(i)}^{(i)}}{\sin\theta_1^{(i)} \sin\theta_2^{(i)} \ldots \sin\theta_{d(i)}^{(i)}}. \tag{2.6.12}$$

We consider only positive angle values, and hence we get $0 < F(v_i) < \infty$.

Lemma 2.6.1 Any triangulation $\mathcal{T} = (V, E, C, \psi)$ satisfies the next constraint.

(C6) $F(v_i) = 1$ for any inner vertex v_i.

Proof Let v_i be an inner vertex of $\mathcal{T}$. As shown in Figure 2.6.3, let $w_1, w_2, \ldots, w_{d(i)}$ be the vertices incident to v_i counterclockwise, let $\phi_j^{(i)}$ and $\theta_j^{(i)}$ be the cc-facing angle and the c-facing angle, respectively, around v_i associated with the triangle $\Delta v_i w_j w_{j+1}$, where $w_{d(i)+1}$ is to be read as w_1. Let $l(v_i, w_j)$ denote the length of the edge $\overline{v_i w_j}$. Then we get

$$l(v_i, w_j)\sin\phi_j^{(i)} = l(v_i w_{j+1})\sin\theta_j^{(i)} \quad \text{for } j = 1, 2, \ldots, d(i). \tag{2.6.13}$$

Substituting these equations in $F(v_i)$, we obtain

$$F(v_i) = \prod_{j=1}^{d(i)} \frac{\sin\phi_j^{(i)}}{\sin\theta_j^{(i)}} = \prod_{j=1}^{d(i)} \frac{l(v_i, w_{j+1})}{l(v_i, w_j)} = 1. \tag{2.6.14}$$

□

Theorem V2 A 2-connected triangulation graph $G(V, E, C)$ is a DT-realizable graph if and only if the set of constraints (C1)−(C6) is satisfiable.

Proof First suppose that G is a DT-realizable graph. Then there exists a Delaunay triangulation $\mathcal{T} = (G, \psi)$. Let us assign the values of the angles realized by $\mathcal{T}$ to the corresponding angle variables. Then, they satisfy (C1), (C2), (C5) and (C6) because $\mathcal{T}$ is a triangulation. Moreover, they satisfy (C3) and (C4) because $\mathcal{T}$ is a Delaunay triangulation.

Next suppose that there exist angle values for G that satisfy (C1)–(C6). Then, we can construct the triangulation using these angle values. First, we choose an arbitrary cell of G and draw it as a triangle of arbitrary size with the given angle values. Next we augment the triangulation by adding adjacent triangles one by one. Since a new triangle added at each step is adjacent to at least one old triangle, its size is determined automatically in such a way that the edges common to the old and the new triangles coincide. Even if the new triangle is adjacent to two or more triangles, it can be glued to the old part of the triangulation consistently because the constraint (C6) is satisfied. Hence we can complete the triangulation $\mathcal{T} = (G, \psi)$. The constraint (C3) implies that the outermost edges form a convex polyhedron, and hence the triangulation is the partition of the convex hull of the vertices whose locations are specified by ψ. The constraint (C4) directly implies that the circumcircle of a triangle does not contain the vertices of the adjacent triangles. This fact, in turn, implies that the circumcircle of a triangle does not contain a vertex, because we can always obtain the Delaunay triangulation by flipping the diagonals of the quadrilaterals that do not satisfy (C4). Thus, the constraints (C3) and (C4) altogether guarantee that $\mathcal{T}$ is a Delaunay triangulation. □

If we restrict the Delaunay triangulations to non-degenerate ones, constraints (C3) and (C4) are respectively changed in the following way.

(C3′) For each outer vertex, the sum of all the associated angle variables is less than 180.

(C4′) For each inner edge, the sum of the associated pair of the angle values facing the edge is less than 180.

Namely, the constraints (C3) and (C4) are represented by inequalities allowing equalities, while the constraints (C3′) and (C4′) are represented by inequalities without allowing equalities.

Thus, we get a non-degenerate version of Theorem V2 as follows.

Theorem V3 A 2-connected triangulation graph $G(V, E, C)$ is a non-degenerate DT-realizable graph if and only if the set of constraints (C1), (C2), (C3′), (C4′), (C5) and (C6) is satisfiable.

Proof The proof of this theorem is straightforward because the addition of the constraints (C3′) and (C4′) simply implies the deletion of the equality symbols from the improper inequalities generated by (C3) and (C4). □

Thus, we get the necessary and sufficient condition for a triangulation graph to be a DT-realizable graph or a non-degenerate DT-realizable graph. Battista and Vismara (1993) pointed out that if actual values are assigned to the angle variables, the constraints (C1)–(C6) can be used to judge whether the given set of angle values corresponds to the actual Delaunay triangula-

tion. However, the condition stated in Theorem V2 or V3 is not useful for the recognition of a DT-realizable graph, because the angle values are unknown variables in our problem, and we do not know a finite-step algorithm for judging the satisfiability of the condition.

If we happen to be able to delete the constraint (C6), we can judge the satisfiability in finite steps because the constraints (C1)–(C5) are linear in the variables and the method for checking their satisfiability has been established in linear programming. Indeed we can delete the constraint (C6). The next two theorems hold.

Theorem V4 (Hiroshima and Sugihara, 1994) A 2-connected triangulation graph $G(V, E, C)$ is a DT-realizable graph if and only if the set of constraints (C1)–(C5) is satisfiable.

Theorem V5 (Hiroshima and Sugihara, 1994) A 2-connected triangulation graph $G(V, E, C)$ is a non-degenerate DT-realizable graph if and only if the set of constraints (C1), (C2), (C3′), (C4′) and (C5) is satisfiable.

As we have already seen in Figure 2.6.2(c), the angle values satisfying (C1)–(C5) cannot be used directly for the construction of a Delaunay triangulation. However, we can show that once we obtain the angle values that satisfy (C1)–(C5), then we can change them so as to satisfy (C6) while (C1)–(C5) are kept unviolated. This is the main story of the proofs of Theorems V4 and V5. The details of the proof are shown in Hiroshima and Sugihara (1994, 1996).